FOOD SAFETY ENGINEERING STRATEGIES FOR COMBATING FOODBORNE BACTERIA IN FOOD PROCESSING ENVIRONMENTS

A Dissertation

Presented to the Faculty of the Graduate School

of Cornell University

In Partial Fulfillment of the Requirements for the Degree of

Doctor of Philosophy

by

Lillian Chieh-hwei Hsu

August 2012

FOOD SAFETY ENGINEERING STRATEGIES FOR COMBATING FOODBORNE BACTERIA IN FOOD PROCESSING ENVIRONMENTS

Lillian Chieh-hwei Hsu, Ph. D.

Cornell University 2012

Food safety engineering is the application of engineering approaches to solve food safety problems. This dissertation showcases two food safety engineering strategies for combating the presence of pathogenic microorganisms in food processing environments and foods.

One strategy for eliminating bacterial presence in foods is by using technologies to inactivate microorganisms. Pulsed light (PL) treatment consists of using short duration, high energy bursts of broad spectrum light to inactivate microorganisms. The antimicrobial effectiveness of PL is directly related to the treatment dose (fluence) received by the microorganism. Treatment effectiveness and uniformity can vary greatly depending on the properties of the substrate and the relative location of the pulsed light source. To gain a better understanding of the sources of non-uniform treatment, a numerical model based on mapping the spatial distribution of fluence in conjunction with Weibull inactivation kinetics to predict the volumetric inactivation in PL treatment of liquid substrates with known optical properties and geometry was developed and validated. Information obtained from this work can help processors determine the viability of using PL as a microbicidal treatment without extensive and costly experiments.

Another approach for eliminating undesirable bacteria in food processing environments is through preventing bacterial attachment to surfaces. Previous work has suggested that substratum surface topography can influence bacterial attachment. However, no universal trends have been

identified. Manipulating surface topography at the nanoscale to control the effective contact area available to the bacterial cells might affect bacterial attachment. The influence of nanoscale surface topography on the attachment behavior of *Escherichia coli, Listeria innocua,* and *Pseudomonas fluorescens* to nanoporous alumina and nanoengineered silica substrates was investigated. Bacterial attachment and biofilm formation were observed by wide field fluorescence microscopy, scanning electron microscopy, and atomic force microscopy. The current results suggest that substratum nanoscale topography influences the number of attached cells, and also the relative orientation of cells to the topographical details. Moreover, morphological differences between attached cells indicate that bacteria utilize different mechanisms of attachment in response to nanoscale substratum topography. Insight gained from this type of work will aid in the design of surfaces that resist bacterial attachment and thereby reduce the risk for cross-contamination.

Overall, these approaches can work synergistically to positively impact the safety and quality of the food supply.

BIOGRAPHICAL SKETCH

Lillian Chieh-hwei Hsu was delivered via Caesarean section after failing to find her way to the exit on a cold February evening in Pittsburgh, PA. Shortly thereafter, the Hsu family moved to New Jersey where Lillian began what has thus far been a 23-year-long career in academia. Following in the tradition set by her older sister, Lillian earned the title of Valedictorian of her graduating class from Whippany Park High School. Four years later, she earned a Bachelor of Arts degree in biochemistry as a Vagelos Scholar under the uniquely memorable mentorship of Dr. Ponzy Lu from the University of Pennsylvania. She simultaneously completed a Master of Science degree in chemistry with Dr. Andrew N. Binns, who taught her, among other things, how essential it is to develop meticulous dish washing skills, especially for microbiological research. In the Binns/Goulian lab, surrounded by the stimulating company of Gauri Nair, Fanglian He, Yvonne Chan, Albert Siryaporn, Elizabeth Libby, Paige Derr, and Dan Cheng, Lillian learned many microbiological and chemical methods while completing her thesis, "Structural and functional analyses of ChvE from *Agrobacterium tumefaciens*", and developed a love for ABBA – all things that would prove very useful during her PhD. Additionally, having unlimited access to cable television for the first time in her life, Lillian discovered the wonders of Alton Brown and instantly fell in love with culinary science. Combining her interest in biochemistry and the culinary arts, food science seemed like the obvious choice for life after Penn.

In August 2007, Lillian ventured to the rolling hills and freezing tundra of Ithaca, NY, where she began her pursuit of a PhD in food science as a National Needs Fellow with Dr. Carmen Moraru. Though her research projects were more food safety than food making, (aside from a particular frozen breakfast food – related project) she was still able to hone her baking

skills to the simultaneous delight and chagrin of many of her roommates, labmates, and other friends. After all is said and done, Lillian feels that, despite the 36-hour growth curves and numerous nights spent sleeping in the old Stocking Hall lab, the past five years at Cornell truly have made for one incredible journey, and she looks forward to embarking on the next exciting adventure.

For the trillions of bacteria that cooperated with me and selflessly gave their lives to the noble cause of improving the safety of the world's food supply.

- & -

For my family, for all of their love, patience, and support.

ACKNOWLEDGMENTS

I would like to acknowledge my advisor, Dr. Carmen I. Moraru, for taking on the role and responsibility of being my primary research mentor. Her support –intellectual, financial, and personal – throughout the past five years was undoubtedly a major contributing factor in my being able to complete the PhD program, and I am very grateful for all she has done. I would also like to thank Dr. Randy W. Worobo for serving as my food microbiology minor committee member and for providing endless plates of bacteria and invaluable advice. I would like to acknowledge Dr. Dennis D. Miller, my nutrition minor committee member, for recommending many interesting nutrition classes and seminars throughout the years, and also for our periodic conversations about life. I would also like to acknowledge Dr. Syed Rizvi for sharing many interesting perspectives with me during the semester that I served as his TA.

The company and camaraderie of past and current members of the Moraru lab were integral in keeping morale up in difficult times and sharing the good times. Mila Wihodo and Dan Michelle Wang – thank you for showing me the ropes during my first year both in and out of the lab. Aaron Uesugi – thank you for teaching me how to zap bacteria with Pulsed Light and for sharing Guittard chocolate and Hawaiian treats throughout the years. Cosmin Beliciu – thank you for many interesting conversations about science and life and the trinkets from Romania. Anne Sauer – thank you very much for keeping the lab in order, partially setting the groundwork for my first two Pulsed Light projects, sharing sweets from Germany, and for being there through it all. Teng Ju Tan – thank you for all of the great food recommendations in upstate New York and for inspiring me with your consistently positive attitude. Dongjun Zhao – thank you for the thoughtful gifts from all your travels and helping to keep the lab an upbeat work environment. Guoping Feng – thank you so much for all of your help, advice, and support with the nanotechnology project.

I would also like to acknowledge the Food Science administrative staff, including Janette Robbins, Cindy Uhrovcik, Shelly Staff, Marva Francis, Andy Melnychenko, and Matt Stratton,

for making sure that all administrative things ran smoothly. I would like to thank Tom Burke for fixing every machine that always broke at the most inconvenient time, and for ensuring my personal safety by installing clever safeguards on certain Pulsed Light apparatuses.

I would also like to acknowledge the many friends I have met throughout the years. Thank you, Richard Bodnar, for believing in me when few others did. Thank you, Kai-wen Cheng, Holly Yang, Vicky Lo, Wei-tong Wang, Po-hsun Lin, Yvonne Young, James Young, Jeffrey Yu, Brad Chen, Joyce Kuo, Sophie Wu, Stanley Huang, Chia-hung Kao, Frank Liu, and Daisy Chiang for being my Cornell Taiwanese family away. Special thanks to Jonathan Shaw for giving me my KitchenAid stand mixer, without which my life at Cornell would have been much less sweet. To the Summerhill boys, thanks for being my "bros". Xiao Wang – thank you for boosting morale when times got tough and for being my reliable fried foods companion. KK Yu – thank you for the extended use of your camera and the late night conversations. Jon Tse – thanks for providing many modes of digital entertainment, allowing me to invade your kitchen, and teaching me invaluable ways to relieve stress. Robert Karmazin – thank you for loving chocolate and fries as much as I do, and for keeping me company during the odd hours at which most other people are asleep. Saugata Ghose – thank you for tolerating me in all my moods good and bad, for indulging on nearly all of my impulsive whims, and for coming through for me time and time again. I suppose I will keep in touch with you, at least for a little while. Josh Phelps – it's been an interesting journey (maybe a little too interesting at times) and overall, my PhD would not have been as great an experience without you. Thank you for the support, adventures, and all the things you do that show me you care.

Finally, I would like to thank my family for their lifelong support. Mom and Dad, thank you for everything you have done for me. I know I would not be who or where I am today without your continued love and dedication. Vivian – thanks for pushing me to forge my own path. Ben – thank you for always being there, and for the duck dinner that powered me through the finish line. And last but not least, Mickey – thanks for all the hilarious memories and joy only a kitty could bring to my life.

TABLE OF CONTENTS

LIST OF FIGURES

LIST OF TABLES

CHAPTER 1

INTRODUCTION

Food safety engineering is a relatively recent and growing field that has emerged in response to the increasing demand and need for safe, healthy, and minimally processed foods. Whereas the field of food safety involves understanding the fundamental microbiological biological principles and mechanisms of action of pathogenic and spoilage microorganisms, as well as identifying chemical hazards, the food safety engineering perspective involves applying engineering principles to solve the microbial and chemical food safety problems at the industrial level. Food safety engineering can be subcategorized into the following broad areas: (1) engineering aspects of microbial control and inactivation; (2) sanitary design of food processing plants and equipment for food safety; and (3) monitoring and detection methods for chemical and microbial contaminants. This dissertation will present two different engineering-based approaches that address the issue of contaminating bacteria in foods and food processing environments that fall under category (1).

Engineering aspects of microbial control and inactivation include developing technologies for achieving microbial inactivation, building predictive models for microbial inactivation, using nanotechnology approaches for ensuring food safety, and designing packaging systems for microbial control. While thermal treatment has been the traditional method for inactivating bacteria in many foods, it also has the effect of altering various quality and nutritional attributes, such as color changes, loss of some vitamins, and texture and flavor changes (López-Gómez et al., 2009). The demand for minimally-processed "fresh" foods has been a major driving force behind the research and development of alternative technologies that do not use high heat as the primary means of microbial inactivation and therefore have a less

negative impact on the nutritional quality and sensory attributes of the food. Such non-thermal processes include high pressure processing, ionizing radiation, pulsed electric fields, pulsed light, and ultrasound. While each of these technologies currently has specific niche applications, either as standalone treatments or as part of hurdle treatment processes, they also have limitations that must carefully be considered when identifying potential applications and designing appropriate treatment protocols. One way to gauge upfront whether or not a particular technology is suitable for a target food safety application without extensive and lengthy experimentation is by using **predictive modeling**. Besides offering estimates on the effectiveness of the treatment, predictive models provide information about the uniformity of the treatment, and can help to identify practical or physical limitations of the process. This type of information is critical for proper application of a technology. This work will offer an example of how predictive modeling can be used in the context of evaluating the feasibility and non-uniformities of Pulsed Light treatment for microbial inactivation.

While devising intervention strategies for microbial inactivation is a very important food safety tool, another approach for eliminating undesirable bacteria in food processing environments is by preventing or minimizing their presence in food processing plants. While such efforts have been made for many years, recent progress in **nanotechnology** has opened new ways in the fight against microorganisms. Applications of **nanotechnology for food safety** primarily include new methods of microbial detection, and the development of materials with antimicrobial properties. For example, biosensors using a nanowire 'barcode' system are purported to be able to detect spores, viruses, and bacterial toxins such as ricin and botulinum toxin, based on the specific configuration of nanoscale wires coated with various metals (Tok et al., 2006). Other nanosensors are capable of detecting the presence of bacteria and/or toxins produced by these bacteria, as well as other chemical contaminants (Zaytseva et al., 2005). In

addition to being portable, these biosensors have the added benefit of being less costly and able to produce results much more rapidly in-house rather than sending samples away for testing. When used for food packaging, some nanomaterials can enhance the protective properties of the packaging components, thereby enhancing product shelf-life (Dingman, 2008; A to Z of Nanotechnology, 2006). Furthermore, nanosensors can be incorporated into packaging materials to aid in the monitoring of product spoilage, alerting the consumer when the product is no longer safe for consumption (Dingman, 2008; A to Z of Nanotechnology, 2006; Sozer and Kokini, 2009; Bhattacharya et al., 2007).

Recently, there has been increasing interest in a different application of nanotechnology for food safety. Manipulating material properties at the nanoscale to hinder bacterial attachment has yielded some success, especially in the biomedical and dental fields. A similar approach, using food-safe materials, might be very useful for the food industry. Thus, the second focus of this dissertation is to develop and use nanoengineered surface topography for controlling bacterial attachment to surfaces as a preventative measure against microbial contamination in food processing plants.

REFERENCES

A to Z of Nanotechnology. (2006). *Nanotechnology and food packaging*. Retrieved August 28, 2006, from http://www.azonano.com/details.asp?ArticleID=857

Bhattacharya, S., Jang, J., Yang, L., Akin, D., Bashir, R. (2007). Biomems and nanotechnology-based approaches for rapid detection of biological entities. *Journal of Rapid Methods & Automation in Microbiology*, 15, 1-32.

Dingman, J. (2008). Nanotechnology: its impact on food safety. *Journal of Environmental Health*, 70 (6), 47-50.

López-Gómez, A., Fernández, P. S., Palop, A., Periago, P. M., Martinez-López, A., Marin-Iniesta, F., & Barbosa-Cánovas, G. V. (2009). Food Safety Engineering: An Emergent Perspective. *Food Engineering Reviews*, *1*(1), 84-104.

Sozer, N., & Kokini, J. L. (2009). Nanotechnology and its applications in the food sector. *Trends in biotechnology*, *27*(2), 82-9. doi:10.1016/j.tibtech.2008.10.010

Tok, J. B.-H., Chuang, F. Y. S., Kao, M. C., Rose, K. a, Pannu, S. S., Sha, M. Y., Chakarova, G., Penn, S.G., and Dougherty, G.M. (2006). Metallic striped nanowires as multiplexed immunoassay platforms for pathogen detection. *Angewandte Chemie* (International ed. in English), 45(41), 6900-4.

Zaytseva, N.V., Goral, V.N., Montagna, R.A., and Baeumner, A.J. (2005). Development of a microfluidic biosensor module for pathogen detection. *Lab-on-chip*, 5 (8), 805-811.

CHAPTER 2

PULSED LIGHT TREATMENT AS A METHOD FOR MICROBIAL INACTIVATION

Chapter 2.1

Pulsed Light Treatment Background

Pulsed light (PL) is a technology that uses short duration, high-energy pulses of UV-rich broad spectrum (λ = 200 – 1100 nm) light to inactivate a range of pathogenic and spoilage microorganisms in foods and on food contact surfaces. PL has been effective in inactivating various species of bacteria, yeasts, molds (Takeshita et al., 2003; Jun et al., 2003; Rowan et al., 1999; MacGregor et al., 1998). The FDA has approved the use of PL in the United States "for surface microorganism control", provided that the cumulative dose does not exceed 12 J/cm^2, the radiation source is a xenon flashlamp that emits broad spectrum light, and the pulse duration is 2 milliseconds or shorter (CFR 21 Part 179.41). Current commercial applications of PL are limited to surface sterilization of packaging materials, such as cups, caps, and lids, used to store a range of ready-to-eat products (www.claranor.com). Though there has been significant research in recent decades on the effectiveness of PL treatment of a wide variety of food products, including fresh fruits and vegetables, beverages, and meat and cheese products (Lagunas-Solar et al., 2006; Bialka and Demirci, 2008; Bialka and Demirci, 2007; Krishnamurthy et al., 2007; Uesugi and Moraru, 2009; Sauer and Moraru, 2009), there has not yet been a true industrial adoption of PL for treatment of foods.

Some of the reasons for the absence of commercial PL treatment of foods include the lack of confidence in overall PL effectiveness, limitations to what PL can inactivate, and challenges associated with appropriate processing design. In Pulsed Light treatment,

microorganisms are inactivated when they are exposed to sufficient doses of light energy primarily in the ultraviolet (UV) range (200 – 400 nm). The incident energy dose, or *fluence*, that the microorganisms receive is directly dependent upon the distance from the flashlamp. Moreover, the uniformity of the lethal effect is directly influenced by the shape of the lamp, orientation of the substrate relative to the lamp, as well as the chemical composition and topography of the liquid or solid substrate, respectively (Woodling and Moraru, 2005; Hsu and Moraru, 2011). Ensuring uniform treatment is one of the main challenges associated with using PL as the sole treatment process for microbial inactivation, and, along with overall efficacy, are two of the major limitations of PL.

Unlike traditional thermal treatments which follow first-order linear inactivation kinetics, microbial inactivation by PL is more appropriately described by the Weibull distribution. The Weibull model is a non-mechanistic and non-linear model that takes into account biological variation and does not assume that every cell in a given population has the same resistance to a particular treatment (Peleg and Cole, 1998). The Weibull model describes microbial inactivation kinetics using the following equation:

$$\log\left(\frac{N}{N_o}\right) = -\alpha \times F^{\beta} \qquad \text{(Eq.2.1)}$$

where N is the number of survivors after treatment, N_o is the initial population, α is the scale parameter, F is fluence, in units of Joules/cm^2, and β is the shape parameter. When $\beta < 1$, the inactivation curve is concave upward and implies that as treatment intensity increases, so does the remaining cellular population's resistance to the treatment. When $\beta > 1$, the inactivation curve is concave downward, indicating that the remaining population becomes more susceptible to the treatment as treatment intensity increases. When $\beta = 1$, the inactivation curve is linear and the inactivation follows first-order kinetics (Uesugi et al., 2007). Thus, the Weibull model captures

both linear and non-linear inactivation kinetics, and has been shown to accurately describe microbial inactivation by PL treatment of various substrates (Woodling and Moraru, 2005; Uesugi et al., 2007; Bialka et al., 2008; Sauer and Moraru, 2009).

While the use of the Weibull model to describe microbial inactivation kinetics is widely accepted, less understood about PL are the mechanisms of inactivation. The microbicidal effect of PL is thought to be predominately the result of the UV portion of the emitted light (Woodling and Moraru, 2007). As with traditional continuous-UV treatment (254 nm), the primary mechanism of microbial inactivation by PL is thought to be the extensive DNA damage induced by UV light. The formation of pyrimidine dimers on adjacent bases causes helix distortion and interrupts DNA replication as well as transcription (Sinha and Hader, 2002). Additionally, both single strand and double strand breakages of DNA exposed to the high energy light pulses from PL treatment contribute to the killing effect (Dunn et al., 1995; Rowan et al., 1999). A recent study conducted by Cheigh *et al*. suggests that, overall, the lethal effect of PL is due to a combination of structural cellular damage, as evidenced by visualization of ruptured cell walls and cytoplasmic membranes in cells exposed to PL but not in cells exposed to continuous UV-C treatment, in addition to UV-induced DNA damage (Cheigh et al., 2012). Since PL treatment can achieve similar levels of microbial reduction in a few seconds that continuous UV treatment does in minutes (Uesugi PhD thesis, 2011), there is reason to believe that there may be other effects unique to PL treatment that contribute to microbial inactivation. More research is needed to fully understand the mechanisms of PL inactivation.

REFERENCES

Bialka, K. L., & Demirci, a. (2007). Decontamination of *Escherichia coli* O157:H7 and *Salmonella enterica* on blueberries using ozone and pulsed UV-light. *Journal of food science*, 72(9), M391-6.

Bialka, K. L., & Demirci, A. (2008). Efficacy of pulsed UV-light for the decontamination of *Escherichia coli* O157:H7 and *Salmonella* spp. on raspberries and strawberries. *Journal of food science*, 73(5), M201-7.

Cheigh, C., Park, M., Chung, M., Shin, J., Park, Y. (2012). Comparison of intense pulsed light- and ultraviolet (UVC)- induced cell damage in *Listeria monocytogenes* and *Escherichia coli* O157:H7. *Food Control*, 25, 654-659.

Claranor company website, available at: www.claranor.com. [Accessed May 22, 2012].

Dunn, J., Ott, T., Clark, W. (1995). Pulsed-light treatment of food and packaging. *Food Technology*, 49, 95-98.

FDA Code of Federal Regulations Title 21. http://www.accessdata.fda.gov/scripts/cdrh/cfdocs/cfcfr/CFRSearch.cfm?CFRPart=179

Hsu, L., and Moraru, C.I. (2011). Quantifying and mapping the spatial distribution of fluence inside a Pulsed Light treatment chamber and various liquid substrates. *J of Food Engineering*. 103, 84 – 91.

Jun, S., Irudayaraj, J., Demirci, A., & Geiser, D. (2003). Pulsed UV-light treatment of corn meal for inactivation of *Aspergillus niger* spores. *International Journal of Food Science and Technology*, 38(8), 883-888.

Krishnamurthy, K., Demirci, a, & Irudayaraj, J. M. (2007). Inactivation of Staphylococcus aureus in milk using flow-through pulsed UV-light treatment system. *Journal of food science*, 72(7), M233-9.

Lagunas-Solar, M. C., Piña, C., MacDonald, J. D., & Bolkan, L. (2006). Development of pulsed UV light processes for surface fungal disinfection of fresh fruits. *Journal of food protection*, 69(2), 376-84.

Peleg, M., & Cole, M. B. (1998). Reinterpretation of microbial survival curves. *Critical reviews in food science and nutrition*, 38(5), 353-80.

Rowan, N. J., Macgregor, S. J., Anderson, J. G., Fouracre, R. A., Mcilvaney, L., & Farish, O. (1999). Pulsed-light inactivation of food-related microorganisms. *Appl Environmental Microbiology*, 65, 1312-1315.

Rowan, N., MacGregor, S., Anderson, J., Fouracre, R., McIlvaney, L., & Farish, O. (1999). Pulsed-light inactivation of food related microorganisms. *Appl. Environ. Microbiol*,

65(3), 1312-1315.

Sauer, A., & Moraru, C. I. (2009). Inactivation of *Escherichia coli* ATCC 25922 and *Escherichia coli* O157:H7 in apple juice and apple cider, using Pulsed Light treatment. *Journal of Food Protection*, 72(5), 937-944.

Sinha, R. P., & Häder, D.-P. (2002). UV-induced DNA damage and repair: A review. *Photochemical & Photobiological Sciences*, 1(4), 225-236.

Takeshita, K., Shibato, J., Sameshima, T., Fukunaga, S., Isobe, S., Arihara, K., & Itoh, M. (2003). Damage of yeast cells induced by pulsed light irradiation. *Int. J. Food. Microbiol*, 85, 151-158.

Uesugi, A. R., & Moraru, C. I. (2009). Reduction of Listeria on ready-to-eat sausages after exposure to a combination of pulsed light and nisin. *Journal of food protection*, 72(2), 347-53.

Uesugi, A. R., Woodling, S. E., & Moraru, C. I. (2007). Inactivation kinetics and factors of variability in the Pulsed Light treatment of *Listeria innocua* cells. *Journal of Food Protection*, 70(11), 2518-2525.

Woodling, S E, & Moraru, C. I. (2005). Influence of surface topography on the effectiveness of pulsed light treatment for the inactivation of *Listeria innocua* on stainless-steel surfaces. *J. Food Sci*. 70:M345-M351.

Woodling, Sarah E, & Moraru, C. I. (2007). Effect of spectral range in surface inactivation of *Listeria innocua* using broad-spectrum Pulsed Light. *Journal of Food Protection*, 70(4), 909-916.

Chapter 2.2

Research Objectives

With the increasing consumer demand for minimally-processed, fresh and safe foods, there exists an urgent need for development of effective strategies to meet this demand. The concern that arises with minimally-processed and ready-to-eat foods, of course, is the microbiological safety of the product. Rather than relying on the reactionary approach of using technologies to treat a food product that potentially harbors pathogenic bacteria, the emerging food safety engineering perspective is to tackle the problem using both reactionary and preventive tactics.

Over the past few decades, alternative technologies which do not rely on high heat as the primary means of inactivating microorganisms have been developed in an effort to ensure a safe food product without drastically altering the nutritional and sensory properties of the food. Identifying the strengths and weaknesses of alternative technologies such as Pulsed Light (PL), which is capable of inactivating various microorganisms in or on many types of foods and surfaces, could help processors seize appropriate opportunities for using this technology in an industrial setting. Specific to PL is the need for understanding the possible causes of non-uniform treatment. To accomplish this goal, the first two objectives of this dissertation are as follows:

Objective 1: Develop a map and quantify the spatial distribution of total and UV fluence in air and within various fluids with known optical properties

Objective 2: Develop a method using a numerical approach for predicting levels and spatial distribution of microbial inactivation after PL treatment of liquid substrates with known optical properties and geometry

Chapter 2.3

Quantifying and Mapping the Spatial Distribution of Fluence Inside a Pulsed Light Treatment Chamber and Various Liquid Substrates

ABSTRACT

Pulsed light (PL) is a technology that uses short, high-energy pulses of UV-rich broad spectrum light to inactivate a range of pathogenic and spoilage microorganisms in foods and on food contact surfaces. Microbial inactivation is directly related to the energy dose (fluence) received by the target microbes. Since fluence decays away from the lamp source due to light absorption and scattering phenomena, it is necessary to accurately quantify the fluence received locally within a substrate in order to design uniform antimicrobial PL treatments. The main objective of this work was to quantify and map the spatial distribution of both total and UV fluence both in air and in liquid substrates with different optical properties. Butterfield's Phosphate Buffer (BPB), Trypticase Soy Broth (TSB), and apple juice (clarified apple cider) were used as substrates and *L. innocua* was used as the challenge microorganism. A pyroelectric head, and a UV-VIS-NIR spectrophotometer connected to a 1000 µm optical fiber, were used to measure the fluence in air and the three liquid substrates. Fluence was measured at incremental distances from the lamp, along the x-, y- and z-axes. As expected, fluence decreased with increasing distance from the lamp, in all three directions. A 3-parameter Gaussian model described well the spatial distribution of fluence, both in air and in the liquid substrates. Overall, this study emphasizes the fact that substrate-light interactions affect the spatial distribution of fluence within a substrate, and these non-uniformities need to be taken into account when developing commercial applications of PL.

INTRODUCTION

Pulsed Light (PL) treatment has been proven to be highly effective for inactivating a broad range of microorganisms on food and food contact surfaces, or in thin-layer fluid substrates (Moraru and Uesugi, 2009). The effectiveness of PL treatment depends on many factors, one of the most significant being the direct exposure of the targeted microorganisms to the incident light. Substrate properties, such as surface topography and reflectivity, as well as physical distance of the substrate from the flash lamp, and the specific microbes being targeted, also play a role in the effectiveness of PL treatment (Gomez-Lopez et al., 2005a).

Depending on the treatment dose, the targeted microorganism, and the substrate being treated, PL treatment has been reported to achieve anywhere from 0.5 to 8 log reduction. Woodling and Moraru obtained a 4 log reduction of *L. innocua* on a stainless steel coupon with up to 12 pulses at a distance of 50.8 mm from the lamp (corresponding to about 12J/cm^2) (Woodling and Moraru, 2005). Gomez-Lopez *et al.* achieved a range of 0.5 to 2.04 log reduction of mesophilic, aerobic microbes naturally found in minimally processed vegetables such as spinach, iceberg lettuce, cabbage, radicchio, celeriac, green bell peppers, and soybean sprouts, using a treatment dose of up to 2700 light pulses (no fluence value reported) (Gómez-López *et al.*, 2005). Bialka and Demirci obtained a 3.9 log reduction of *E. coli* O157:H7 and a 3.4 log reduction of *Salmonella* on raspberries, with a treatment dose of 72 J/cm^2 and 59.2 J/cm^2. They observed slightly lower reductions of *E. coli* and *Salmonella*, 2.1 and 2.8 log reductions respectively, in strawberries treated with 25.7 and 34.2 J/cm^2 respectively (Bialka and Demirci, 2008). Sharma and Demirci exposed a 6.25 mm layer of alfalfa seeds to PL for 90 seconds at a distance of 8 cm from the lamp and observed a 4.89 log reduction of *E.coli* O157:H7 (Sharma and Demirci, 2003). Ozer and Demirci observed a maximum of 1.09 and 1.02 log reduction of *E. coli O157:H7* and *L. monocytogenes* on raw salmon fillet skins after a 60 second treatment at a

distance of 8 cm from the lamp, with a lamp output of 5.6 J/cm^2 at the surface of the strobe (Ozer and Demirci, 2006). Uesugi and Moraru obtained a 1.39 log reduction of *L. innocua* on the surface of Vienna sausages, after exposure to a treatment dose of 9.4 J/cm^{2,} (Uesugi and Moraru, 2009). Fine and Gervais obtained a 2.93 log reduction of *S. cerevisiae* on black pepper subjected to a dose of 31.12 J/cm^2, and a 0.7 log reduction on wheat flour (Fine and Gervais, 2004).

The wide range in levels of inactivation achieved indicates that on one hand, PL can be an effective treatment against food borne pathogens in certain substrates, but also that there are many factors that influence the effectiveness of PL treatment. Moreover, it is difficult to make cross-comparisons between studies, due to the absence of a standardized system for reporting treatment dose. Some studies report treatment dose in terms of lamp output or number of pulses. While this information gives insight into total treatment time, it is the treatment dose that actually results in inactivation. Therefore, it is necessary to accurately quantify the energy that reaches the substrate in order to make meaningful comparisons and conclusions about PL effectiveness.

Compared to solid foods and food surfaces, less work has been done on using PL to treat liquid substrates. While heat treatment is the most widely used method for decontaminating beverages, PL might be an attractive alternative treatment for beverages if comparable levels of microbial inactivation were achieved without the accompanying negative changes in the sensory and nutritive properties associated with thermal processes. Sauer and Moraru found 5.76 log and 7.15 log reductions of *E.coli* O157:H7 in apple cider and apple juice, respectively, after PL treatments performed under turbulence, at fluence levels of up to 12 J/cm^2 (measured at the liquid surface) (Sauer and Moraru, 2009). Uesugi *et al.* obtained a 6.04 log reduction of *L. innocua* in Butterfield phosphate buffer exposed to 13.3 J/cm^2 of PL (Uesugi *et al*., 2007). Krishnamurthy *et al*. obtained a 7.5 log reduction of *S. aureus* in phosphate buffer after a

treatment dose of 84 J/cm^2, and achieved up to 7 log reduction *S. aureus* in milk flowing at a rate of 20 mL/min at the same distance from the lamp (Krishnamurthy *et al*., 2007).

These results suggest that, as with solid substrates, liquid substrate properties can affect the outcome of PL treatment. Substrate opacity, turbidity, and homogeneity can affect the way light propagates throughout the liquid substrate, and consequently affect the efficiency and uniformity of PL treatment. Additionally, the depth of the fluid column and the spatial location of the column relative to the light source will most likely affect the degree of microbial inactivation that can be achieved. Thus, how light behaves inside each liquid substrate must be understood to ensure successful design of PL applications.

The spatial decay of light intensity from a point source is usually described by the inverse square law (Chang *et al*., 2008). For non-point source lamps, mathematical corrections can be made to take into account the geometry of the light source. DiLazzaro *et al.* analyzed the spatial distribution of light from an excimer lamp and developed a model based on the inverse square law to describe the light distribution as a function of distance from the lamp (Di Lazzaro *et al*., 2004). Other models that were used to describe the spatial distribution of light include the Lorentzian distribution and the simpler Gaussian distribution, both of which are characterized by symmetrical bell-shaped curves. Both distributions are commonly used to describe different phenomena in optics and laser research, including the spatial distribution of light (Davis, 1996).

The equations for the Lorentzian and Gaussian distributions are defined by Eqs. 2.2 and 2.3, respectively (Li, 1992):

$$I(x) = \frac{A}{\left[1 + \left(\frac{x}{\gamma}\right)^2\right]^2} \qquad \text{(Eq. 2.2)}$$

where I is irradiance, A is the amplitude, γ is the ¼ irradiance width, and x represents the position at which I is being determined;

$$I(x) = Be^{\left(-\frac{2x^2}{\sigma^2}\right)} \qquad \text{(Eq. 2.3)}$$

where B is the amplitude and σ is the e^{-2} width along the x-axis. When comparing the Gaussian and Lorentzian distributions, the Gaussian shows a faster decay from the peak, while the Lorentzian distribution has a lower peak and wider tails than the Gaussian, for the same full width at half maximum (Blom and Björk, 2009).

In this study, the spatial distribution of total and UV fluence in air and three liquid substrates (BPB, TSB, and apple juice) was investigated. The objectives of this study were to quantify and to generate a map of both the total fluence distribution and the UV fluence distribution both in air and within various fluids with known optical properties (°Brix, pH, absorbance), in order to better understand potential sources of non-uniformity in PL treatments.

MATERIALS AND METHODS

Cultures. L. innocua (FSL-C2 008) was chosen as a representative organism for measuring fluence in inoculated liquids. Prior to the experiment, the culture was streaked onto tryptic soy agar (TSA) plates from the frozen stock maintained by the Cornell University Food Safety Laboratory and incubated for 24 ± 2 h at 37 ± 2°C.

Liquid substrate preparation. A single isolated colony was transferred into trypticase soy broth (TSB) and incubated for 20 ± 2 hours at 35 ± 2°C. A 1:10 dilution of the bacterial culture in the working substrate (autoclaved BPB) was made just before PL treatment, resulting in a population of approximately 10^8 CFU/mL. TSB and apple juice were autoclaved prior to taking fluence measurements. Only BPB was inoculated, as the presence of the bacteria significantly altered the turbidity of the otherwise clear liquid. The properties of these three liquid substrates were determined prior to conducting the fluence measurements. For BPB, TSB, and apple juice

respectively, the Brix values were 0.5, 3.25, and 11.25°Brix and the pH values were 6.8, 7.4, and 4.0, respectively. The spectral irradiance profiles were measured as part of this study and are shown in Figure 5.

Pulsed Light treatment unit. The PL unit used in this study was a bench-top RS-3000C SteriPulse System (Xenon Corporation; Woburn, MA, USA), which consists of a controller unit and a treatment chamber. A Xenon flashlamp suspended from the ceiling of the treatment chamber and encased in a 40.64 cm lamp housing with a 2.54 cm footprint emits short duration, high-energy light pulses in the near IR to UV range (λ = 180 – 1100 nm).

PL fluence measurements in air. A pyroelectric head (Ophir Optronics, MA) with a Nova II display (Ophir Optronics Inc.; Wilmington, MA) was used to measure the fluence in the PL unit, at incremental distances from the lamp: one centimeter increments along the x-direction (along the direction of the lamp); 0.5 centimeter increments along the y-axis (across the direction of the lamp), and 1.1 centimeter increments along the z-direction (vertically away from the lamp). The pyroelectric head was placed on an adjustable stainless steel shelf in the PL unit. A stainless steel aperture cover was placed over the detector's head, which completely covered the top surface of the head except for a 1-cm^2 circular opening that exposed the detector's surface. The opening of the aperture cover was centered on the detector's surface, and the upper limit of detection was 2.0 J. Fluence measurements were performed in triplicate, and pauses of at least 30 seconds between measurements were allowed in order to prevent saturation of the pyroelectric head.

PL fluence measurements in liquid substrates. Fluence measurements through columns of the three liquid substrates were performed in a similar manner as described for air, with some notable differences. Varying volumes of substrate (BPB inoculated with *L. innocua*, TSB, and apple juice) that corresponded to liquid columns of specific thickness were placed into a flat-

bottomed crystallizing dish (Pyrex, 125 mm x 65 mm) and placed at a fixed vertical distance of 14 cm from the quartz face of the lamp housing. A pyroelectric head was centered beneath the crystallizing dish, and fluence measurements were performed in triplicate. Pauses of at least 30 seconds in between measurements were taken to prevent saturation of the pyroelectric head. Ideally, the pyroelectric head should have been placed at the base of the fluid column inside the crystallizing dish, and the dish should have been moved systematically away from the lamp as was the case for air (no dish). However, since the pyroelectric head could not be immersed in liquid, the decay of fluence through the liquid substrates was captured by adding fixed volumes of each liquid substrate to the glass Pyrex dish, thereby generating liquid columns of varying thickness. This introduces some error into the model, as the decay of fluence is faster in the liquids than in air. The incident fluence at the air-liquid interface will be higher than in actuality, especially for thinner columns of liquid, leading to slight over-prediction of fluence values.

Measuring absolute irradiance and quantification of UV fluence. An Ocean Optics HR2000 spectrophotometer (Ocean Optics; Dunedin, FL) attached to a 1000μm optic fiber was used to measure absolute irradiance (fluence) per wavelength per pulse emitted by the PL unit, in air and through the liquid substrates. Spectrasuite® software package (Ocean Optics; Dunedin, FL) was used to integrate the area beneath the irradiance curves from λ=200-400 nm (UV spectrum) and from λ=200-1000nm (full spectrum). The ratio of these areas gave the proportion of fluence that was contributed by the UV spectral range.

To measure irradiance as a function of wavelength in air, the optic fiber was centered inside the PL chamber along the x- and y- axes. Irradiance was measured per pulse at various z-distances from the lamp. To ensure that the entire pulse was captured, the spectrophotometer was triggered just before the pulse was triggered by the PL unit. To measure irradiance through the liquids, the optic fiber was placed centrally beneath a flat-bottomed crystallizing dish (Pyrex,

125 mm x 65 mm) containing various volumes of liquid substrate, corresponding to liquid columns of specific height. Irradiance was measured per pulse as described for air. All measurements were performed in triplicate. It is important to note that the glass Pyrex dish used to hold the liquid substrates does absorb some of the light energy, including wavelengths in the UV range. This affects irradiance measurements and is corrected for in the model.

Mapping fluence distribution. To generate the equation describing the three-dimensional decay of fluence, the fluence vs. distance data was analyzed using Microsoft Excel (Microsoft Corp; Redmond, WA) and SigmaPlot (Systat Software Inc; San Jose, CA). Measured fluence values along each of the three axes were curve-fitted to a 3-parameter Gaussian model in the x- and y-directions, and to an exponential model in the z-direction. The Gaussian model was chosen over the Lorentzian to describe the fluence distribution in the x- and y-direction due to the ease of subsequent coupling of fluence with the inactivation Weibull kinetics equations.

Statistical analysis. The goodness of fit of the 3-parameter Gaussian model to the experimental data was analyzed using SigmaPlot. Microsoft Excel was used to analyze the goodness of fit of the exponential model to the experimental data obtained in the z-direction. The experimental v. predicted values in the x-z and y-z planes were also plotted using Microsoft Excel, and the R^2 values determined and used to evaluate the goodness of the fit.

RESULTS AND DISCUSSION

1. Distribution of total fluence

1.a. Distribution of total fluence in the PL chamber

The coordinate axes were defined such that the linear flashlamp was parallel to the x-axis (along the lamp), the y-axis was perpendicular to the lamp (across the lamp), and the z-axis was

vertically perpendicular to the lamp. Since it has been previously determined that there is a linear relationship between fluence and the number of pulses (Uesugi *et al*., 2007), it was only necessary to measure the fluence per pulse at each (x, y, z) coordinate.

The spatial distribution of light intensity is a result of absorption, reflection, and scattering of light. Generally, the distribution of light intensity as a function of distance from the lamp source follows a Lorentzian distribution (Li, 1992). However, the simpler Gaussian model was chosen to facilitate coupling of the fluence-distance relationship with the Weibull model of microbial inactivation kinetics. Figure 2.1 compares how well the measured fluence values fit the Gaussian and Lorentzian models. The R^2 values were essentially identical for the x- and y-axes at a vertical distance of 3.2 cm from the lamp (0.889, 0.97), and for the x-axis at a vertical distance of 9.7 cm (0.999) (Fig. 1a, c, d). Along the y-axis at a vertical distance of 9.7 cm, the R^2 value was actually slightly higher (0.970) for the Gaussian fit compared to the Lorentzian fit (0.905), further confirming the legitimacy of using the simpler Gaussian model. SigmaPlot software was used to fit the total fluence data in air and in the liquid columns to a 3-parameter Guassian model (x and y axes) of the form:

$$F_x = Ae^{-0.5\left(\frac{x-x_0}{b_x}\right)^2} \qquad \text{(Eq. 2.4)}$$

where A, x_o, and b_x are constants and F is fluence (J/cm^2). An analogous equation was used for the y-axis, substituting y and y_o for x and x_o, respectively. Using nonlinear regression, the constants were determined to be:

x_o: *-1.04*

y_o: *0.87*

b_x: *21.48*

b_y: *2.11*

Figure 2.1. Comparison of the Gaussian and Lorentzian fits at a vertical distance of 9.7cm and 3.2 cm. Figures a and b show the measured fluence values along the x (a) and y (b) axes at a vertical distance of 9.7 cm from the lamp. Figures c and d show the measured fluence values along the x (c) and y (d) axes at a vertical distance of 3.2 cm from the lamp.

(a)

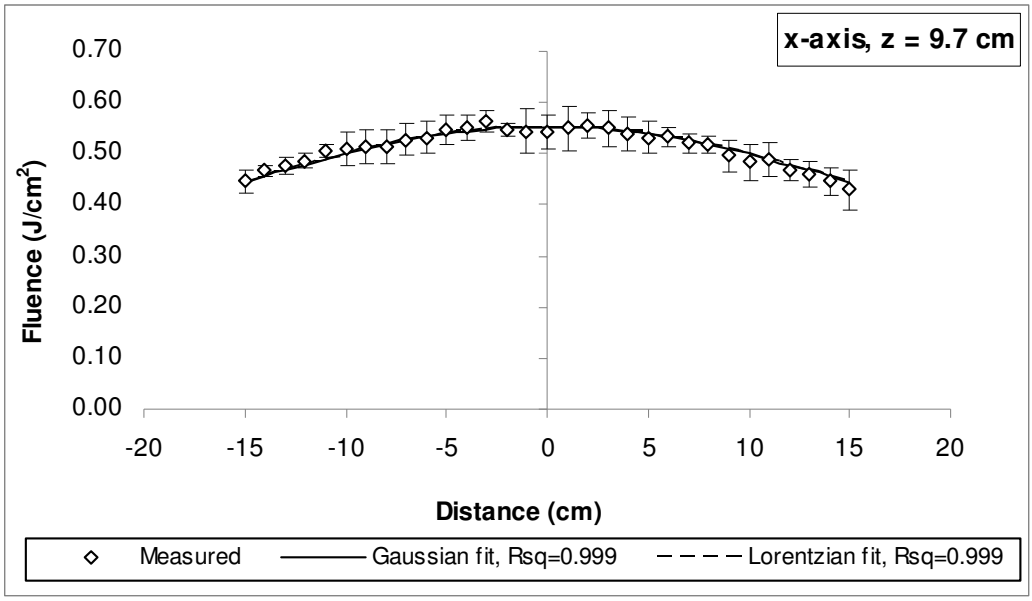
x-axis, z = 9.7 cm
Fluence (J/cm²)
0.70
0.60
0.50
0.40
0.30
0.20
0.10
0.00
-20
-15
-10
-5
0
5
10
15
20
Distance (cm)
Measured
Gaussian fit, Rsq=0.999
Lorentzian fit, Rsq=0.999

(b)

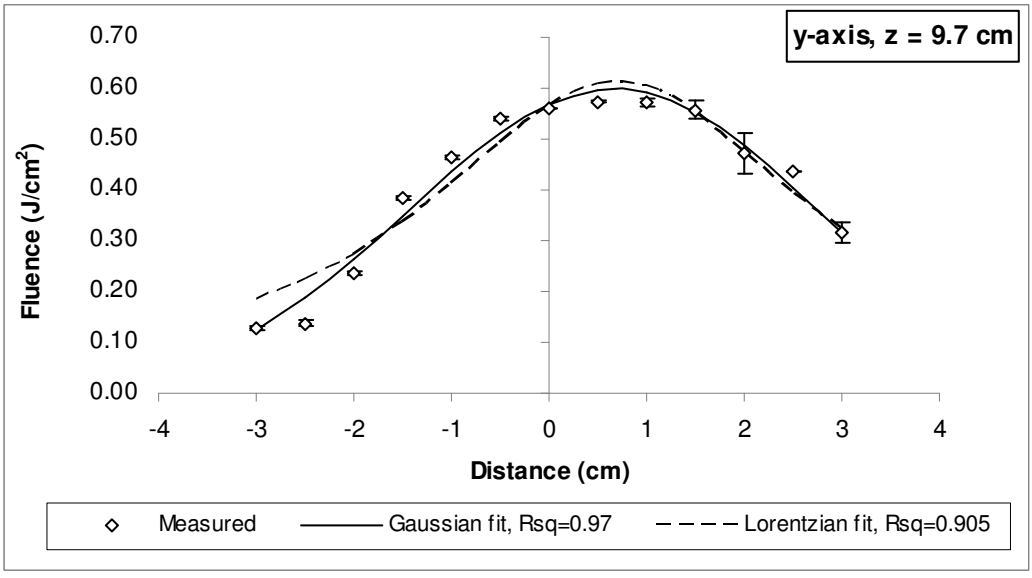
y-axis, z = 9.7 cm
Fluence (J/cm²)
0.70
0.60
0.50
0.40
0.30
0.20
0.10
0.00
-4
-3
-2
-1
0
1
2
3
4
Distance (cm)
Measured
Gaussian fit, Rsq=0.97
Lorentzian fit, Rsq=0.905

Figure 2.1 (continued)

(c)

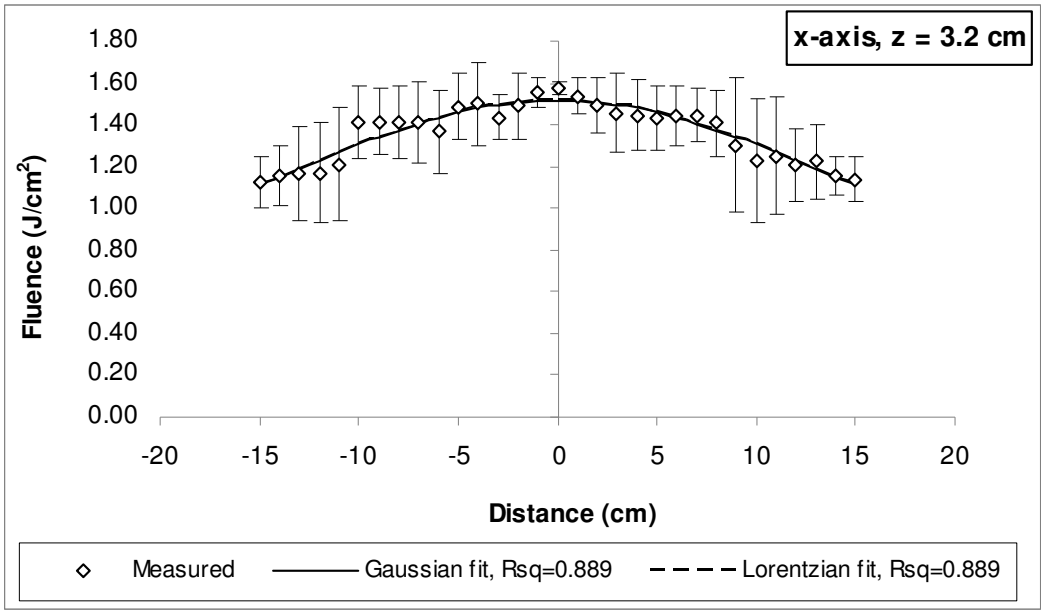

(d)

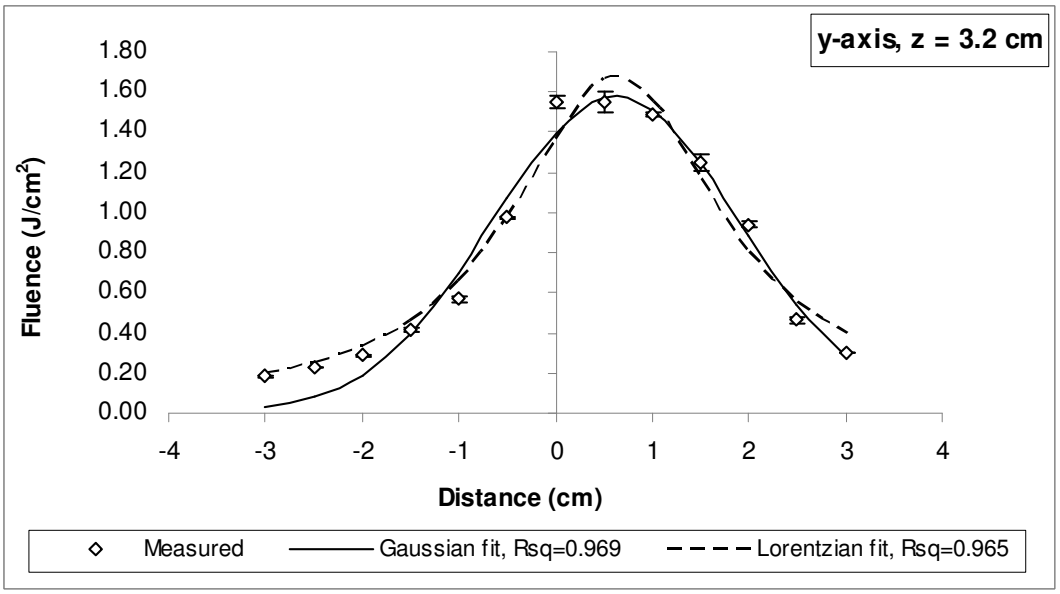

Table 2.1 shows the R^2 values that were obtained from fitting the measured fluence data to the Gaussian or exponential models. Along the x-axis, the model was able to better

approximate the experimental data as vertical distance from the lamp increased (further away from the lamp), as evidenced by higher R^2 values with increasing distance from the lamp (R^2 from 0.83 to 0.98 at vertical distance of 3.2 cm and 9.7 cm, respectively). Along the y-axis, the model approximated well the experimental distance at all vertical distances from the lamp (R^2 between 0.95 and 0.98). Figure 2.2 shows plots of the experimental v. predicted values. Along the lamp axis (x-axis), the calculated and experimental values matched fairly well, with an R^2 value of 0.97 and a slope very close to one (0.99). Along the y-axis, the calculated values were more accurate as distance from the lamp increased: R^2 = 0.72, 0.86, and 0.94; slopes = 0.80, 0.95, and 1.05 at 3.2, 5.8, and 9.7 cm, respectively, vertically from the lamp. Slope values greater than 1 indicate an under-prediction of fluence, while slopes greater than 1 indicate over-prediction. The model tended towards a very slight under-prediction for distances farther from the lamp, and over-prediction for distances close to the surface of the lamp.

Table 2.1 R^2 values obtained from curve-fitting measured data to the Gaussian (x- and y-axes) or exponential functions (z-axis) using SigmaPlot.

Vertical distance from lamp (cm)	x-axis	y-axis	z-axis
3.2	0.83	0.96	0.99
5.8	0.89	0.98	
7.1	0.96	0.95	
9.7	0.98	0.97	
12.3	0.96	0.95	

(a)

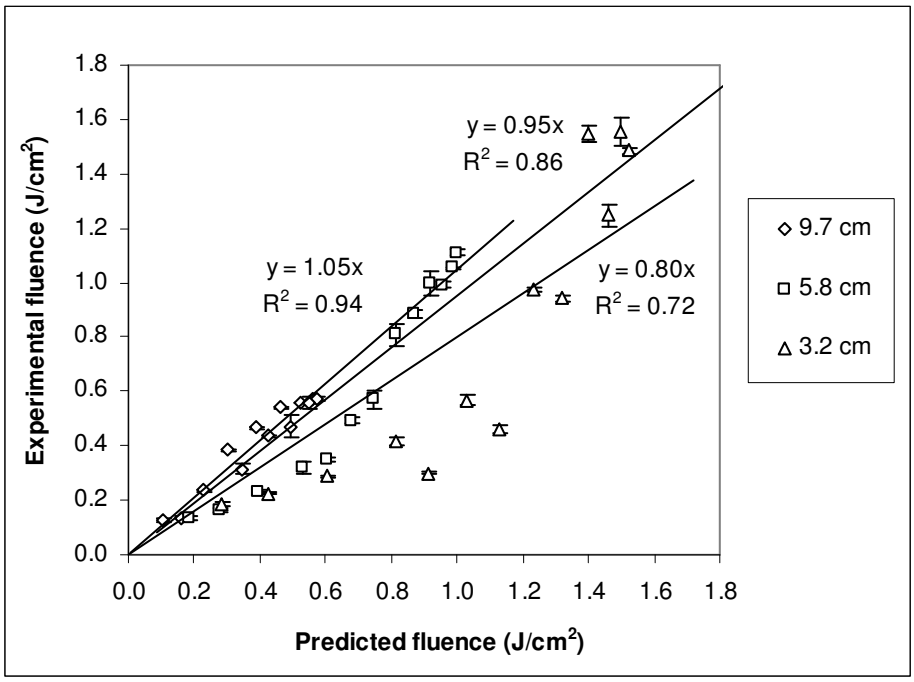

(b)

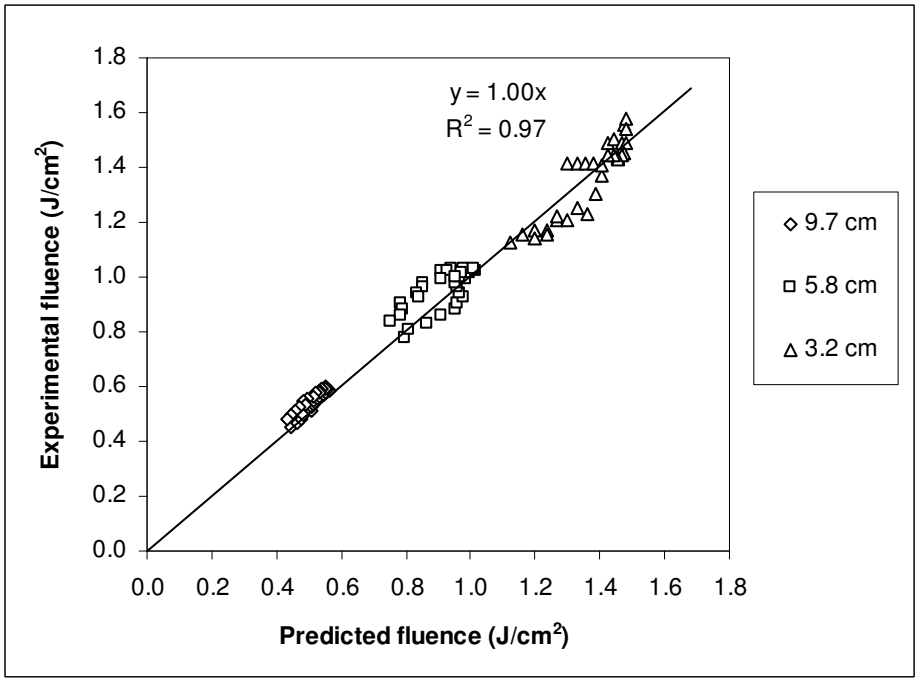

Figure 2.2 Graphs of Predicted v. Experimental fluence values in air in the (a) y-z direction and (b) x-z directions

To determine the value for "*A*", as well as the exponential coefficient for the decay along the z-axis, the fluence measurements taken along the z-axis were fitted to an exponential curve of the form:

$$F_z = Ae^{-Cz} \qquad \text{(Eq. 2.5)}$$

where F = fluence (J/cm^2) and A & C are constants. The decay along the z-axis also follows a Gaussian distribution, but because the Gaussian distribution is symmetric with respect to the lamp, and in this case due to the equipment design, light was only distributed below the lamp, an exponential model was used for simplification purposes. After curve-fitting the data to an exponential function using Microsoft Excel, the values for A were determined to be 2.32, 0.30, 0.29, and 0.28 for air, BPB, TSB, and apple juice, respectively. "*C*" was determined to be 0.14 for air, 0.06 for BPB, 0.27 for TSB, and 0.24 for apple juice. The exponential model was an appropriate approximation, as evidenced by a coefficient of determination between the measured and predicted data $R^2 = 0.99$.

The mathematical form of the three dimensional fluence distribution ($F_{x,y,z}$) in the PL chamber was then obtained by multiplying equations 2.4 and 2.5:

$$F_{x,y,z} = 2.32e^{-\left[0.5\left(\frac{x+1.04}{21.48}\right)^2+0.5\left(\frac{y-0.87}{2.11}\right)^2+Cz\right]} \qquad \text{(Eq. 2.6)}$$

where x, y, and z represent distances from the origin (0, 0, 0). A two-dimensional representation of the calculated fluence distribution in the PL chamber and each substrate is shown in Figures 2.3 and 2.4. The shapes of the fluence curves along the x and y axes are consistent with those of Di Lazzaro *et al*., who measured the spatial distribution of light from an excimer lamp (Di Lazzaro *et al.*, 2004). Fluence decays exponentially with increasing vertical distance from the lamp, both in air and in fluids. Moving away from the focal point of the lamp along the x- and y-axes, fluence follows a Gaussian distribution. It is interesting to note that the fluence distribution

is not perfectly symmetrical about the origin along the x- and y-axes. In air, along the x-axis in a given xy-plane, the fluence distribution is approximately symmetrical about the origin (i.e. the focal point of the lamp). However, along the y-axis in a given xy-plane, fluence was centered 1-centimeter in front of the origin along the y axis. This was attributed to asymmetries within the PL treatment chamber. Also significant is the fact that, at a fixed vertical (z) distance from the lamp, fluence decays much more rapidly along the y-axis as compared to the x-axis. Along the x-axis, fluence drops by less than 1 Joule across a distance of 18 centimeters (the edge of the treatment chamber) to the right or left of the origin. However, along the y-axis, fluence drops to less than half of the maximal value at a distance of 3 centimeters to the front or back of the origin. This is caused directly by the shape and size of the lamp (linear lamp with a 40.64 cm x 2.54 cm footprint).

Figure 2.3 Calculated distribution of fluence in the xz-planes in (a) Empty Chamber, (b) BPB, (c) TSB, (d) Apple Juice

a)

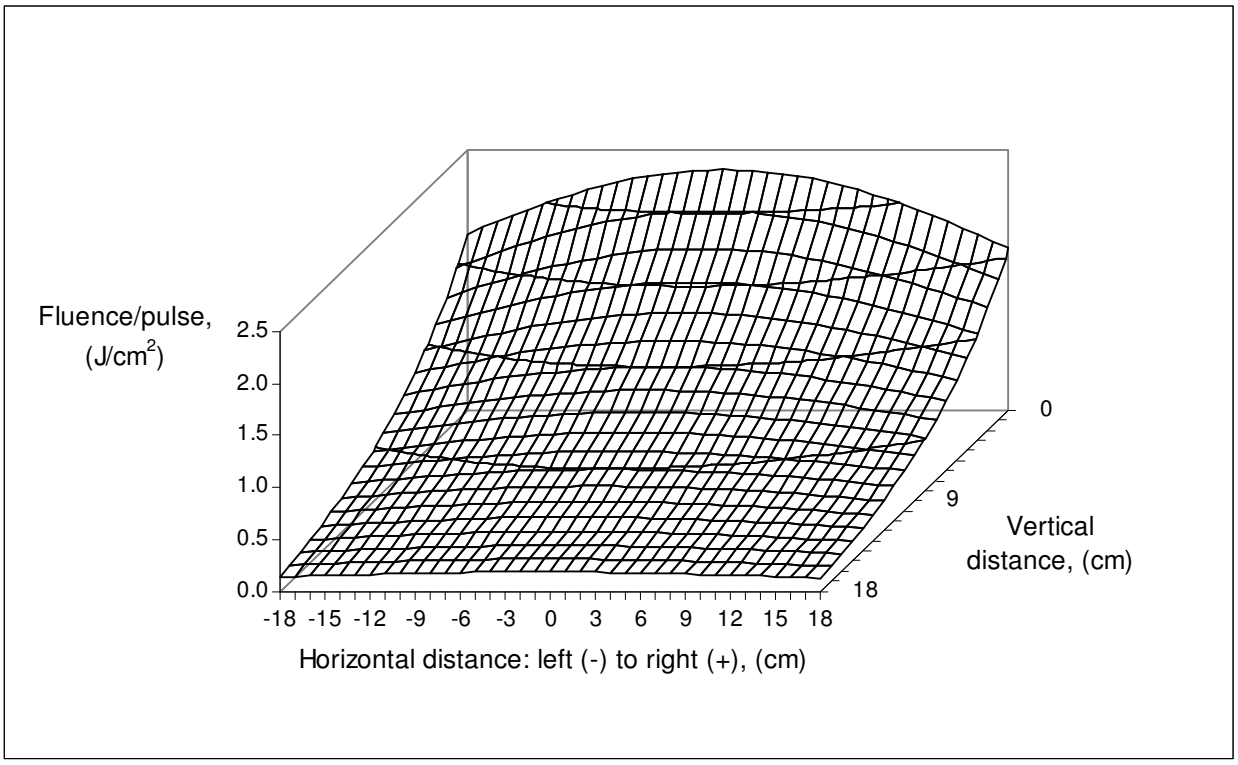
Fluence/pulse,
(J/cm2)
2.5
2.0
1.5
1.0
0.5
0.0
-18 -15 -12 -9 -6 -3 0 3 6 9 12 15 18
Horizontal distance: left (-) to right (+), (cm)
0
9
18
Vertical
distance, (cm)

(b) BPB

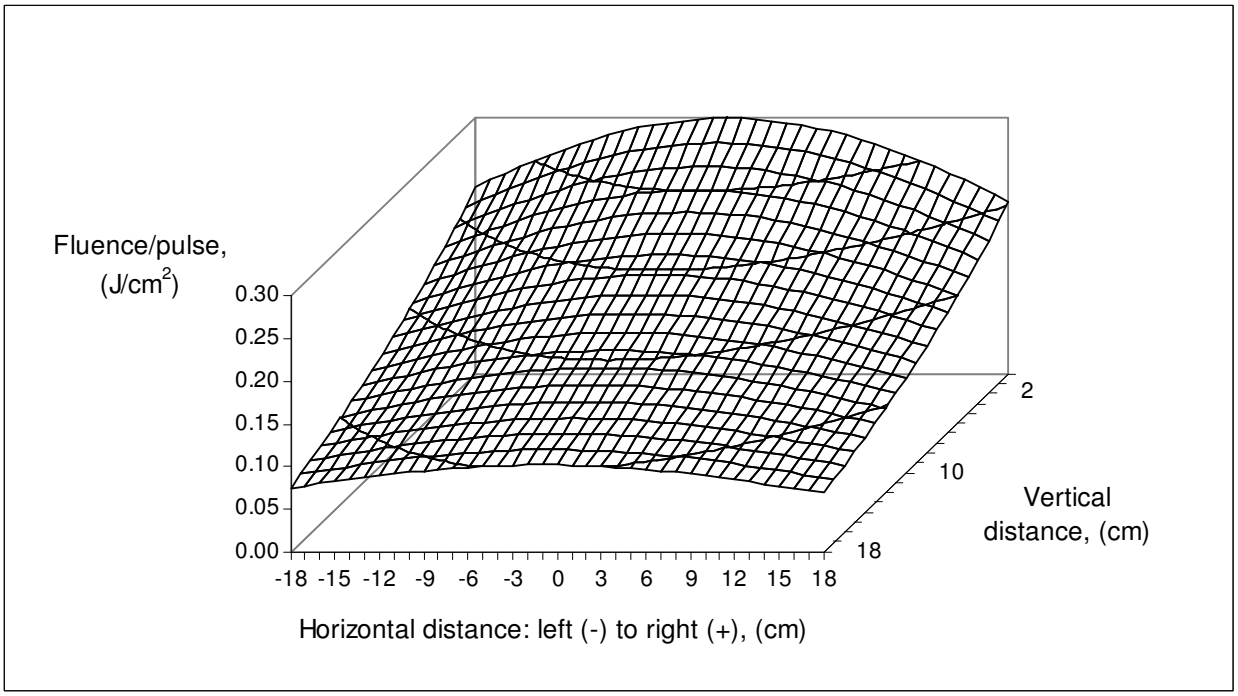
Fluence/pulse,
(J/cm2)
0.30
0.25
0.20
0.15
0.10
0.05
0.00
-18 -15 -12 -9 -6 -3 0 3 6 9 12 15 18
Horizontal distance: left (-) to right (+), (cm)
2
10
18
Vertical
distance, (cm)

Figure 2.3 (continued)

(c) TSB

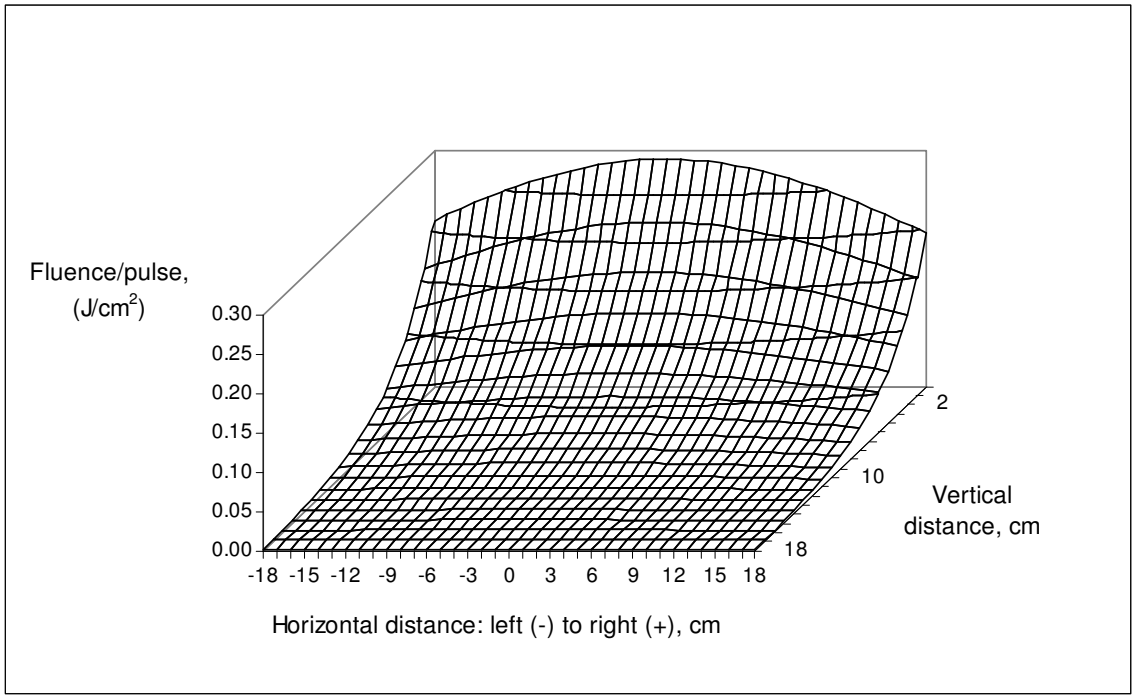

(d) Apple Juice

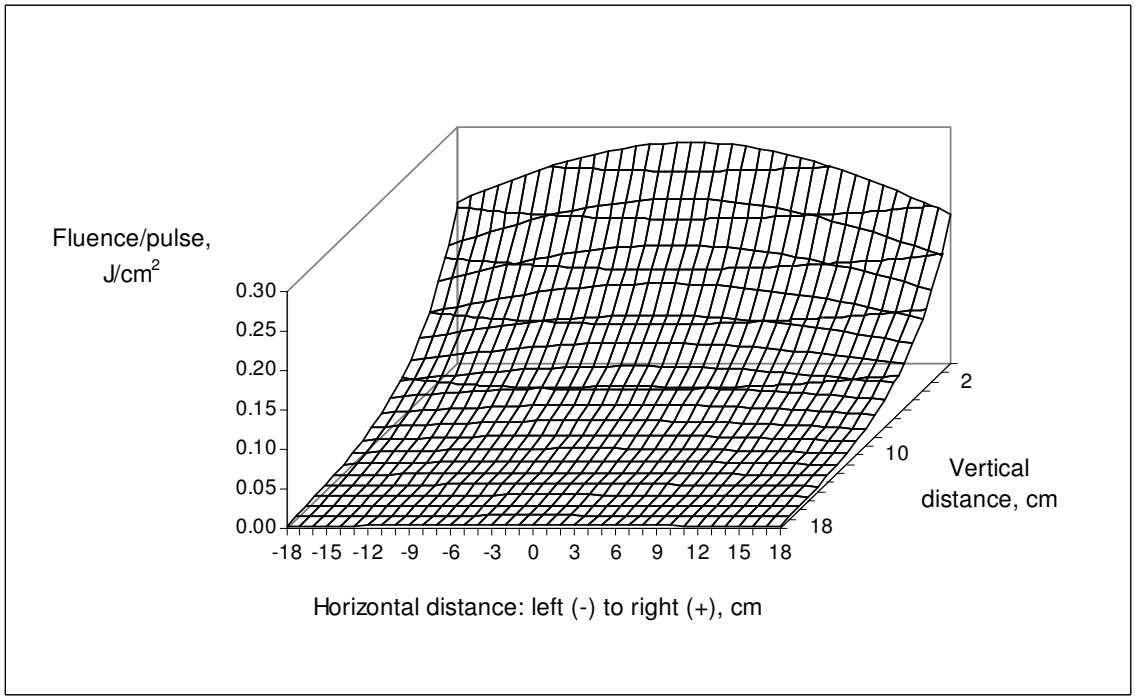

Figure 2.4. Distribution of fluence in the yz-planes in (a) Empty chamber, (b) BPB, (c) TSB, (d) Apple Juice

(a) Empty Chamber

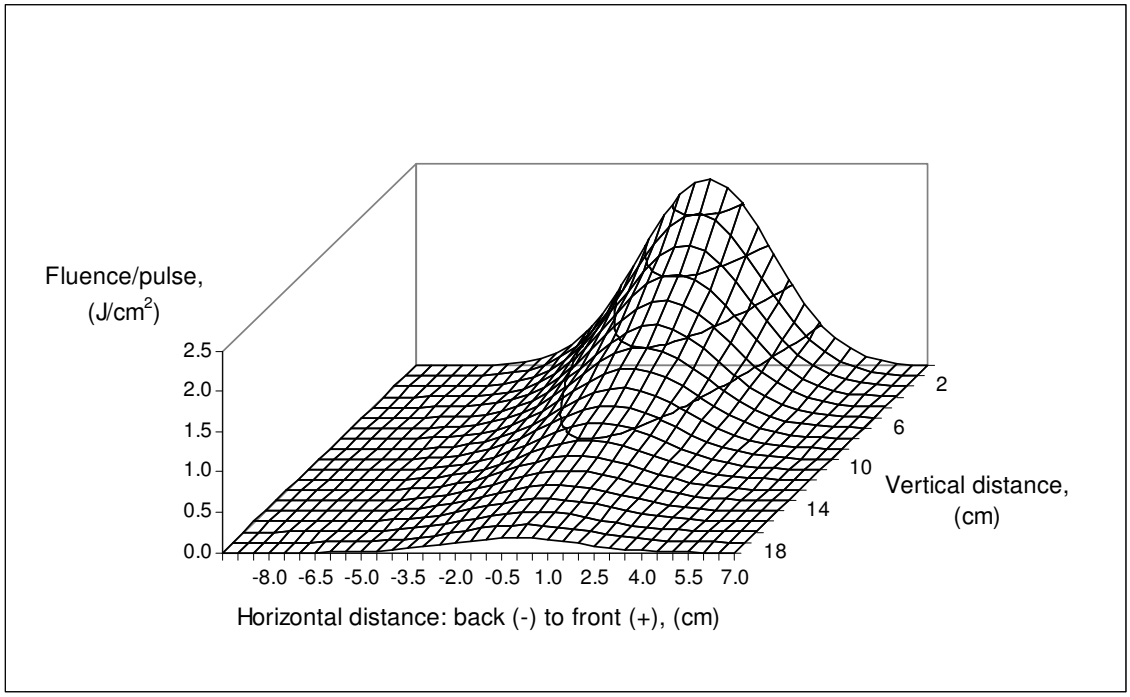

(b) BPB

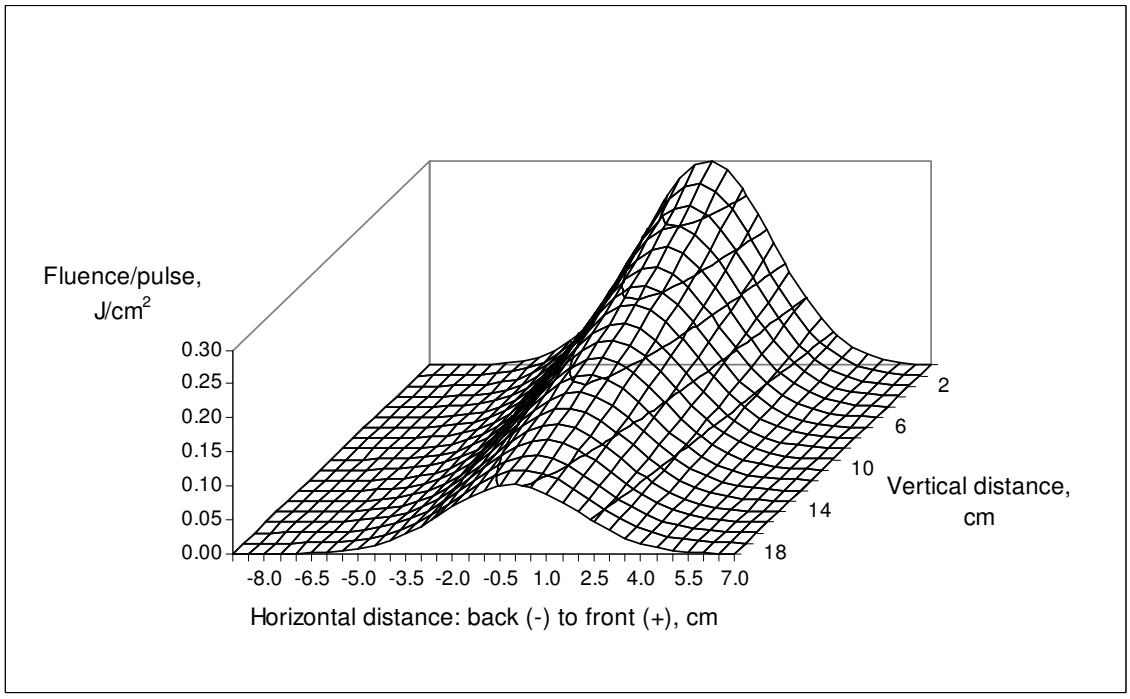

Figure 2.4 (continued)

(c) TSB

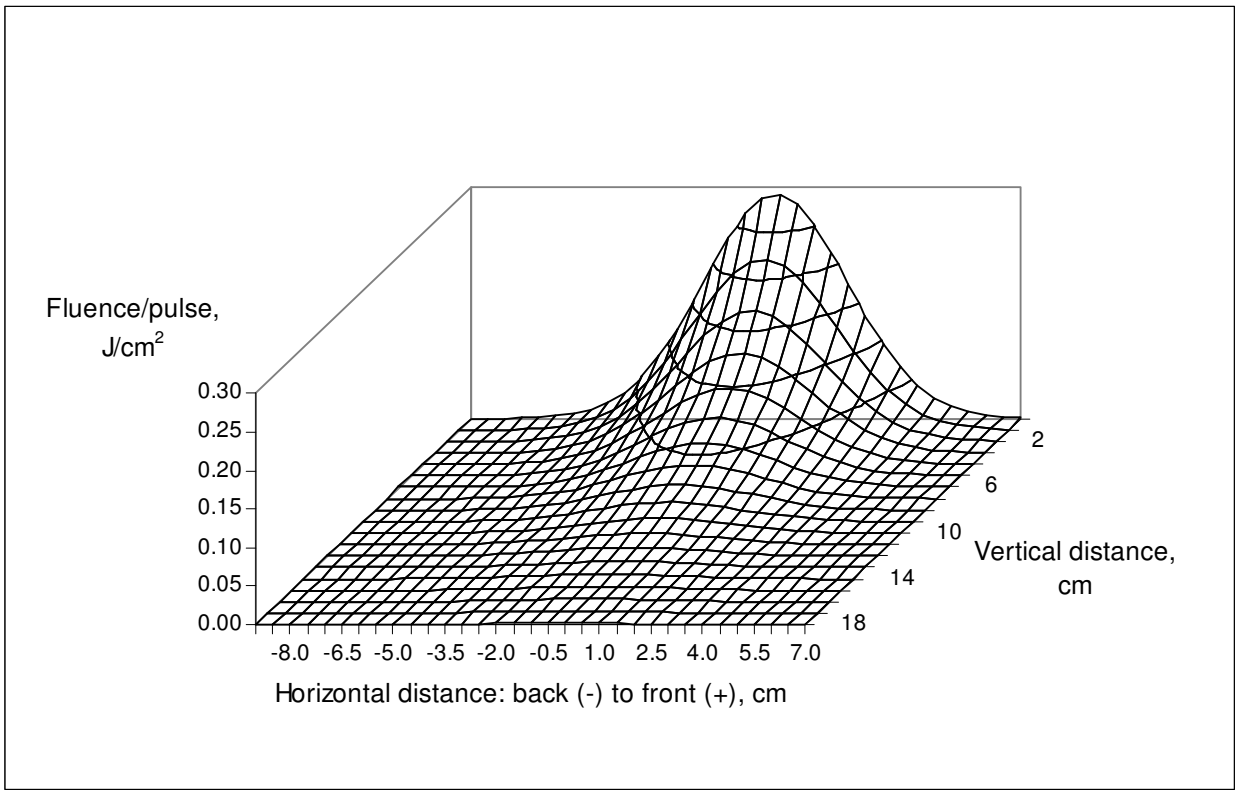

Figure 2.4 (continued)

(d) Apple Juice

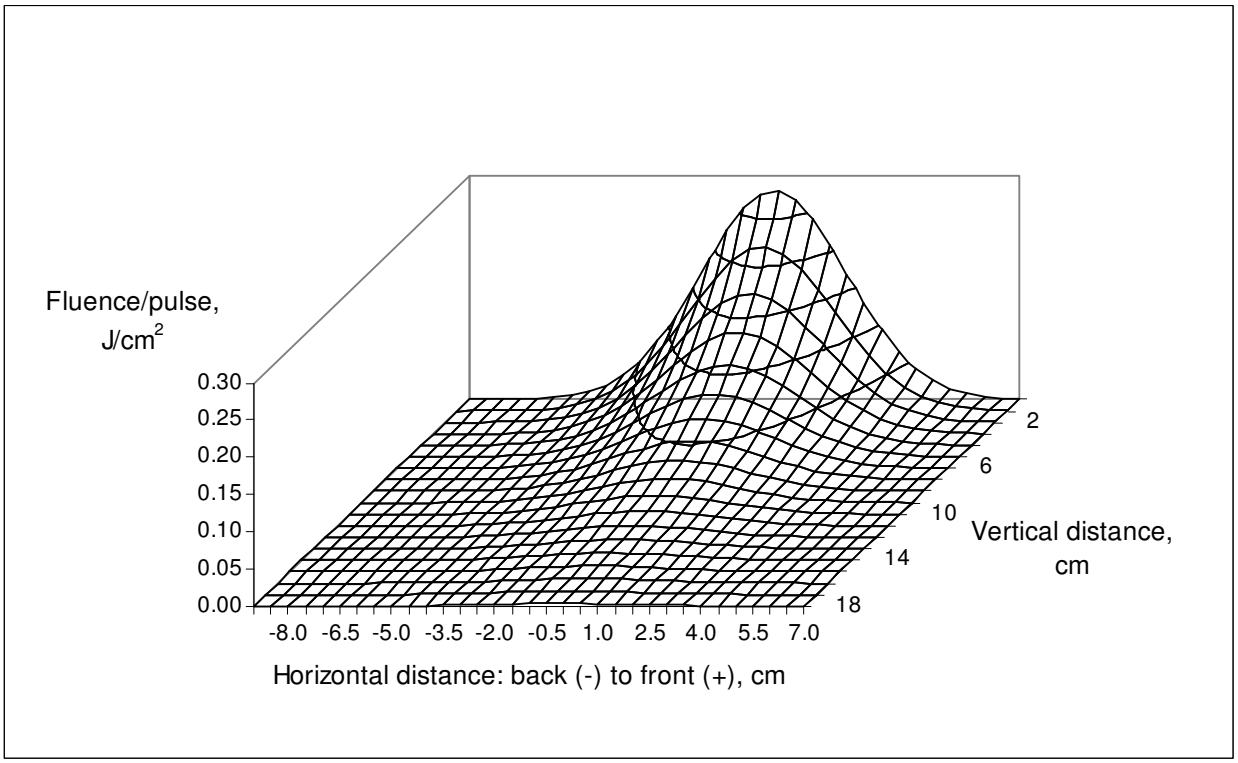

1.b. Distribution of total fluence in liquid substrates

In the case of PL treatment of a fluid substrate, the fluid itself will affect the actual fluence that reaches the microbial cells suspended in the liquid, due to absorption and scattering effects. Therefore, fluence measurements were carried out in order to quantify the attenuation of fluence by the fluid substrates.

Before discussing the actual fluence distribution inside the liquid substrates, it is important to make some comments about the method used to measure the fluence. Ideally, fluence should have been measured directly in a liquid-filled chamber. However, since it was not possible to expose neither the pyroelectric head nor the optic fiber directly to the liquid substrate,

measurements were made through the bottom of a crystallizing dish containing various volumes of liquid. In order to minimize as much as possible the effect of the crystallizing dish on the measurements (i.e. secondary reflections), the crystallizing dish used to measure both total fluence and irradiance, was much wider than the exposed 1-cm^2 area of the detector. A simplifying assumption also made in this study was that within a given xy-plane (a horizontal plane parallel to the plane of the lamp), the liquid substrate will attenuate fluence uniformly throughout that plane. This means that the influence of the liquid substrate on fluence was factored only into the decay of fluence in the vertical direction, perpendicular to the lamp. While this is a realistic and satisfactory assumption in a homogenous liquid substrate, in semi-turbid or turbid liquids, this assumption will introduce some error due to anomalous light scattering that could be caused by suspended particles (including microbial cells) of non-uniform size and distribution. Therefore, the simplifying assumption used in this work could result in some deviation of the predicted fluence values as compared to measured values at a particular (x,y) coordinate.

Fluence values measured through all liquid substrates indicated that fluence followed a Gaussian distribution through the liquid substrates, similar to the fluence distribution in air. The maximal fluence values for the liquid substrates, obtained at points directly under the lamp and within the 2.54 cm footprint of the lamp, were lower than the fluence at the same spatial coordinates but in air, primarily due to absorption of light energy by the liquid. Colored liquids tended to absorb more total energy than clearer liquids, thereby decreasing maximal fluence values, as well as resulting in faster decay with vertical distance from the lamp. Thus, though the maximal fluence values for the three liquids were similar, (0.30 J/cm^2, 0.29 J/cm^2, and 0.27 J/cm^2 for BPB, TSB, and apple juice, respectively) the exponential decay through each substrate differed drastically (exponential parameters of 0.06, 0.27, and 0.24 for inoculated BPB, TSB, and

apple juice, respectively), resulting in a much stronger decay of fluence in thick layers of TSB and apple juice as compared to BPB. For a fluid layer of a given thickness, BPB consistently had the highest fluence value.

2. Quantification of UV fluence

While the Xenon lamp in the PL unit emits broad spectrum energy, much of the microbicidal effect of PL comes from energy emitted in the high energy UV wavelength range (λ = 200 – 400 nm) (Woodling and Morrau, 2007; Moraru and Uesugi, 2009). Thus, it is useful to understand not merely the total fluence distribution, but also the proportion of the total fluence contributed by the UV wavelengths.

To determine the proportion of total fluence contributed by the UV range, a spectrophotometer was used to measure the absolute irradiance per wavelength from λ = 200 – 1000 nm. As with the pyroelectric head, the optical fiber could not be immersed into the liquid, and thus the fiber was placed under a glass Pyrex dish containing the liquid substrates. However, the glass dish does absorb some light, including wavelengths in the UV region. To correct for this error, both the total irradiance and the UV irradiance through the empty glass dish was also measured. The ratio of the UV irradiance in air (without a glass dish) and through the bottom of the glass dish was taken, and the values for UV irradiance proportion were corrected for by multiplying by this ratio. Thus, the UV absorption by the glass dish was accounted for in the model.

Figure 2.5 shows the absolute irradiance curves and the proportion of UV irradiance, for air, the glass Pyrex dish, inoculated BPB, TSB, and apple juice. The Spectrasuite® software, the default program for the spectrophotometer, was used to obtain the total energy received per pulse, in Joules, by integrating the irradiance curves from λ = 200 nm to λ = 1000 nm. Integration of the irradiance curves from λ = 200 nm to λ = 400 nm gave the energy contributed

by the UV wavelengths. The ratio of total energy to UV energy yielded the percentage of total fluence contributed by the UV wavelengths. This ratio was determined for air, the glass Pyrex dish, and the three liquid substrates. These ratios, after correcting for the absorbance by the glass Pyrex dish, were then used as multipliers in the equation describing total fluence in the PL chamber and the liquid substrates to obtain equations describing the 3D distribution of UV fluence in air and the liquid substrates:

$$F_{x,y,z} = Ae^{-\left[0.5\left(\frac{x+1.04}{21.48}\right)^2+0.5\left(\frac{y-0.87}{2.11}\right)^2+Cz\right]} \qquad \text{Eq. 2.7}$$

where the values for *A* were determined to be 0.93, 0.14, 0.12, and 0.13 for air, inoculated BPB, TSB, and apple juice, respectively. The values for *C* remained the same as those describing the decay of total fluence.

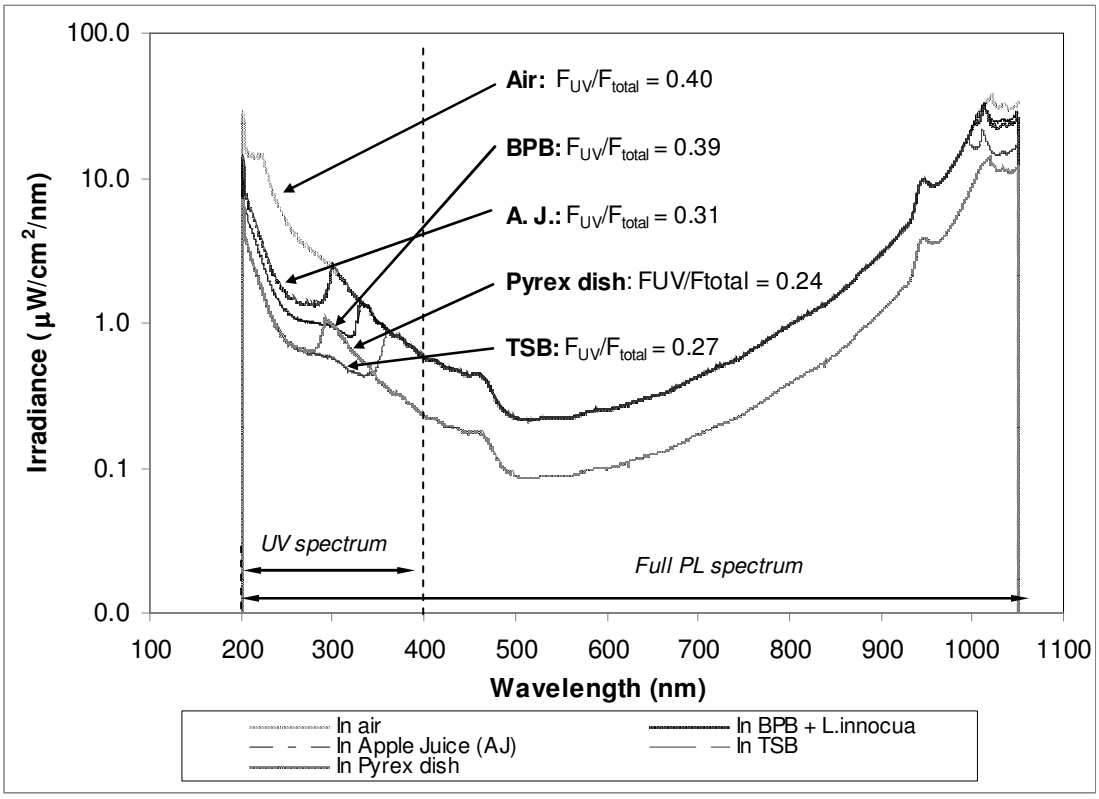

Figure 2.5 Spectral distribution of measured irradiance in air and liquid substrates

As seen in Figure 2.5, the proportion of UV fluence changes depending on the substrate. In air, the UV fluence represented about 40% of the total fluence. In the 1:10 dilution of bacterial culture in BPB, the UV fluence was ~ 39% of the total fluence, indicating that the substrate itself (BPB) did not absorb much of the UV, and most of the UV absorption was caused by the suspended cells. However, in TSB and apple juice, the UV fraction dropped to 27% and 31%, respectively, suggesting that these substrates absorb UV preferentially. Light absorption by the substrate depends both on the chemical composition of the substrate and on the wavelength of the radiation. In BPB, the only chemical in solution is monobasic potassium phosphate, which does not have significant UV absorption. For TSB, the major components are digested proteins (pancreatic digest of casein, papaic digest of soybean meal) and sodium chloride. Proteins, especially those containing the amino acids tyrosine, phenylalanine, and tryptophan, will absorb UV, thereby contributing to the greater absorption of the UV wavelengths as compared to BPB. Apple juice contains mostly sugars, including fructose, sucrose, and glucose, as well as organic acids, such as ascorbic acid, all of which absorb UV wavelengths (200 nm for the sugars, and 220-300 nm for ascorbic acid) (Koutchma *et al.*, 2009). These differences in chemical composition account for the different absorption profiles exhibited by the liquids, with the more chemically complex liquids absorbing more of the higher-energy, shorter wavelengths as compared to BPB. Liquids that preferentially absorb UV are less suitable for PL treatment, since the microbicidal portion of the PL spectrum will be diminished by the substrate itself.

Perhaps the most significant finding of this work is not the measurement of the absolute values of total or UV fluence, as these values will vary between PL treatment units, but rather the large variability in spatial distribution of fluence. For the PL chamber used in this study, the most notable decay of fluence took place in the *y* direction (perpendicular to the direction of the lamp),

due to the departure from the 1 in footprint of the lamp in that direction. Additionally, fluence drops along the x- and z- axes were non-trivial, further emphasizing the importance of substrate position relative to the lamp. It is critical to either stay within the footprint of the lamp when using this PL setup, or to install additional lamps positioned in a manner that can ensure uniform PL exposure and minimize the risk of dead spots.

CONCLUSIONS

This study describes methods for both quantifying the total and UV fluence at a given spatial location per pulse within a PL treatment chamber, and for mapping the fluence distribution both in air and in liquid substrates. The findings are of great use in pre-determining the potential effectiveness of PL treatment for a certain application, as well as furthering understanding of the inherent non-uniformities of the treatment.

Quantifying the fluence per pulse will allow a more meaningful comparison of PL effectiveness, as treatment should be reported in terms of fluence at the substrate surface or within the substrate, rather than merely at the lamp surface. Additionally, as most of the microbicidal effect of PL results from the UV wavelengths, knowing the proportion of total fluence contributed by UV wavelengths will allow an even more accurate comparison of PL effectiveness. The microbial reduction observed can then be related to both total and UV fluence, providing a standardized basis for comparing PL effectiveness.

This study also emphasizes the importance of spatial location of the substrate relative to the lamp in PL treatment. Fluence varies significantly with distance from the lamp, in all directions. Knowing the spatial distribution of fluence within the PL chamber and within different liquids within the PL chamber will help processors determine where to place their substrates relative to the lamp, or to use multiple lamps to maximize PL effectiveness and ensure

homogeneous treatment. This work also opens the possibility of predicting expected microbial inactivation by coupling the spatial fluence distribution within a liquid substrate with the kinetics of microbial inactivation, and will be the subject of a future study. This will help processors evaluate whether or not PL is a viable treatment for a specific substrate, as well as facilitate the design of effective and uniform PL treatments.

ACKNOWLEDGEMENTS

Support for this work was provided by the USDA National Needs Graduate Fellowship Competitive Grant No. 2007-38420-17751 from the National Institute of Food and Agriculture, and the Cornell University Agricultural Experiment Station federal formula funds, Project No. NYC 143400, CSREES/USDA. Any opinions, findings, conclusions, or recommendations expressed in this publication are those of the authors and do not necessarily reflect the view of the U.S. Department of Agriculture.

REFERENCES

Bialka, K. L., Demirci, A. (2008). Efficacy of pulsed UV-light for the decontamination of *Escherichia coli* O157:H7 and Salmonella spp. on raspberries and strawberries. *Journal of Food Science*, 73(5), M201-7.

Blom, H., Björk, G. (2009). Lorentzian spatial intensity distribution in one-photon fluorescence correlation spectroscopy. *Applied Optics*, 48(31), 6050-8.

Chang, C., Liu, H., Peng, C., Fang, H., Tsao, T., Lan, C.(2008). Evaluation of erythemal UV effective irradiance from UV lamp exposure and the application in shield metal arc welding processing. *Health Physics*, 94(4), 318-27.

Davis, C. (1996). Lasers and Electro-Optics: Fundamentals and Engineering. New York, NY: Cambridge University Press.

Di Lazzaro, P., Murra, D., Felici, G., Fu, S. (2004). Spatial distribution of the light emitted by an excimer lamp used for ultraviolet-B photo-therapy: experiment and modeling. *Review of Scientific Instruments*, 75(5), 1332.

Fine, F., Gervais, P. (2004). Efficiency of pulsed UV light for microbial decontamination of food powders. *Journal of Food Protection*, 67(4), 787-92.

Gómez-López, V., Devlieghere, F., Bonduelle, V., Debevere. (2005a). Factors affecting the inactivation of micro-organisms by intense light pulses. *Journal of Applied Microbiology*, 99, 460-470.

Gómez-López, V. M., Devlieghere, F., Bonduelle, V., Debevere, J. (2005b). Intense light pulses decontamination of minimally processed vegetables and their shelf-life. *International Journal of Food Microbiology*, 103(1), 79-89.

Koutchma, T.N., Forney, L.J., Moraru, C.I. *Ultraviolet Light in Food Technology*. Boca Raton. CRC Press: 2009.

Krishnamurthy, K., Demirci, A., Irudayaraj, J. M. (2007). Inactivation of *Staphylococcus aureus* in milk using flow-through pulsed UV-light treatment system. *Journal of Food Science*, 72(7), M233-9.

Li, Y. (1992). Focusing of diode laser beams: a simple mathematical model: Comment. *Applied Optics*, 31(18), 3392.

Moraru, C. I., Uesugi, A. R. (2009). Pulsed-light treatment: principles and applications. In T. N. Koutchma, L. J. Forney, & C. I. Moraru, *Ultraviolet Light in Food Technology* (pp. 235-265). Boca Raton: CRC Press.

Ozer, N. P., Demirci, A. (2006). Inactivation of *Escherichia coli* O157:H7 and *Listeria monocytogenes* inoculated on raw salmon fillets by pulsed UV-light treatment. *International Journal of Food Science and Technology*, 41(4), 354-360.

Sauer, A., Moraru, C. I. (2009). Inactivation of *Escherichia coli* ATCC 25922 and *Escherichia coli* O157:H7 in apple juice and apple cider, using pulsed light treatment. *Journal of Food Protection*, 72(5), 937-944.

Sharma, R., Demirci, A. (2003). Inactivation of *Escherichia coli* O157:H7 on inoculated alfalfa seeds with pulsed ultraviolet light and response surface modeling. *Journal of Food Science*, 68(4), 1448-1453.

Uesugi, A. R., Moraru, C. I. (2009). Reduction of *Listeria* on ready-to-eat sausages after exposure to a combination of pulsed light and nisin. *Journal of Food Protection,* 72(2), 347-53.

Uesugi, A. R., Woodling, S. E., Moraru, C. I. (2007). Inactivation kinetics and factors of variability in the pulsed light treatment of *Listeria innocua* cells. *Journal of Food Protection*, 70(11), 2518-2525.

Woodling, S. E., Moraru, C. I. (2005). Influence of surface topography on the effectiveness of pulsed light treatment for the inactivation of *Listeria innocua* on stainless-steel surfaces. *Journal of Food Science*, 70(7) 345-351.

Woodling, S. E., Moraru, C. I. (2007). Effect of spectral range in surface inactivation of *Listeria innocua* using broad-spectrum pulsed light. *Journal of Food Protection*, 70(4), 909-916.

Chapter 2.4

A Numerical Approach for Predicting Volumetric Inactivation of Food Borne Microorganisms in Liquid Substrates by Pulsed Light Treatment

ABSTRACT

Pulsed light (PL) technology is able to effectively destroy a wide variety of food spoilage and pathogenic microorganisms. However, the effectiveness of PL treatment depends on direct exposure of the target microorganisms to the short, high energy pulses of light. The complex physical and chemical properties of foods affect the way light propagates through a given food substrate, and thus there is a real potential for insufficiently or non-uniformly treated products. The objective of this work was to develop a method for predicting levels and spatial distribution of microbial inactivation in PL treatment of liquid substrates, and to validate the predictions with experimental data. Three liquids with different composition and optical properties (BPB, TSB, apple juice) were inoculated with either *Escherichia coli* ATCC 25922 or *Listeria innocua* FSL C2-008 and treated with PL, in two different geometries. The Weibull model was used to describe the microbial inactivation kinetics for each organism. The kinetic equations were coupled with previously determined equations describing either the total fluence (F_{total}) or UV fluence (F_{UV}) distribution in each of the liquids, for either cylindrical or rectangular prismatic geometries. COMSOL simulation software was used to generate maps of spatial distribution of microbial inactivation and to predict the average volumetric inactivation for each substrate. Overall, the model that used F_{total} provided gross over-estimations for microbial inactivation. Using F_{UV} as the treatment dose yielded reasonably good predictions of expected microbial inactivation, especially for the more opaque and turbid substrates. This approach can help

processors determine which substrates would be suitable for PL treatment, and to design highly effective and uniform PL treatments.

INTRODUCTION

Pulsed light (PL) technology has emerged in recent years as a promising alternative to traditional heat-based methods for killing spoilage and pathogenic microbes in foods and on food contact surfaces. PL treatment consists of exposing microbes to short, high-power pulses of broad range light emitted from a light source such as a Xenon lamp. While the exact mechanism of cellular inactivation has not yet been fully elucidated, it has been shown that the UV portion of the light spectrum is largely responsible for causing cell death (Wuytack *et al.* 2003; Woodling and Moraru 2007).

Since PL is a light-based technology, its effectiveness is directly dependent on the dose of light energy that is experienced by the target microorganisms. As such, the possibility for non-uniform treatment is nontrivial, as there are many factors in food systems that could easily lead to non-uniform exposure of microbial cells to the light. Characteristics inherent to a particular substrate that may lead to non-uniform treatment include substrate homogeneity, topography, and optical penetration depth (Woodling & Moraru, 2005); (Moraru & Uesugi, 2009); (Sauer & Moraru, 2009). There are also spatial factors that must also be considered, with distance from and position relative to the lamp being the most salient factors.

Traditional experiments following a standard procedure for determining the efficacy of PL treatment can only give the average level of microbial inactivation achieved under a given set of conditions. While average values give insight into whether or not PL is a viable option for treating a given substrate, they do not provide any indicator of whether or not the substrate has been uniformly treated. A non-uniformly treated food product is undesirable and potentially

unsafe for consumption. Due to the many variables that ultimately affect the amount of light energy that reaches a specific spatial location, as well as the non-linear inactivation kinetics of PL (Uesugi et al, 2007), it would be very useful to be able to determine the spatial distribution of microbial inactivation in a substrate, which would help in understanding possible non-uniformities of PL treatment. Achieving this through experimentation would be a very complex task, with numerous practical limitations. Therefore, the best approach to solve such a problem is to use the predictive power of numerical simulation.

The use of numerical methods for modeling changes in various parameters to identify potential treatment non-uniformities during food processing is common. Several researchers have used numerical methods to model pressure and temperature changes that occur during hydrostatic high pressure (HHP) processing. Ghani and Farid (2007) used a numerical approach to track the temperature distribution, and pressure and velocity fields during HHP processing of a solid-liquid food mixture. Khurana and Karwe (2008) employed numerical methods to map the temperature distribution within the pressurizing medium during HHP in order to determine areas of non-uniform temperature that could potentially result in a non-uniformly treated final product. Researchers have also employed numerical methods for investigating the distribution of electric field strength and temperature during food processing by pulsed electric field (PEF) technology, which can also result in treatment non-uniformities. Toepfl *et al*. (2007) used numerical simulation to study how the presence of common food constituents, such as fat globules, and microbial cell agglomeration affected the distribution and intensity of electric fields. Lindgren *et al*. (2002) and Fiala *et al*. (2001) investigated the relationships between rate of fluid flow, ohmic heating of the fluid, and electric field intensity to better understand how local temperature changes as a result of the electric field, convection and conduction. Qin *et al*. (1995) developed a finite element method to describe the distribution of the electric field in the treatment chamber,

and used data obtained from their model to design two different treatment chambers that would experience a uniform electric field throughout the treatment region. Information gained from numerical modeling may ultimately allow for better process design to maximize microbial inactivation while minimizing over-processing.

With regard to light-based treatments such as PL and continuous UV, the single most important factor that dictates the effectiveness of the treatment is the dose of energy received by the target microbes. The distribution of light energy may vary throughout a substrate, depending on the optical properties of the substrate and spatial location of the substrate relative to the light source (Hsu and Moraru, 2011). Thus, the potential for non-uniform treatment of the substrate must be addressed before commercial applications of PL are developed. For continuous UV applications, the spatial distribution of energy dose in various substrates such as water and apple cider has been modeled using numerical methods (Unluturk *et al.* 2004; Cabaj *et al.* 1996). Comparatively little work has been done with regard to dose distribution and treatment uniformity for PL applications. Previous work done by Hsu and Moraru (2011) focused on generating maps of the spatial distribution of both fluence and UV fluence within an empty PL chamber and three liquid substrates. In that study it was found that the spatial distribution of fluence varied greatly not only with distance from the lamp, but also spatial location relative to the focal point of the lamp (Hsu and Moraru, 2011). As a result of the non-uniform distribution of fluence, it can be expected that the microbial inactivation achieved throughout the substrate will also be non-uniform. This clearly indicates a need for developing a numerical method to predict the spatial distribution of microbial inactivation rather than merely quantifying a volumetric average inactivation.

The overall objective of this study was to develop a method using a numerical approach for predicting levels and spatial distribution of microbial inactivation after PL treatment of liquid

substrates with known optical properties and geometry. The specific objectives were to: (1) develop kinetic models to characterize PL inactivation of food related microorganisms, *Escherichia coli* ATCC 25922 (as a surrogate for *Escherichia coli* O157:H7) and *Listeria innocua* (as a surrogate for *Listeria monocytogenes*) as a function of treatment dose; (2) predict the spatial distribution of microbial inactivation and the average microbial inactivation in three different fluids and two different geometries; and (3) validate the numerical predictions using experimental data.

MATERIALS AND METHODS

Liquid substrates. Three liquid substrates of different degrees of clarity were used in this work: apple juice (apple cider clarified by cold microfiltration), trypticase soy broth (TSB), and Butterfield's phosphate buffer (BPB). For BPB, TSB, and apple juice, the ºBrix values were 0.5, 3.25, and 11.25°Brix, respectively, and the pH values were 6.8, 7.4, and 4.0, respectively (Hsu and Moraru, 2011). The substrates, including their spectral irradiance profiles, are described in detail in the paper by Hsu and Moraru (2011).

Cultures. *E. coli* (ATCC 25922) and *L. innocua* (FSL C2-008) were used as challenge organisms. *E. coli* (ATCC 25922) was obtained from the frozen culture collection of Dr. Randy Worobo at Cornell University (Geneva, NY), and *L. innocua* (FSL C2-008) was obtained from the frozen culture collection maintained by the Food Microbiology and Safety Laboratory in the Food Science Department at Cornell University (Ithaca, NY). Prior to the experiment, the cultures were streaked onto tryptic soy agar (TSA) plates and incubated for 24 ± 2 h at 37 ± 2°C.

Microbial inactivation experiments by PL. Microbial inactivation data for the two challenge organisms and two different geometries was obtained. The geometries used were a cylindrical geometry and a prismatic geometry. The inactivation data for the cylindrical

geometry, for all three substrates, was taken from the work by Sauer and Moraru (2009). The inactivation data for the prismatic geometry was generated in this study. The methodology for the microbial inactivation experiments is described below.

Liquid substrate preparation. A single isolated colony of the challenge organism was transferred into trypticase soy broth (TSB) and incubated for 20 ± 2 hours at 37 ± 2°C. A 1:10 dilution of the bacterial culture in the working substrate (which was autoclaved before use) was made just before PL treatment, resulting in a population of approximately 10^9 CFU/mL.

Pulsed Light treatment unit. The PL unit used in this study was a bench-top RS-3000C SteriPulse System (Xenon Corporation; Wilmington, MA, USA), which consists of a controller unit, a treatment chamber and a fan. A Xenon flashlamp is mounted in the ceiling of the treatment chamber and is encased in a lamp housing with a quartz face. The lamp is 40.64 cm long with a 2.54 cm footprint and emits short duration, high-energy light pulses in the near IR to UV range (λ = 180 – 1100 nm).

PL fluence measurements. A pyroelectric head (Ophir Optronics, MA) with a Nova II display (Ophir Optronics Inc.; Wilmington, MA) was used to measure the fluence inside the PL chamber and for each substrate, using the methodology described by Hsu and Moraru (2011). Fluence is the dose of total radiant energy that reaches the substrate, and is expressed in J/cm^2.

Pulsed Light treatment. For the microbial inactivation experiments in a prismatic geometry, sterile and transparent Lab-Tek II Chamber Slide 1 well slides (Nagle Nunc International; Naperville, IL) with chamber dimensions of 23.2 mm × 53.3 mm x 11.0 mm were used to hold the liquid cell suspensions during the PL treatment. The bottom of the chamber was made of glass, while the walls were made of polystyrene. Immediately before the treatment 1 mL (thin layer treatment) or 10mL (thick layer treatment) of the inoculated liquid was placed in the chamber of the Lab-Tek II Chamber Slide, resulting in a liquid layer of 1.1 mm or 11 mm,

respectively. The chamber with the inoculated liquid substrate was placed in the PL unit at a distance of 3.2 cm from the surface of the lamp housing, and exposed to PL treatment doses of up to 13.2 J/cm^2 (12 pulses). All experiments were performed in triplicate.

For the inactivation experiments in cylindrical geometry performed by Sauer and Moraru, varying volumes of inoculated liquid were placed in sterile, Pyrex flat-bottomed tubes (25.0 mm x 120.0 mm), resulting in film thicknesses of 2.6, 4.4, 6.6, 8.8 and 17.6 mm (Sauer and Moraru, 2009). The inoculated Pyrex tubes were placed at the base of the PL chamber, at a vertical distance between surface of the lamp housing and base of the flat-bottomed glass tubes of 13.6 cm, and subjected to PL treatment doses of up to 13.2 J/cm^2 (12 pulses). All experiments were performed in triplicate.

Enumeration of survivors. Following the PL treatment, 1 mL of the treated inoculum was transferred into 7 mL of TSB and the glass chamber was rinsed twice with 1 mL of TSB, adding the rinse TSB to the treated inoculum. The resulting liquid (10 mL) was serially diluted in Butterfield's phosphate buffer (BPB), after which 100 μL was spread-plated onto TSA and incubated for 24 ± 2 h at 37 ± 2°C. Survivors were enumerated by standard plate counting (SPC). In some instances, for the treatments performed using the cylindrical geometry (Sauer and Moraru, 2009), plate counts fell below 25 CFU/plate, and therefore estimation of survivors was performed using the most probable number technique (MPN). The MPN methodology is described in detail in the paper by Sauer and Moraru (2009).

Evaluation of PL efficiency. The inoculum (N_0) and survivor counts (N) were expressed in log CFU or log MPN for the liquid substrates. The level of microbial reduction was calculated as log (N/ N_0).

Modeling of microbial inactivation. The non-linear Weibull model was used to describe inactivation kinetics. For microbial inactivation by PL the function takes the form (Uesugi and

Moraru, 2007):

$$\log\left(\frac{N}{N_o}\right) = -\alpha \times F^{\beta} \qquad \text{Eq. 2.8}$$

where: N/N_0 is the ratio of survivors after treatment (N) over the initial number of organisms (N_0), α is the scale parameter, β is the shape factor, which describes the shape of the survivor curve, and F is the treatment intensity or fluence (J/cm^2). The Weibull parameters α and β were obtained by linearizing eq. (1), using Excel (Microsoft Inc., Redmond, WA). As treatment dose, both total fluence (F_{total}) and UV fluence (F_{UV}) were used, and Weibull parameters for both cases were determined.

Predicting the volumetric distribution of microbial inactivation. Fluence equations describing the spatial distribution of light in the PL chamber, described in previous work done by Hsu and Moraru (2011), were coupled with the Weibull inactivation parameters, for all substrates and geometries. COMSOL Multiphysics Modeling and Simulation Software (COMSOL Inc., Burlington, MA) was used to calculate the microbial inactivation for different sized cylindrical geometries, for each of the three liquid substrates. The methodology used for determining the volumetric distribution of microbial inactivation, including the type of mesh and mesh size, will be discussed in detail in this next section.

RESULTS & DISCUSSION

Microbial inactivation kinetics by PL

An example of a microbial inactivation curve for *E. coli* ATCC 25922 is shown in Figure 2.6. For all liquid substrates, tailing was observed at higher treatment levels, and all inactivation curves exhibited a concave upward shape, which is in agreement with previous findings (Uesugi et al., 2007; Sauer and Moraru, 2009). According to previous work by Uesugi *et al.* (2007), the

Weibull model describes well the microbial inactivation achieved by PL; thus, this model was applied to determine volumetric microbial inactivation in all liquid substrates. The Weibull model relates the survivor ratio to treatment intensity and can assume both a linear or non-linear relationship (Eq. 2.8). The survivor curve is concave downward when the shape parameter, β, is greater than 1, concave upward when $\beta < 1$, and linear when $\beta = 1$. If $\beta < 1$, this suggests that cells die rapidly at the beginning of treatment, but as treatment intensifies, the remaining cells exhibit greater resistance to the treatment and do not die off as rapidly. If $\beta > 1$, the cells do not die off as quickly initially, but as treatment intensifies, the cells become increasingly susceptible to the treatment. If $\beta = 1$, then the inactivation curve is linear and follows first order kinetics.

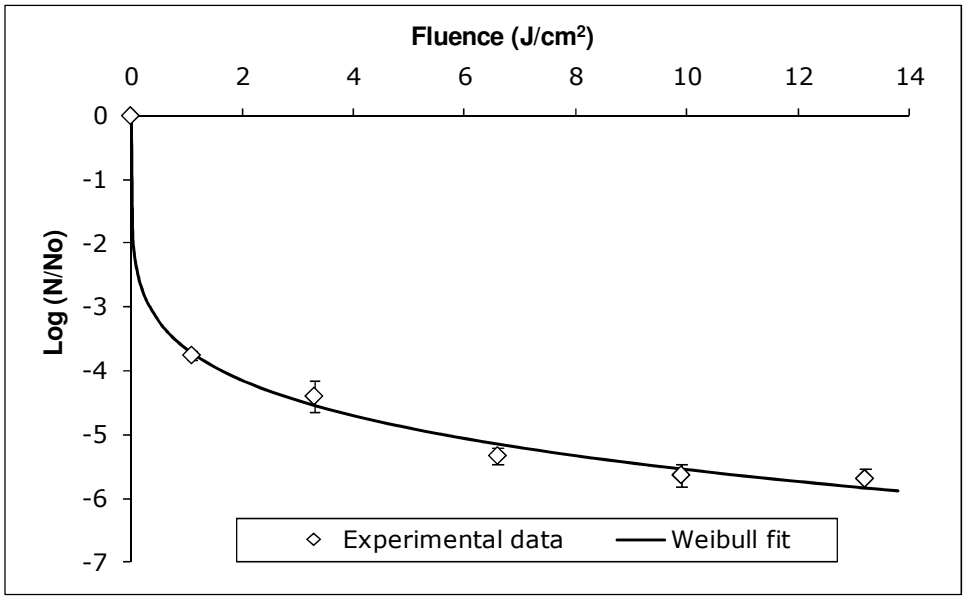

Figure 2.6. Inactivation of *E. coli* ATCC 25922 in BPB by Pulsed Light treatment.

Table 2.2 summarizes the Weibull parameters for BPB, TSB, and apple juice, calculated based on both total fluence (F_{total}) (from Sauer and Moraru, 2009) and UV fluence (F_{UV}) (this work). It can be observed that $\beta<1$ for all substrates, which reflects the upward concavity of the inactivation curves. The scale parameter (α) had smaller values for the cloudy substrates (TSB

and apple juice) than for the clear substrate (BPB). Another observation is that the values for the scale parameter, α, differ when using F_{total} vs. F_{UV} for the same liquid substrate, but the shape parameters remain the same.

Table 2.2. Weibull parameters for PL inactivation of *E. coli* and *L. innocua*, calculated based on inactivation data obtained from the PL treatment of 1 mL of suspension of initial concentration of 10^9 and 10^8 cfu/mL in BPB.

Substrate	Weibull parameters for PL inactivation of *E. coli* ATCC 25922			
	F_{Total}		F_{UV}	
	A	β	A	B
BPB	5.70	0.17	7.53	0.17
TSB	1.66	0.25	2.55	0.25
Apple Juice	1.60	0.20	2.25	0.20
	Weibull parameters for PL inactivation of *L. innocua* FSL C2-008			
BPB	3.47	0.23	5.03	0.23

It is important to note that the Weibull inactivation kinetic parameters determined for *L. innocua* and *E. coli* were based on fluence values determined by measuring the incident light with a pyroelectric head centered beneath the liquid substrate, and on the assumption that fluence value is uniformly distributed throughout the substrate. While the Weibull parameters determined this way do provide a very good description of the experimentally observed *average* microbial inactivation, they cannot provide any information on the uniformity of the treatment, which is a critical detail in practical applications.

Development of a model describing the spatial distribution of microbial inactivation

To gain insight into the spatial distribution of microbial inactivation, the spatial distribution of fluence must be first determined. The fluence does decay away from the light source in all three directions: along the lamp (x), perpendicular to the lamp (y) and vertically

away from the lamp (z), due to the absorption by chemical components and scattering by particulates in the medium the light travels through. In previous work it was shown that for the three liquid substrates evaluated in this study, the spatial distribution of total fluence within a volume of fluid could be defined by the following equation (Hsu and Moraru, 2011):

$$F_{x,y,z} = Ae^{-\left[0.5\left(\frac{x+1.04}{21.48}\right)^2+0.5\left(\frac{y-0.87}{2.11}\right)^2+Cz\right]} \quad \text{Eq. 2.7}$$

where A was determined to be 0.30, 0.29, and 0.28 for BPB, TSB, and apple juice, respectively. When considering only the UV component of fluence (F_{UV}), the values of A were determined to be 0.14, 0.12, and 0.13, respectively. The value of "C" was determined to be 0.06 for BPB, 0.27 for TSB, and 0.24 for apple juice, for both F_{total} and F_{UV} (Hsu and Moraru, 2011).

With both the spatial distribution of fluence and the Weibull inactivation kinetics known, it becomes possible to calculate the average microbial inactivation that can be expected for a cylindrical column of fluid exposed to a given PL dose (fluence). Calculations were made using numerical simulation for two different geometries.

First, a rectangular prism representing the PL chamber was created in COMSOL Multiphysics®, and the coordinate axes defined: the x-axis was parallel to the axis of the lamp, the y-axis was perpendicular to the lamp in the plane of the lamp, and the z-axis was perpendicular to the lamp in the vertical direction. A cylinder was inserted inside the rectangular PL chamber, with the vertical (z) distance from the top of the rectangular prism to the top of the cylinder representative of the vertical distance between the Xenon lamp and the surface of the liquid column. The rectangular prism and cylinder were defined as Geometry 1 and Geometry 2, respectively. A similar procedure was followed for the thin-layer and in-depth PL treatments of the challenge organisms in a rectangular prism geometry, in which case the dimensions of the Lab-Tek II glass chambers were used.

Next, the microbial inactivation kinetics equation, described by Eq. 2.8, was re-written as:

$$N = N_0 \times 10^{-\alpha \times F^{\beta}} \qquad \text{Eq. 2.9}$$

In order to determine the spatial distribution of survivors, fluence (F) in Eq. 2.9 was substituted with the equations describing the spatial distribution of fluence shown in Eq. 2.7, which resulted in the following overall equation:

$$N = N_0 \times 10^{-\alpha \times \left(Ae^{-\left[0.5\left(\frac{x+1.04}{21.48} \right)^2 + 0.5\left(\frac{y-0.87}{2.11} \right)^2 + Cz \right]} \right)^{\beta}} \qquad \text{Eq. 2.10}$$

This equation was used to generate survivor data for each of the geometries, substrates and challenge organisms. The COMSOL software first calculated the number of survivors (N) for each unit volume of the geometry, after which a volumetric average was calculated. The average was obtained by calculating the total number of survivors for the entire volume by integrating Eq. 2.10 over the volume of the geometry, and dividing this total by the volume of the geometry. Two separate calculations were performed: one based on F_{total} and one on F_{UV}, using the values of the model constants A and C mentioned above.

Calculation of PL inactivation in liquid substrates as a function of spatial location

Using the number of survivors N, the logarithm of the survivor ratio, $Log\ (N/N_0)$, was then calculated to determine the level of inactivation. The volumetric inactivation was calculated for *E. coli* and *L. innocua* in both cylindrical and rectangular prismatic columns of BPB, as well as for *E. coli* in cylindrical columns of TSB and apple juice.

When using numerical simulation software to perform volumetric integrations, the

accuracy of the predictions depends on the mesh used to discretize the geometry. To investigate whether the level of mesh refinement significantly affected the microbial inactivation predictions, the mesh was repeatedly refined until the software reached its limit, using a total of four refinement iterations. The default mesh used by COMSOL to carry out the volumetric integration was initially coarse, with 21 tetrahedral elements for the cylindrical geometry and 68 tetrahedral elements in the rectangular prismatic geometry. After four refinements, the cylindrical mesh contained 34,940 tetrahedral elements, while the rectangular prismatic geometry contained 5,434 elements. The finest mesh for each of the two geometries is shown in Figures 2.7 a & b.

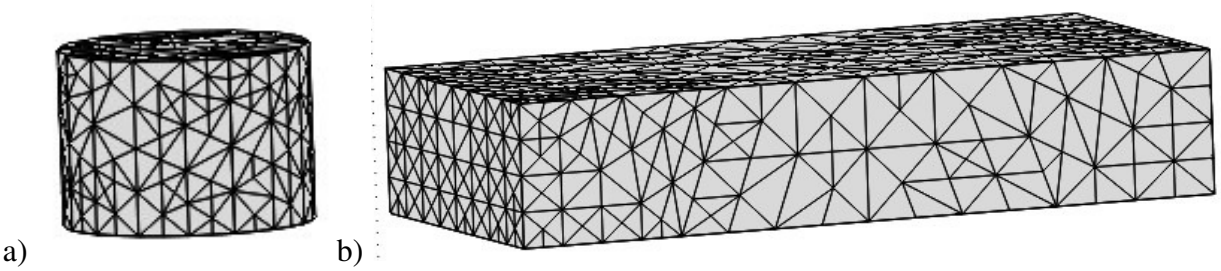

Figure 2.7. Pictorial representation of the mesh used to discretize the (a) cylindrical and (b) rectangular prism geometries. The cylindrical geometry has a radius of 1.25 cm and height of 1.76 cm. The rectangular prism had dimensions of 2.32 x 5.33 x 1.1 cm (length x width x height). The cylindrical mesh contains 34,940 tetrahedral elements, while the rectangular prismatic geometry contains 5,434 elements.

As seen in Table 2.3, which shows the mesh statistics for each level of refinement for BPB, in both cylindrical and rectangular prismatic geometries, the volumetric integrations did not yield *Log* (N/N_0) values that were significantly different upon refining the mesh. Therefore, the default mesh was considered sufficiently accurate for this application, and was used for all the calculations in this study.

Table 2.3. Mesh statistics for BPB in cylindrical and rectangular prismatic geometries for *E. coli* ATCC 25922 after 12 pulses of treatment

Level of refinement	Cylinder		Rectangular prism	
	# of tetrahedral elements	Log (N/N_0)	# of tetrahedral elements	Log (N/N_0)
Default	251	-4.08	68	-5.84
1st refinement	1,032	-4.08	141	-5.84
2nd refinement	3,411	-4.07	593	-5.84
3rd refinement	11,076	-4.07	1,796	-5.84
4th refinement	34,940	-4.07	5,434	-5.84

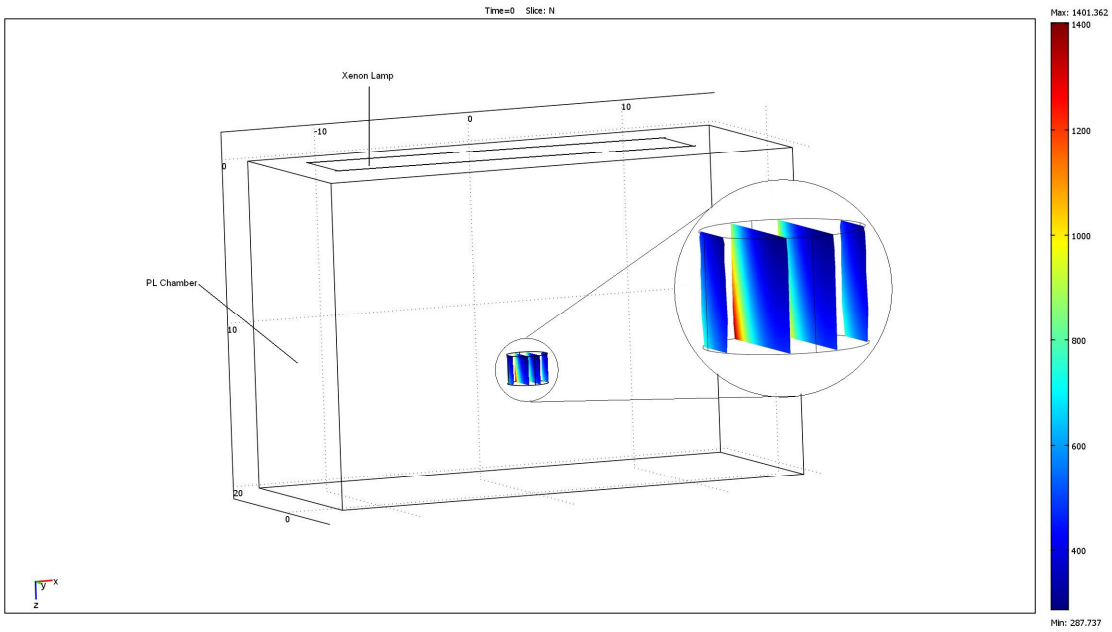

a)

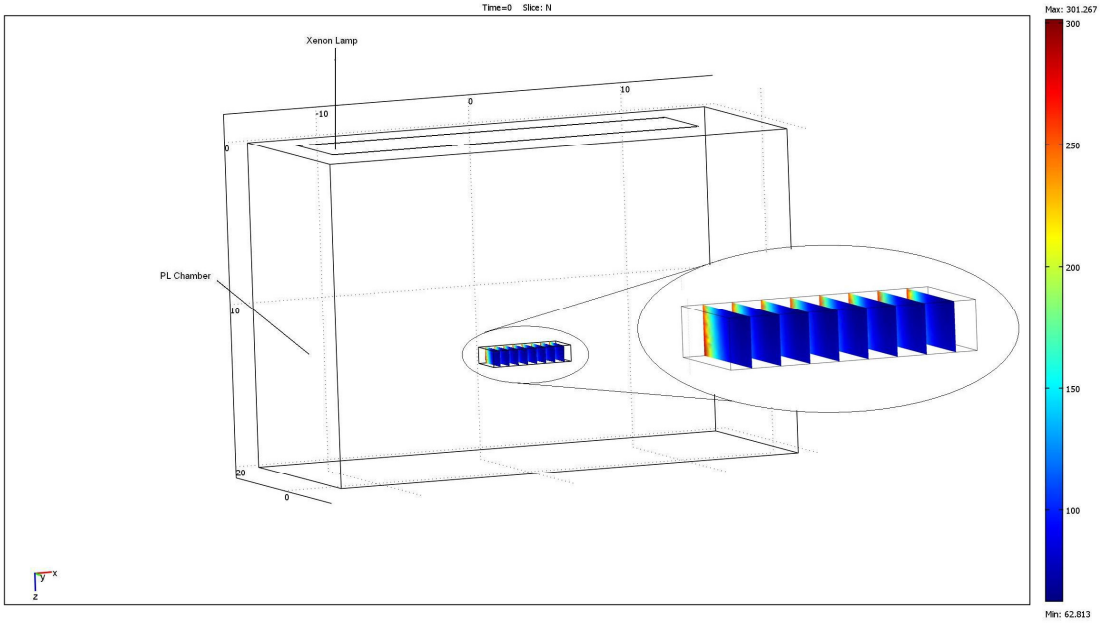

b)

Figure 2.8. Spatial distribution of survivors of for PL treatment of *E.coli* ATCC 25922 in BPB in (a) a cylinder and (b) rectangular prism geometries. Cross-sections are made in the *yz*-plane, and the color gradient represents levels of survivors from low (blue) to high (red).

As expected, the number of surviving cells increases as the vertical distance from the lamp increases, for both geometries. Additionally, along the *x*-, and especially *y*-axes, the levels of inactivation also vary, even when the thickness of the fluid layer stays constant, a direct artifact of the spatial distribution of fluence within the substrate. The lowest levels of survivors (thus the highest levels of inactivation), represented by the deep blue color, occur at the surface of the cylinder and rectangular prism geometry, within the 2.54 cm footprint along the *y*-axis of the lamp. The presence of red, yellow, and green colors along the negative *y*-axis (which corresponds to areas further away from the focal point of the lamp) for each geometry indicate greater numbers of surviving bacterial cells in areas that experience a lower dose of light energy than areas of the geometry closer to the focal point of the lamp. It is interesting to note that the variability in the number of survivors (thus the inactivation drop) is not as striking along the *x*-axis as compared to the *y*-axis. This can clearly be observed for the rectangular prismatic geometry, which is nearly twice as wide along the *x*-axis as the diameter of the cylindrical geometry. These observations further emphasize the importance of not only absolute distance of the target from the lamp, but its spatial location relative to the lamp.

The theoretical microbial inactivation was calculated based on the number of survivors for cylindrical fluid columns both for the clear substrate and for more turbid liquids: tryptic soy broth (TSB) and apple juice, which are representative of possible commercial applications of PL treatment. As expected, overall levels of inactivation were much lower in these chemically complex substrates as compared to BPB. In BPB, more than 6 log reduction was observed after exposure to a cumulative dose of 12.6 J/cm^2 treatment (slightly higher than the maximum dose (12 J/cm^2 allowed by the FDA for commercial applications of PL), as compared to 1-1.5 log reduction in TSB and apple juice. As with BPB, lower inactivation was predicted for thicker

fluid columns than thin-layer columns. Additionally, as predicted in BPB, the survivor levels (thus the microbial inactivation) in TSB and apple juice were not uniform throughout the volume of the cylinder. Along the *x*- and *y*-axes, a notable increase in survivors (drop in inactivation levels) was predicted, corresponding to the decrease in fluence as distance from the lamp increases. Overall, the calculated drop in inactivation through the thicker layers of fluid was larger for TSB and apple juice than for BPB, as light is attenuated more by the former substrates.

Validation of theoretical calculations

The calculated data was validated for the three fluids (BPB, TSB and apple juice) by comparing calculated volumetric inactivation averages with experimentally determined inactivation data. When microbial inactivation was calculated based on F_{total}, values of inactivation were higher than what was observed experimentally, for all three substrates, with the exception of the thinnest layer (2.2 mm) of BPB in a cylinder. The accuracy of the model was significantly improved when F_{UV} was used to predict microbial inactivation, for all three substrates and for all fluid layer thicknesses (Table 2.4). As most of the microbicidal effect of PL is due to wavelengths in the UV range (Woodling and Moraru, 2007), it follows that predictions with F_{UV} instead of F_{total} would be more accurate.

Table 2.4. Evaluation of goodness of models for *E. coli* ATCC 25922 and comparison of the goodness of models based on F_{total} and F_{UV}.

BPB inoculated with *E. coli* ATCC25922						
Column Height, mm	**Inactivation after 12 pulses treatment**			**Inactivation after 39 pulses treatment**		
	Coefficient of variance*	Relative error **		Coefficient of variance*	Relative error **	
		Using F_{total}	Using F_{UV}		Using F_{total}	Using F_{UV}
2.2	19%	1%	27%	11%	*-21%*	4%
4.4	17%	*-9%*	25%	19%	*-6%*	20%
6.6	8%	*-20%*	20%	19%	*-14%*	17%
8.8	5%	*-37%*	12%	8%	*-43%*	*-2%*
17.6	*2%*	*-83%*	*-10%*	7%	*-92%*	*-31%*
Apple Juice inoculated with *E. coli* ATCC25922						
Column Height, mm	**Inactivation after 12 pulses treatment**			**Inactivation after 39 pulses treatment**		
	Coefficient of variance*	Relative error **		Coefficient of variance*	Relative error **	
		Using F_{total}	Using F_{UV}		Using F_{total}	Using F_{UV}
2.2	9%	*-50%*	6%	12%	*-42%*	10%
4.4	9%	*-69%*	19%	1%	*-90%*	2%
6.6	11%	*-73%*	33%	1%	*-111%*	6%
8.8	17%	*-82%*	40%	9%	*-112%*	16%
17.6	7%	*-90%*	65%	9%	*-108%*	40%
TSB inoculated with *E. coli* ATCC25922						
Column Height, mm	**Inactivation after 12 pulses treatment**			**Inactivation after 39 pulses treatment**		
	Coefficient of variance*	Relative error **		Coefficient of variance*	Relative error **	
		Using F_{total}	Using F_{UV}		Using F_{total}	Using F_{UV}
2.2	6%	*-46%*	28%	2%	*-36%*	32%
4.4	2%	*-55%*	45%	8%	*-95%*	23%
6.6	5%	*-62%*	55%	13%	*-114%*	28%
8.8	12%	*-72%*	62%	n.a.	*-104%*	39%
17.6	4%	*-71%*	84%	48%	*-181%*	41%

Note: *Italicized values indicate over-prediction; non-italicized values indicate under-prediction.*

* Coefficient of variance = Standard deviation/experimental value (absolute value)

** Relative error = (Predicted value – Experimental value)/Experimental value

Figure 2.9 compares the experimentally observed inactivation to predicted inactivation, for *E. coli* in all three liquid substrates in a cylindrical geometry, and Figure 2.10 shows the same for *E. coli* and *L. innocua* in BPB in a rectangular geometry. Generally, the calculated inactivation based on F_{UV} gave a good prediction of microbial inactivation, with a tendency towards under-prediction. From a food safety perspective, under-prediction (i.e. predicted inactivation lower than that obtained experimentally), is more favorable than over-prediction, which can give a false sense of safety. Interestingly, the model based on F_{UV} gave more accurate predicted levels of microbial inactivation in the more chemically complex substrates, TSB and apple juice, as compared to the clear phosphate buffer, BPB, especially in thicker columns. Both the F_{total} and F_{UV} calculations over-predicted inactivation for BPB in fluid columns of 8.8 and 17.6 mm thickness. This is most likely due to more accurate fluence values for TSB and apple juice, as these measurements were less affected by secondary reflections, which were experienced mostly in the clear substrate (Hsu and Moraru, 2011). In the cases of TSB and apple juice, the total fluence, as well as the UV fluence, drops greatly as liquid column thickness increases, due to significant absorption by the substrate, which was much more significant than scattering or reflection effects.

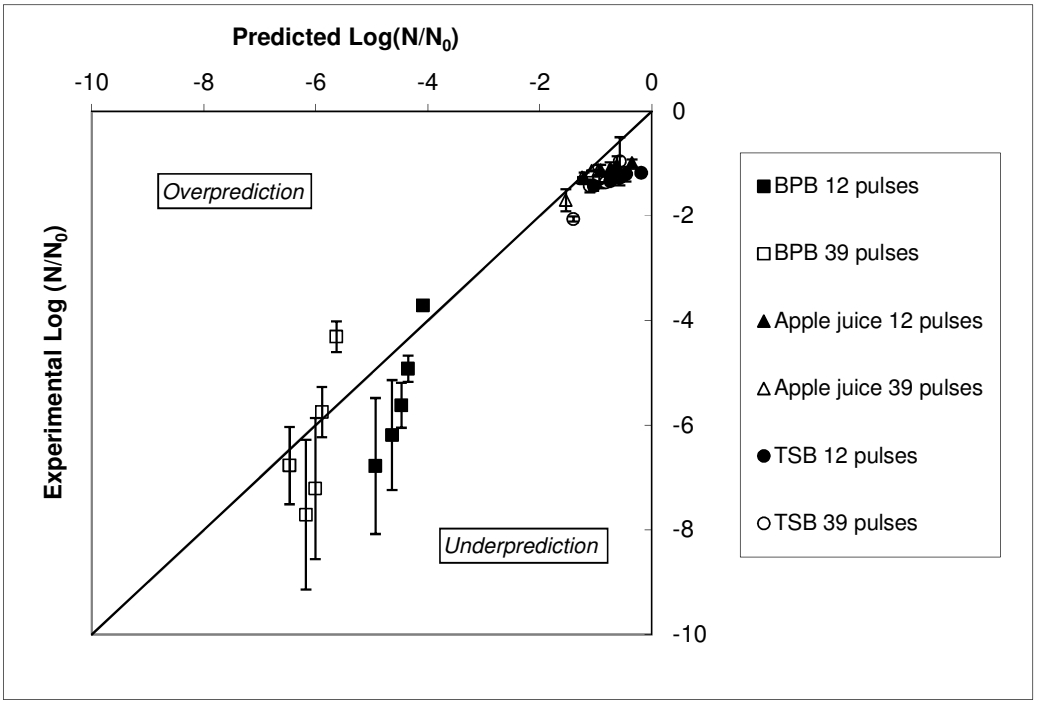

Figure 2.9. Experimental versus predicted survivor ratios for *E. coli* in cylindrical columns of inoculated fluids. Error bars represent one standard deviation of the data.

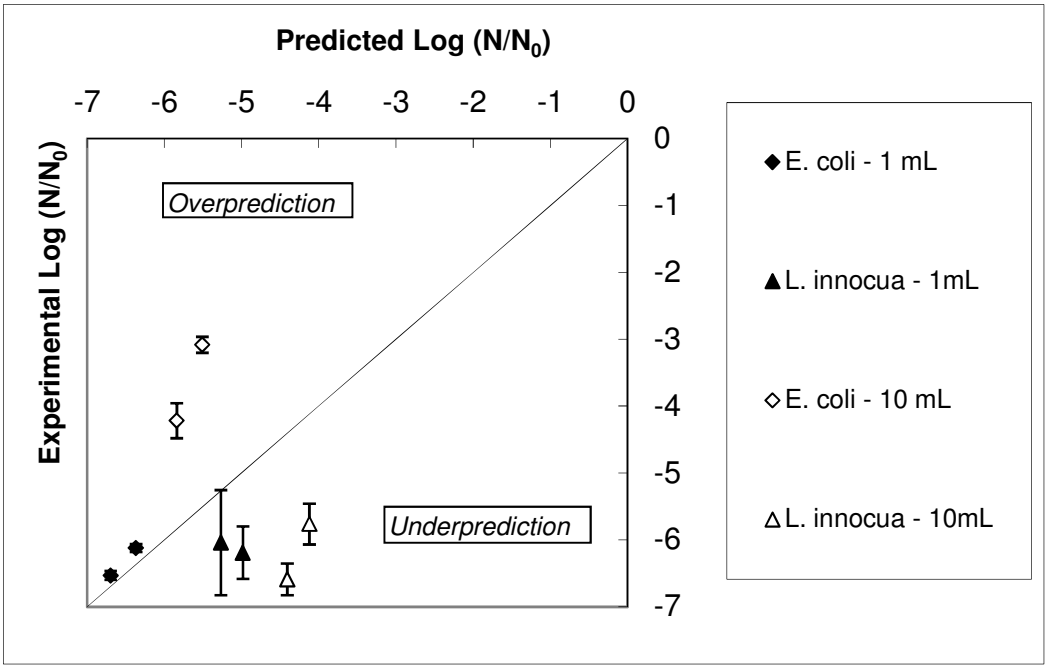

Figure 2.10. Experimental versus predicted survivor ratios for *E. coli* and *L. innocua* in rectangular prismatic geometries of inoculated BPB. Error bars represent one standard deviation of the data.

CONCLUSIONS

This study demonstrates that it is possible to use numerical methods to predict the level and distribution of PL inactivation in both a column and a rectangular prism of fluid, based on the spatial distribution of fluence and inactivation kinetics for the specific microorganism and substrate. The Weibull model based on F_{UV} gave a more accurate prediction of microbial inactivation, compared to that based on F_{total}, with a tendency towards under-prediction. Moreover, the model predicted reasonably well the microbial inactivation in more complex substrates (TSB and apple juice), which suggests that this approach could be useful when designing potential applications of PL in liquid food substrates, such as beverages. Further refinement of the model is theoretically possible, but due to natural variability amongst common

food-borne microorganisms or the composition of the food substrate, such refinement is not necessarily practical. Perhaps the most significant result of this study is the large potential for non-uniform PL treatment of the substrate, when the treatment is performed in static mode. The spatial relationship between the light source and the substrate must carefully be considered to ensure a homogeneously safe final product. Additionally, the use of turbulent treatments can alleviate to a great extent the non-uniformities observed for static treatments, and can also increase the overall effectiveness of PL treatment, as previously demonstrated by Sauer and Moraru (2009).

ACKNOWLEDGEMENTS

This research was supported by the USDA National Needs Competitive Grant no. 2006-04257 from the National Institute of Food and Agriculture and the Cornell University Agricultural Experiment Station federal formula funds, Project No. NYC 143400, CSREES/USDA. The authors also wish to thank Dr. Amit Halder from the Department of Biological and Environmental Engineering at Cornell University for his assistance with using the COMSOL software.

REFERENCES

Cabaj, A, Sommer, R., and Schoenen, D. (1996). Biodosimetry: Model calculations for U.V. water disinfection devices with regard to dose distributions. *Water Research* 30(4): 1003-1009.

Fiala, A., Wouters P., van den Bosch, E., Creyghton, Y. (2001). Coupled electrical-fluid model of pulsed electric field treatment in a model food system. *Innovative Food Science & Emerging Technologies* 2(4):229-238.

Ghani, A, Farid, M. (2007). Numerical simulation of solid-liquid food mixture in a high pressure processing unit using computational fluid dynamics. *Journal of Food Engineering* 80:1031-1042.

Hsu, L., Moraru, C.I. (2011). Quantifying and mapping the spatial distribution of fluence inside a Pulsed Light treatment chamber and various liquid substrates. *Journal of Food Engineering* 103:84–91

Khurana, M., Karwe, M. (2008). Numerical prediction of temperature distribution and measurement of temperature in a high hydrostatic pressure food processor. *Food and Bioprocess Technology* 2 (3): 279-290.

Lindgren, M., Aronsson, K., Galt, S., Ohlsson, T. (2002). Simulation of the temperature increase in pulsed electric field (PEF) continuous flow treatment chambers. *Innovative Food Science & Emerging Technologies* 3(3): 233-245.

Moraru, C. I., Uesugi, A. R. (2009). Pulsed-light treatment: principles and applications. In T. N. Koutchma, L. J. Forney, & C. I. Moraru, *Ultraviolet Light in Food Technology* (pp. 235-265). Boca Raton: CRC Press.

Qin, B., Zhang, Q., Barbosa-Canovas, G.V., Swanson, B.G., Pedrow, P.D. (1995). Pulsed electric field treatment chamber design for liquid food pasteurization using a finite element method. *Transactions of the ASAE* 38(2): 557-565.

Sauer, A., Moraru, C.I. (2009). Inactivation of *Escherichia coli* ATCC 25922 and *Escherichia coli* O157:H7 in apple juice and apple cider, using Pulsed Light treatment. *Journal of Food Protection* 72(5): 937-944.

Toepfl, S, Heinz, V., Knorr, D. (2007). High intensity pulsed electric fields applied for food preservation. *Chemical Engineering and Processing* 46: 537–546.

Uesugi, A.R., Woodling, S. E., Moraru, C.I. (2007). Inactivation kinetics and factors of variability in the Pulsed Light treatment of *Listeria innocua* cells. *Journal of Food Protection* 70(11): 2518-2525.

Unluturk, S., Arastoopour, H., Koutchma, T. (2004). Modeling of UV dose distribution in a thin-film UV reactor for processing of apple cider. *Journal of Food Engineering* 65: 125-136.

Woodling, S E, and C I Moraru. (2005). Influence of surface topography on the effectiveness of pulsed light treatment for the inactivation of *Listeria innocua* on stainless-steel surfaces. *Journal of Food Science* 70:M345-M351.

Woodling, S.E., Moraru, C.I. (2007). Effect of spectral range in surface inactivation of *Listeria innocua* using broad-spectrum pulsed light. *Journal of Food Protection* 70: 909-916.

Wuytack, E., Doung Thi Phuong, L., Aertsen, A., Reyns, K.M.F., Marquenie, D., De Ketelaere, B., Masschalck, B., Van Opstal, I., Diels, A.M.J., Michiels, C.W. (2003). Comparison of sublethal injury induced in *Salmonella enterica* serovar Typhimurium by heat and by different nonthermal treatments. *Journal of Food Protection* 66(1): 31-7.

CHAPTER 3

CONTROLLING BACTERIAL ATTACHMENT BY NANOENGINEERING SUBSTRATUM SURFACE TOPOGRAPHY

Chapter 3.1

Effect of surface topography on bacterial attachment

While the use of non-thermal treatments for microbial inactivation might be a viable solution for specific foods or food-related products, a more comprehensive approach to improving food safety includes reducing or preventing the presence of pathogenic bacteria food processing environments. Adopting measures to prevent bacteria from persisting in food processing environments could greatly improve the overall safety and quality of foods, particularly minimally processed foods and ready-to-eat (RTE) foods, by reducing the risk of cross-contamination. The attachment of unwanted bacteria to various surfaces often has adverse consequences. In food processing facilities, the presence of spoilage or pathogenic microorganisms opens the possibility of transfer from food contact surfaces and processing equipment to the foods themselves. Consequences of such transfer events range from dramatic losses of food products due to more rapid spoilage, to financial losses due to recalls and product loss, and to mild to severe illness resulting from consumption of contaminated foods.

While planktonic cells can cause problems in the food industry, they usually can be effectively removed by physical means and/or killed by chemical sanitizers. Unfortunately, under favorable circumstances, nearly all bacteria can potentially form biofilms, which are notoriously difficult to remove. Many potentially deadly food pathogens, including *Escherichia*

coli O157:H7*, Listeria monocytogenes, Bacillus cereus, Salmonella typhimurium,* and *Campylobacter jejuni*, are known to form biofilms. Moreover, biofilms formed by these microorganisms may aid in trapping other harmful microbes that do not typically form biofilms, thereby allowing these species to survive and proliferate when they otherwise might not.

A biofilm is essentially a community of microbial cells, which includes both viable and non-viable cells, irreversibly associated with a surface and enclosed in a polymeric matrix of predominantly polysaccharide material (Carpentier & Cerf, 1993; Donlan, 2002). Populations of microorganisms in a biofilm may be of a single species, but often include multiple bacterial species. The cells are embedded in a complex matrix consisting of extracellular polymeric substances such as polysaccharides, proteins, phospholipids, teichoic acids and nucleic acids, and water. This complex matrix offers protection to the cells by preventing harmful chemicals from reaching the cells, concentrating nutrients from the environment, and preventing dehydration.

Biofilm formation consists of the following events: initial reversible attachment by the bacterial cell to a surface; production of EPS and/or specific adhesins that lead to irreversible attachment; development of early biofilm architecture; and biofilm maturation. The mature biofilm consists of complex pedestal-like structures that contain water channels and pores that allow for nutrient harvesting and waste exchange and ensure adequate hydration. Cells that reside in biofilms are known to be physiologically and metabolically different from their planktonic counterparts. The last step is the eventual release of some cells into the environment and their return to the planktonic state (Van Houdt & Michiels, 2005).

As biofilms can persist in spite of harsh chemicals and sanitizers such as trisodium phosphates, chlorine, ozone, hydrogen peroxide, peracetic acid, and quaternary ammonium compounds (Frank & Koffi, 1990; Robbins et al., 2005) it is clear that sanitation and surface disinfection by chemical means is not sufficient. One approach to combating this problem is to

prevent bacterial attachment altogether. Thus, understanding the effects of material surface properties on bacterial adhesion might be an effective approach to ultimately enabling the design of materials that can resist or promote bacterial attachment.

While the mechanisms of biofilm formation are complex and are influenced by many factors, including nutrient availability, the specific microbial species that are present and their interactions, and fluid dynamics, the most critical step that must occur before a biofilm can form is the ***irreversible attachment*** of the cell to the substratum surface. There are also many factors that influence whether or not a bacterium will be able to irreversibly attach to a surface. These include contact time and physicochemical interactions between the bacterial cell and the substratum surface, which are dictated by the surface characteristics of the cell and substratum.

Contact time. The initial reversible attachment of a bacterium to a surface may happen randomly, but irreversible attachment requires sufficient contact time between the cell and the substratum surface. Generally, the contact time required is short, ranging from seconds to minutes (Collignon and Korsten, 2010; Nguyen et al., 2010).

Bacterial cell surface. The bacterial cell surface itself is complex and constantly changing to adapt to environmental conditions. Generally, bacteria have a net negative surface charge. The surface structures that protrude from the cell membrane, including lipopolysaccharides, proteins, and lipoteichoic acids, contribute to the charge and hydrophobicity of the cell. Additionally, projections, including flagella and fimbriae/pili, have been implicated in helping to mediate adhesion to a surface, though there are conflicting reports about the exact roles of these structures. For example, several groups have found that many strains of *E. coli* require Type 1 fimbriae (rod-shaped appendages that are 7 nm wide and 1 μm long) to mediate stable attachment to cell surfaces (Beloin et al., 2004; Pratt & Kolter, 1998; Ren et al., 2004). Another filamentous projection prevalent in *E. coli* and other bacteria that may play a role in

mediating attachment and subsequent biofilm formation is curli. Ryu *et al*. found that curli does not appear to affect attachment, but does enhance biofilm formation on stainless steel (Ryu et al., 2004). In contrast, for certain Shiga toxin producing *E. coli* (STEC), adhesion to abiotic stainless steel surfaces was enhanced when *curli* was expressed (Cookson et al., 2002; Pawar et al., 2005). These differences are most likely the result of strain-specific behavior, environmental factors, and other mechanistic events that have not been investigated. Though there are no concrete relationships between cell surface appendages and bacterial adhesion, one hypothesis is that the presence of certain cell surface projections may help overcome the electrostatic repulsive forces and allow attachment of negatively-charged bacteria to negatively charged surfaces (Busscher & Weerkamp, 1987).

Substratum surface topography. Substratum surface properties have a strong influence on bacterial adhesion, with chemical composition, surface charge, hydrophobicity, topography, surface conditioning being prominent factors (Bryers, 2000; Li & Logan, 2004; Mitik-Dineva et al., 2008). Bacterial adhesion occurs when surface forces, including polar interactions and van der Waals forces, overcome the repulsive electrostatic forces and hold the cell close to the substratum surface. Due to the multiplicity of factors involved, clear trends regarding bacterial adhesion and any single surface property have not been established.

To date, the majority of studies attempting to elucidate the effects that substratum surface topography have on bacterial adhesion have focused on topographical features that are approximately the size of the target microorganism or larger (micrometric scale). With recent advancements in nanofabrication technologies and the development of atomic force microscopy, it is now possible to both fabricate materials with deliberate nanoscale features. Several studies suggest that bacteria also show different responses to nanoscale topographical details as compared to micrometric scale topography, in terms of quantity of attached cells, orientation

relative to the substratum surface details, and cellular morphology. Hochbaum and Aizenberg found that *P. aeruginosa* cells aligned themselves horizontally in trenches when the vertical posts were spaced far enough apart to accommodate the cells. However, cells aligned themselves parallel to the vertical posts when the inter-post spacing was smaller than the diameter of the cell (Hochbaum and Aizenberg, 2010). Using atomic force microscopy (AFM), Diaz *et al.* found that *P. fluorescens* aligned themselves very specifically to the nanoscale patterns (channels 90 nm deep and 900 nm wide) in a gold surface, positioning themselves in trenches and crevices (Díaz et al., 2007). Park *et al*. found that *P. fluorescens* and *P. putida* exhibited greater adhesion to titania with nanophase compared to conventional topography (Park et al., 2008), though they did not notice any differences in spatial distribution of adhered bacteria between the surfaces.

Although all the studies to date have suggested that bacteria *do* respond differently to nanoscale topographical features as compared to micro-scale features, the contrasting findings regarding the specific effect of nanoscale topographical features on bacterial attachment indicate that bacterial adhesion at the nanoscale is a very complex process. Elucidating the mechanisms behind this complex phenomenon would significantly advance our understanding of how bacteria respond to nanoscale surface topography, which would enable the design and manufacture of materials that can effectively control bacterial attachment.

Chapter 3.2

Research Objective

It is generally accepted that substratum topography, both at the micro- and at the nanoscale, is a significant factor that affects bacterial attachment. Recent studies attempting to understand the factors that affect bacterial attachment and long-term adhesion to solid surfaces with nanosclae topography have yielded sometimes conflicting findings.

Thus, the main objective of this work was to systematically evaluate the influence of nanoscale surface topography on the attachment of food-related microorganisms in order to elucidate the rules of bacterial attachment.

Based on a good understanding of the rules governing attachment behavior, surfaces can be deliberately engineered to either promote or hinder bacterial attachment, which could have significant applications both in food processing environments as well as in biomedical applications.

Chapter 3.3

The Effect of Nanoscale Topography on the Adhesion of Food-Related Bacteria to Solid Surfaces

ABSTRACT

Controlling bacterial attachment to material surfaces is a very important issue for many fields, including the biomedical, dental, environmental, and =food processing fields. Recent work suggests that of the many factors that play a role in the attachment process, surface topography at the submicrometric and nanometric scales have a significant influence on bacterial attachment. In this study, the attachment behavior of food-related bacteria including *Escherichia coli, Listeria, and Pseudomonas fluorescens*, to nanoengineered silica and nanoporous alumina surfaces was investigated. Silica surfaces with specifically engineered topographical patterns, and commercially available nanoporous alumina membranes were characterized in terms of surface roughness and degree of hydrophobicity. The effect of nanoscale surface topography on bacterial attachment was analyzed both qualitatively and quantitatively. Fluorescence microscopy with LIVE/DEAD dyes and scanning electron microscopy were used to visualize cells that had attached to both types of surfaces after 30 minutes, 24 hours, and 96 hours. The orientation of attached cells relative to the engineered topographical silica patterns suggested a preferential arrangement that maximized the contact area between cell and surface. Consistent quantitative trends were less obvious, but statistically significant differences in the numbers of attached cells were observed at certain time points. Most strikingly, bacterial cells exhibited different morphology when attached to different surfaces, suggesting that bacteria utilize different mechanisms of attachment in response to surface topography. Altogether, the results of

this work indicate that substrate nanotopography is an important factor in the bacterial attachment process and should be considered in the design of microbial repellant food contact materials.

INTRODUCTION

In the United States, foodborne pathogens have been estimated to cause 48 million illnesses, 128,000 hospitalizations, and about 3,000 deaths each year (Scallan et al., 2011). Many foodborne illness cases can be traced back to consumption of foods that have been contaminated with pathogenic bacteria. Oftentimes, this contamination occurs in the food processing and manufacturing facilities. If pathogenic and spoilage microorganisms are present on food contact surfaces, the risk for cross contamination into the foodstuffs is significant. Regular disinfection practices help eliminate these bacteria, but chemical cleaners cannot completely remove adherent bacteria. Moreover, under the right circumstances, adherent bacteria may form biofilms, which are notoriously difficult to remove. Even potent sanitizers including quaternary, ammonium compound, iodine, anionic sanitizers, and chlorine cannot completely remove bacteria that have formed biofilms (Chmielewski and Frank, 2003). Persisting bacteria in food processing facilities increases the chance for transfer onto foods and consequently, the risk for transmitting foodborne illnesses.

Among the many factors affecting bacterial attachment and subsequent biofilm formation, the topography and physicochemical properties of the substrate itself play a large role in mediating attachment. For instance, surface roughness is believed to greatly affect bacterial adhesion. Surfaces with R_a (arithmetic mean roughness) values ≤ 0.8 µm are typically considered "hygienic" or easy to clean, whereas those with $R_a > 0.8$ µm are more difficult to clean and more susceptible to bacterial deposition (Flint et al., 2000). It is generally accepted that bacteria are

more able to attach to crevices and pits where they are protected from unfavorable environmental disturbances (Mitik-Dineva et al., 2008). Scheuerman *et al*. proposed that bacteria attach to rougher surfaces for three reasons: higher surface area for attachment; protection from shear forces; and local chemical changes in the surface that favor attractive physicochemical interactions (Scheuerman et al., 1998). Additionally, surface irregularities make cleaning more difficult (Verran et al., 2001). Boyd *et al.* found a strong correlation between attachment and surface topography, with stronger adhesion of *S. aureus* occurring on rougher stainless steel surfaces compared to smooth surfaces. Moreover, the stainless steel surfaces with topographical features that were on the same scale as the *S. aureus* cells themselves (1 μm) appeared to promote the strongest bacterial attachment, most likely due to maximal cell-substratum contact area (Boyd et al., 2002). Whitehead *et al*. also observed similar patterns with bacterial species of different sizes (Whitehead et al., 2005). Nonetheless, bacteria have been found to colonize quite well even very smooth surfaces, such as electropolished stainless steel (Sarah E Woodling & Moraru, 2005). The conclusion that can be drawn from these findings is that surface roughness alone is not a sufficient parameter for predicting bacterial attachment behavior.

The quest for a better understanding of the role surface topography plays on bacterial attachment has led many researchers to investigate the cellular response to nanoscale topography. Probing the cellular response to nanomaterials has been the subject of several studies in recent years, though they mostly focus on mammalian cellular responses to materials used in surgical and dental materials (Dalby et al., 2003; Balasundaram & Webster, 2006; Popat et al., 2006). A few studies have suggested that bacteria show different responses to nanoscale topographical details, although no universal rules of attachment have yet been determined. Using atomic force microscopy (AFM), Diaz *et al.* found that *P. fluorescens* aligned themselves very specifically to the nanoscale patterns (channels 90 nm deep and 900 nm wide) in a gold surface,

positioning themselves in trenches and crevices (Díaz et al., 2007). Additionally, the individual bacterial cells appeared to be shorter compared to those adhered to smooth surfaces and produced less EPS. Park *et al*. found that *P. fluorescens* and *P. putida* exhibited greater adhesion to titania with nanophase compared to conventional topography (Park et al., 2008), though they did not notice any differences in spatial distribution of adhered bacteria between the surfaces. Mitik-Dineva *et al*. assessed the attachment behaviors of *E. coli* K12, *P. aeruginosa* ATCC 9027, and *S. aureus* CIP 68.5 on glass with nanotopographical features etched onto the surface and found that *E. coli* and *P. aeruginosa* exhibited larger cell size while attached to the modified glass surfaces relative to the control surfaces (Mitik-Dineva et al., 2009) - in contrast to what Diaz et al. found (2007), and deposited substantial amounts of extracellular polymeric substances (EPS) onto the modified surfaces.

These apparently conflicting findings are probably the result of many factors, including using different analytical tools and bacterial strains used in the different studies, but also of the fact that bacterial adhesion is a very complex process. Nonetheless, all the studies that have been done have suggested that bacteria do in fact respond differently to nanoscale topographical features compared to conventional topographies. If nanoscale surface topographies could be designed in ways that would reduce or hinder bacterial attachment, this would be very useful in improving the hygienic quality of food processing surfaces and reducing the incidence of foodborne illness. This study probed the attachment behavior of food-related bacteria to surfaces constructed out of silica and alumina. Specifically, the relationship between the size and shape of the bacterium relative to the size and shape of the nanoscale surface details was examined.

MATERIALS AND METHODS

Bacterial strains

Bacterial strains were selected after screening a two nonpathogenic *Escherichia coli* strains, four *Pseudomonas fluorescens* strains, and seven pathogenic *E. coli* O157:H7 strains for biofilm formation using a slightly modified rapid crystal violet assay from the method of Cookson *et al*. (2002). A single colony of each bacterial strain was inoculated into 2 mL TSB and incubated overnight at 30 and 37°C for *P. fluorescens* and *E. coli* strains, respectively, with shaking at 225 rpm. A 10 µL loopful of culture was inoculated into fresh tubes containing 2 mL TSB and grown statically for 48 hours at 30 or 37°C for *P. fluorescens* and *E. coli* strains respectively. After 48 hours, spent culture was removed from each test tube. Test tubes were rinsed three times with 3 mL sterile deionized water, inverted, and allowed to dry at 65°C for 30 minutes. 3 mL of a 0.2% crystal violet solution was aliquoted into each test tube, incubated for 30 minutes are room temperature, and then removed. Test tubes were rinsed three times with 5 mL sterile deionized water and allowed to dry at room temperature overnight. 3 mL of 95% ethanol was aliquoted into each test tube to elute the crystal violet. Absorbance readings were taken at 570 and 595 nm using a SpectraMax Plus 384 spectrophotometer (Molecular Devices, Sunnyvale, CA). The results of the crystal violet assay led to the selection of *E. coli* ATCC 25922 and *P. fluorescens* as the nonpathogenic strains to use, and *E. coli* O157H7 as the pathogenic strain (data not shown). A nonpathogenic strain of *Listeria, Listeria innocua* FSL C2-008, was also analyzed in this study. The nonpathogenic strains of *E. coli* and *L. innocua* were obtained from the Food Safety Laboratory at Cornell University (Ithaca, NY). The pathogenic *E. coli* strains, as well as the *P. fluorescens* strains were obtained from the collection of Dr. Randy Worobo (Cornell University, Geneva, NY).

Electrophoretic mobility of bacterial cells

The electrophoretic mobility of bacterial cells was determined by dynamic light scattering using a Malvern Zetasizer Nano-ZS (Malvern Instruments Ltd, Worcestershire, UK). Briefly, a 1:10 dilution of stationary phase culture was made in TSB and gently vortexed to ensure thorough mixing. A one-milliliter sample was aliquoted into the cuvette and inserted into the chamber. Measurements were taken in triplicate, and each replicate consisted of at least 15 measurements.

Substrates

Chemically identical but topographically distinct silica dice and alumina membranes were used as substrates. For the silica substrates, commercially available silicon wafers were purchased from Silicon Quest International, Inc. (San Jose, CA). Three distinct nano- and microscale patterns of pores were created in 200 nm thick thermally grown silicon dioxide in the Cornell NanoScale Science and Technology Facility (Ithaca, NY). The features ranged in size from 500-1500 nm and were defined by deep ultraviolet (DUV) lithography using an ASML PAS5500/300C DUV Stepper (ASML, Veldhoven, Netherlands). Subsequent dry etching was used to realize pores with a depth of 25-30 nm. Pore depth was confirmed using a Veeco 6M profilometer (Veeco, Plainview, NY) and pore size and shape were verified by scanning electron microscopy (SEM) using a Zeiss LEO 1550 FE-SEM (Zeiss, Oberkochen, Germany) located in the Cornell Center for Materials Research. Alumina membranes with pores of 20 or 200 nm were purchased from Whatman (GE Healthcare, United Kingdom), and nanosmooth alumina substrates were purchased from Alfa Aesar (Ward Hill, MA).

Contact angle measurements

Contact angle measurements were performed using a Rame-Hart 500 goniometer (Rame-Hart, Inc., Succasunna, NJ) using the sessile drop method. Briefly, 15 μL droplets of water were

allowed to contact the surface of each substrate, and advancing and receding angles were measured. Reported values are an average of advancing and receding angles. All measurements were performed in triplicate.

Surface roughness

Surface roughness characterization of the alumina and silica substrates was performed by atomic force microscopy (AFM) using Veeco DI-3100 (Veeco, Plainview, NY) and PicoPlus microscopes (Molecular Imaging, Tempe, AZ), respectively. The average roughness (R_a), root-mean-square roughness (R_{rms}) and ten-point height (R_z) were extracted from the AFM images by using free source software, Gwyddion.

Substrate preparation

Alumina membranes were rinsed with 100% ethanol and air-dried in a laminar flow hood prior to use. Nanosmooth alumina substrates and silica surfaces were rinsed with 100% ethanol and autoclaved in sterilizing pouches (Thermofisher Scientific, Pittsburgh, PA) for 15 minutes at 121°C prior to use. Surfaces with nanotopographies were not reused, but the nanosmooth alumina substrates were cleaned and reused. Immediately after visualization of attached cells by fluorescence microscopy was completed, the substrates were sonicated for 30 minutes in a heated solution of Alconox and water. After rinsing, the substrates were again sonicated in 95% ethanol for 30 minutes. Substrates were then rinsed, air-dried, and autoclaved prior to re-use. Surfaces that were reused were periodically visualized using SEM to confirm that surface details were not altered and that the cleaning regimen was able to remove all organic matter.

Bacterial cell culture preparation

A single colony of each bacterial strain was streaked out onto Tryptic Soy Agar (TSA) plates and incubated at the appropriate temperature overnight. The following day, a single colony was inoculated into test tubes containing Tryptic Soy Broth (TSB) and grown overnight at 30˚C

or 37˚C, as appropriate, with shaking at 225 rpm. A loopful of culture was transferred into a fresh tube of TSB and incubated with shaking until stationary phase was reached (12-18 hours). The stationary phase culture contained approximately 10^8 cfu/mL.

Attachment and biofilm studies

For the experiments with alumina substrates, one of each type of substrate (porous 20 nm and 200 nm membranes, and nanomooth substrate) were placed into a 60 x 15 mm Petri dish (VWR) containing 5 mL of culture. For the silica substrates, a single dice containing the three designed substrates and the nanosmooth control was inserted directly into a test tube containing stationary phase bacterial cells. All substrates were incubated for 30 minutes or 24 hours for bacterial attachment analysis or 96 hours for observation of biofilm development. Experiments were conducted in duplicate.

Fluorescence microscopy

A wide-field fluorescence Olympus BX-51 microscope (Olympus, Center Valley, PA) equipped with a Roper CoolSnap HX CCD camera (Roper Scientific, Ottobrunn, Germany) was used for epifluorescent imaging of cells stained with the LIVE/DEAD dyes (Molecular Probes, Invitrogen). Substrates with attached bacteria were removed from the cell culture with tweezers and gently rinsed three times with sterile de-ionized water to remove any loosely adherent cells and excess media and placed in new Petri dishes. A solution containing equal parts SYTO 9 and propidium iodide dyes were mixed with sterile de-ionized water and aliquoted into the Petri dishes according to the manufacturer's protocol. Substrates were incubated with the fluorescent dyes in the dark for at least 15 minutes prior to visualization. Each substrate was visualized under a 100x oil immersion lens, and ten fields of view were randomly chosen for analysis. Images were processed using Fireworks (Adobe) and cell counts were performed using ImageJ (NIH).

Scanning electron microscopy

Bare substrates were visualized directly with a Zeiss LEO 1550 FE-SEM (Zeiss, Oberkochen, Germany). Substrates exposed to bacterial cells were immersed in nitrogen slush for 10 seconds, freeze-dried using a Labconco FreeZone Freeze Dryer (Labconco Corp., Kansas City, MO) for 24 hours, and then mounted onto stubs. Carbon was evaporated onto the freeze-dried surfaces prior to visualization.

Statistical analysis

Statistical analysis was performed using JMP 9 (SAS, Cary, NC). The significant differences for the number of adhered cells to the various surfaces compared to control surfaces were tested using multivariate analysis of variance (MANOVA), with surface topography as a fixed variable and the effect of replicate as a random variable. A similar procedure was used for analyzing differences in cell morphology. A p-value of < 0.05 was considered significantly different.

Quantification of numbers of appendages per cell

Images obtained by scanning electron microscopy were visually analyzed to determine the number of appendages that were visible on attached cells, when possible. The number of appendages was categorized into the following groups: 0 – 5, 6 – 10, 11 – 15, > 15, and >> 15. Cells categorized as > 15 had approximately 20+ appendages, whereas cells categorized as >> 15 had too many to count.

RESULTS

Bacterial electrophoretic mobility

The electrophoretic mobility of the bacterial strains used in this study was used as an indicator of the electrical charge of the cell surface. The electrophoretic mobility of *E. coli* ATCC 25922, *L. innocua,* and *P. fluorescens 1150* cells was determined to be -0.87 ± 0.11, -

1.37 ± 0.06 and -0.24 ± 0.02 $\mu s^{-1}/(V/cm)$, respectively. Due to the negative surface charge of the bacteria, the substrate surfaces were deliberately constructed using negatively charged materials, in order to maximize electrostatic repulsion. Alumina and silica, which are both negatively charged, were chosen as the materials from which the substrates were designed. Moreover, alumina has Generally Recognized As Safe (GRAS) status and thus can be considered an acceptable material for food contact surfaces.

Substrate properties

SEM micrographs of bare silica and alumina substrates, as well as those same substrates with attached cells, are shown in Figures 1 and 2, respectively. The dimensions of the topographical details for silica were designed to be similar to the size and shape of the bacterial cells. Four distinct topographies were designed on the silica substrates: circular wells with a diameter of approximately 500 nm and interwell spacing of 200 nm (Figure 1a); narrow rounded rectangular wells with dimensions of 1.5 x 1 µm and interwell spacing of 2 µm (Figure 1b); wide rounded rectangular wells with dimensions of 2 x 1 µm and intewell spacing of 500 nm (Figure 1c); and a nanosmooth surface (Figure 1d) used as a control. All the wells were approximately 27 – 32 nm deep. Alumina substrates had pores of 20 and 200 nm (Figure 2), which were chosen because they were much smaller than the size of the cell, thereby minimizing effective contact area between bacterium and surface.

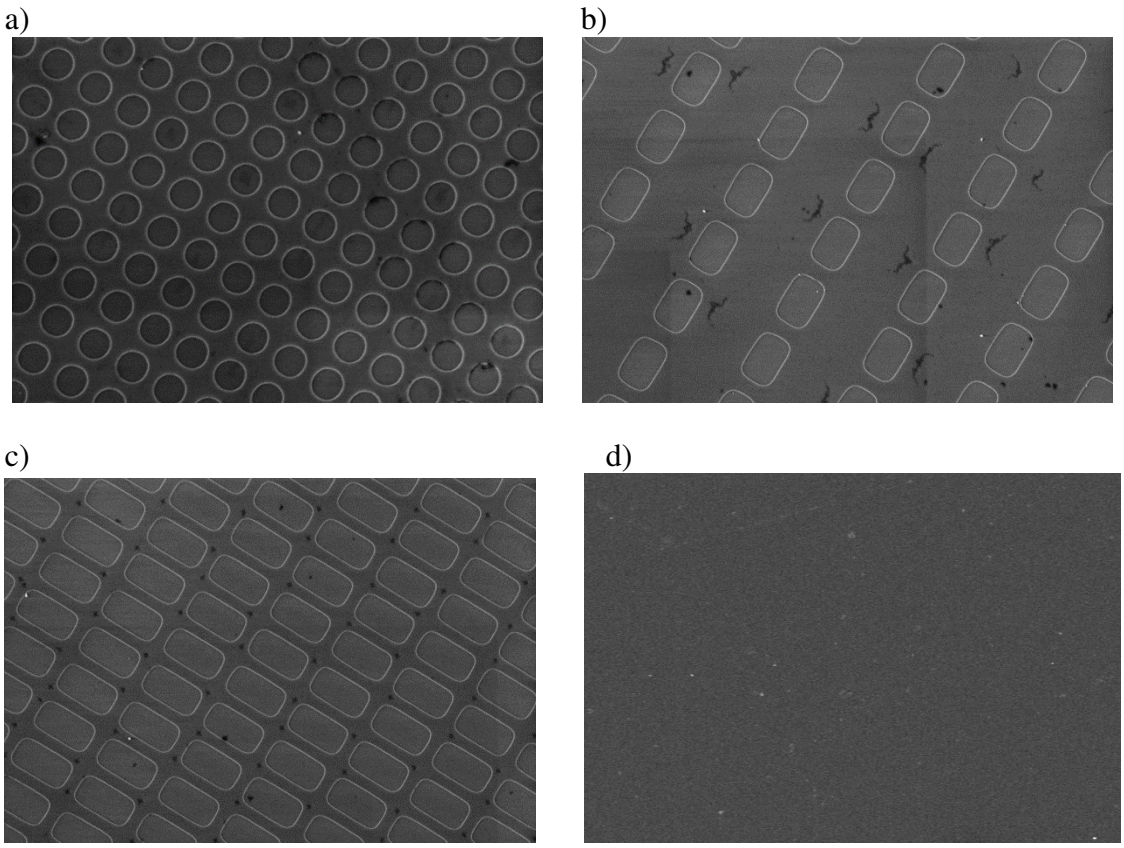

Figure 3.1. Scanning electron micrographs of nanoengineered silica substrates: a) circular wells; b) thin wells; c) wide wells; d) smooth control

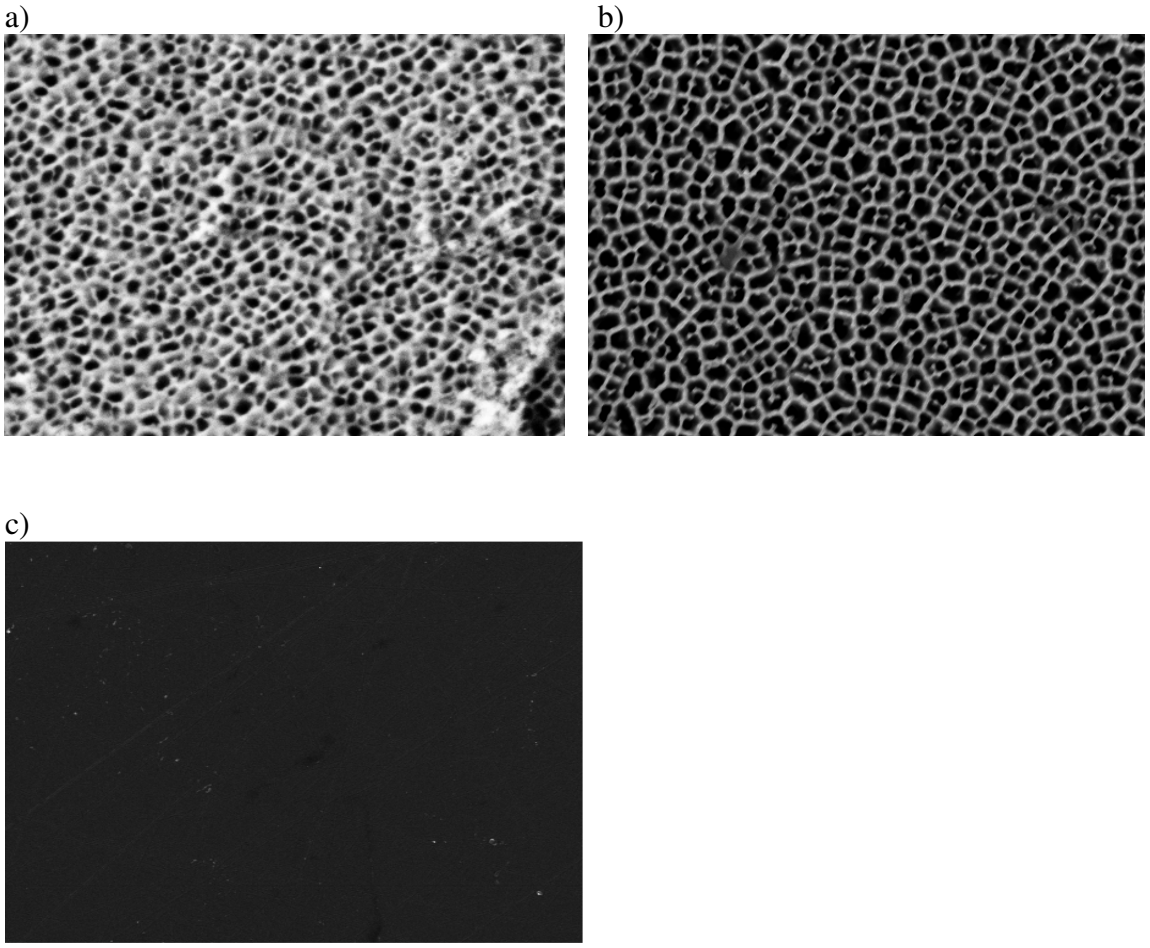

Figure 3.2. Scanning electron micrographs of alumina substrates: a) 20 nm nanoporous membrane; b) 200 nm nanoporous membrane; c) smooth control

Table 3.1 summarizes the roughness parameters and contact angles obtained for all surfaces. The alumina substrates had average roughness (R_a) values of 13 and 15 nm for the 20 nm and 200 nm porous membranes, respectively. The root mean square roughness (R_{rms}) was found to be 19 nm for 20-nm pore membrane and 20 nm for 200-nm pore membrane. The ten-point height (R_z), values, which are defined as the absolute value of the five highest peaks and the five lowest valleys over a given sample length, were 83 and 98 nm for the 20 nm and 200 nm membranes, respectively. Silica substrates had lower values of R_a and R_{rms} and R_z, with R_a values ranging from 5.2 – 6.7 nm for the non-smooth surfaces, and 0.3 nm for the smooth

surface. R_{rms} ranged from 6.1 to 7.5 nm, and R_z values ranged from 19.3 to 26.7 nm. All the surfaces used in this study had roughness values in the "hygienic" range (Ra < 0.8 μm) (Flint et al., 1997).

Table 3.1. **Substrate roughness parameters and contact angle values**

Substrate	**R_a (nm)**	**R_{rms} (nm)**	**R_z (nm)**	**Contact angle (°)**
Alumina, nanosmooth	4.9	6.3	27	83 ± 2°
Alumina membrane, 20 nm wells	13	19	83	-
Alumina membrane, 200 nm wells	15	20	98	-
Silica, nanosmooth	0.3	0.3	1.6	89 ± 2°
Silica, circular wells	6.7	7.5	26.7	98 ± 8°
Silica, thin rectangular wells	6.4	7.3	23.3	94 ± 7°
Silica, wide rectangular wells	5.2	6.1	19.3	95 ± 7°

Contact angle measurements revealed that all of the surfaces were hydrophobic, with the silica wafers slightly more hydrophobic than the smooth alumina substrate (Table 3.1). As bacteria are relatively hydrophilic, using hydrophobic surfaces in this study was expected to contribute to a repellant effect. Smooth silica had a contact angle of 89º whereas smooth alumina had a contact angle of 83º. Nanoengineered silica surfaces were slightly more hydrophobic than the smooth silica, with contact angles ranging from 94 – 98º. It was not possible to measure the contact angles of the alumina membranes due to their porosity.

Visualization of attached bacteria using fluorescence microscopy

Bacterial presence on both the silica and alumina substrates and silica were analyzed after 30 minutes, 24 hours, and 96 hours using fluorescence microscopy. Figure 3.3 shows representative images of *E. coli* ATCC 25922 and *P. fluorescens* cells attached to alumina and silica substrates. Figure 3.3a depicts a representative image of E. coli ATCC 25922 cells attached to nanosmooth alumina, exhibiting no apparent attachment pattern. While it was not possible to observe the topographical details of the alumina nanoporus membranes, some interesting attachment patterns were noticed on certain silica substrates for some of the bacterial strains. For

example, the surfaces with narrow rounded rectangular wells and wide interwell spacing tended to have cells aligned parallel to the long side of the rectangular wells (Figure 3.3b, c). Moreover, cells seemed to preferentially attach to the smooth areas of the surface between the wells rather than inside the wells (Figure 3.3b, c). Similarly, cells tended to align with the long side of the wide rounded rectangular wells with small interwell spacing (Figure 3.3d). The attachment patterns observed on these silica surfaces suggest that cells responded to nanotopography by maximizing contact area between the cell and the surface. Over longer periods of time, microcolonies and the beginnings of biofilm formation were observed, and the newer cell layers did not exhibit any specific orientation.

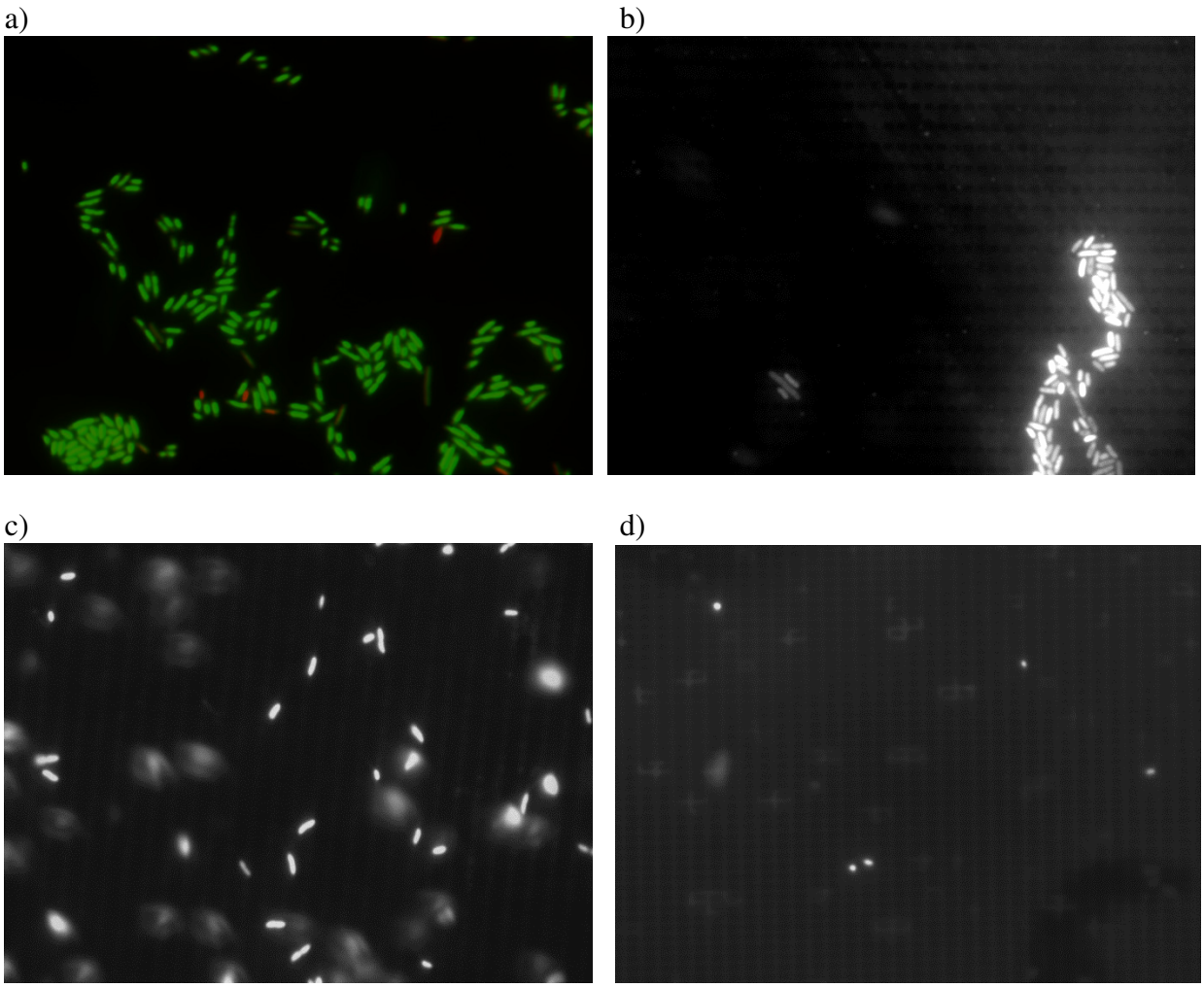

Figure 3.3. Fluorescent microscopic images of attached cells after 30 minutes; a) *E. coli* ATCC 25922 on smooth alumina after 30 minutes, showing no particular arrangemet in attachment; [b) - d)] bacterial cells showing preferential alignment to surface topography: b) *E. coli* ATCC 25922 on silica with thin wells; c) *P. fluorescens* 1150 attached to silica with thin wells; d) *P. fluorescens* 1150 attached to silica with wide wells

Quantification of bacterial attachment

The fluorescent images were analyzed to yield insight into the total number of attached cells at the various time points, as well as the relative proportions of live and dead cells present on the surfaces. Figures 3.4 – 3.6 show the average numbers of live, dead, and total cells attached to the substrates. Bacterial attachment to the engineered silica surfaces revealed trends that were strain specific. *E. coli* ATCC 25922 consistently exhibited higher levels of attachment to the nanosmooth silica control surfaces for all time points. Additionally, there were greater numbers of live cells attached to all surfaces compared to dead cells, except at the 96 hour time point, where a greater population of dead cells attached to controls compared to the nanoengineered surfaces. The pathogenic *E. coli* strain showed significantly greater attachment to the nanoengineered silica surfaces with narrow rounded rectangular wells and wide inter-well spacing, and lower attachment to the surfaces with circular wells, at both the 30 minute and 24 hour time points, However, after 96 hours, control surfaces exhibited significantly greater levels of attachment compared to both the surfaces with either wide or narrow rounded rectangular wells. *P. fluorescens* did not exhibit any obvious trends, with similar levels of attachment to all surfaces. The only notable difference was that attachment to the narrow rounded rectangular wells was almost negligible after 30 minutes, but significantly higher than controls after 24 hours ($p<0.05$). These differences disappeared after 96 hours. Interestingly, as with *E. coli* ATCC 25922, more dead cells than live cells were attached to controls after 96 hours. The Gram positive *L. innocua* also did not exhibit any notable trends in attachment to the silica substrates. At the 30 minute time point, the wide rectangular wells had significantly fewer cells compared to controls, whereas the narrow rectangular wells had significantly higher levels of attachment. However, after 24 hours, significantly fewer cells were attached to the narrow rectangular wells compared to controls.

Attachment trends seen with alumina substrates were also species specific. At the 30 minute time point, all three Gram negative bacterial species exhibited greater attachment on the nanoporous membranes compared to controls. The average numbers of both *E. coli* ATCC 25922 and *E. coli* O157:H7 4477 cells attached to the 200 nm membranes were statistically significantly different from controls. The average numbers of *E. coli* O157:H7 and *P. fluorescens* cells attached to the 20 nm membranes were also significantly different from controls. However, the Gram positive *L. innocua* showed the opposite trend: the greatest amount of cellular attachment was seen on the control surfaces, and the number of cells attached to the 200 nm membranes was significantly lower than that of the control surfaces ($p<0.05$). Also notable was that for the *P. fluorescens* strain used in this study, a greater number of dead cells were found on the nanoporous membranes, whereas a greater number of live cells were found on the control surfaces.

At the 24 and 96 hour time points, attachment trends were less obvious. After 24 hours, *E. coli* ATCC 25922 attached more to control surfaces than the nanoporous membranes, though these differences were not statistically significant. Additionally, a greater proportion of dead cells attached relative to live cells. For the pathogenic strain, the fewest number of cells attached to the control surfaces, though these differences were not statistically significant. *P. fluorescens* showed preferential attachment to the 200 nm membranes and very sparse attachment to the 20 nm membranes. *L. innocua* also showed statistically significantly greater attachment to the 200 nm membrane compared to controls. Attachment to the 20 nm membrane was also greater than controls, though not statistically significantly so. After 96 hours, fewer non-pathogenic *E. coli* cells attached to the nanoporous membranes compared to controls, with the number of cells attached to the 200 nm membranes statistically significantly less than controls. For *L. innocua*, attachment to both nanoporous membrane types was statistically significantly less than

attachment to controls. Conversely, both the pathogenic *E. coli* strain and P. *fluorescens* had greater levels of attachment to the nanoporous membranes compared to controls, though only *P. fluorescens* attachment to the 20 nm membranes was statistically significant.

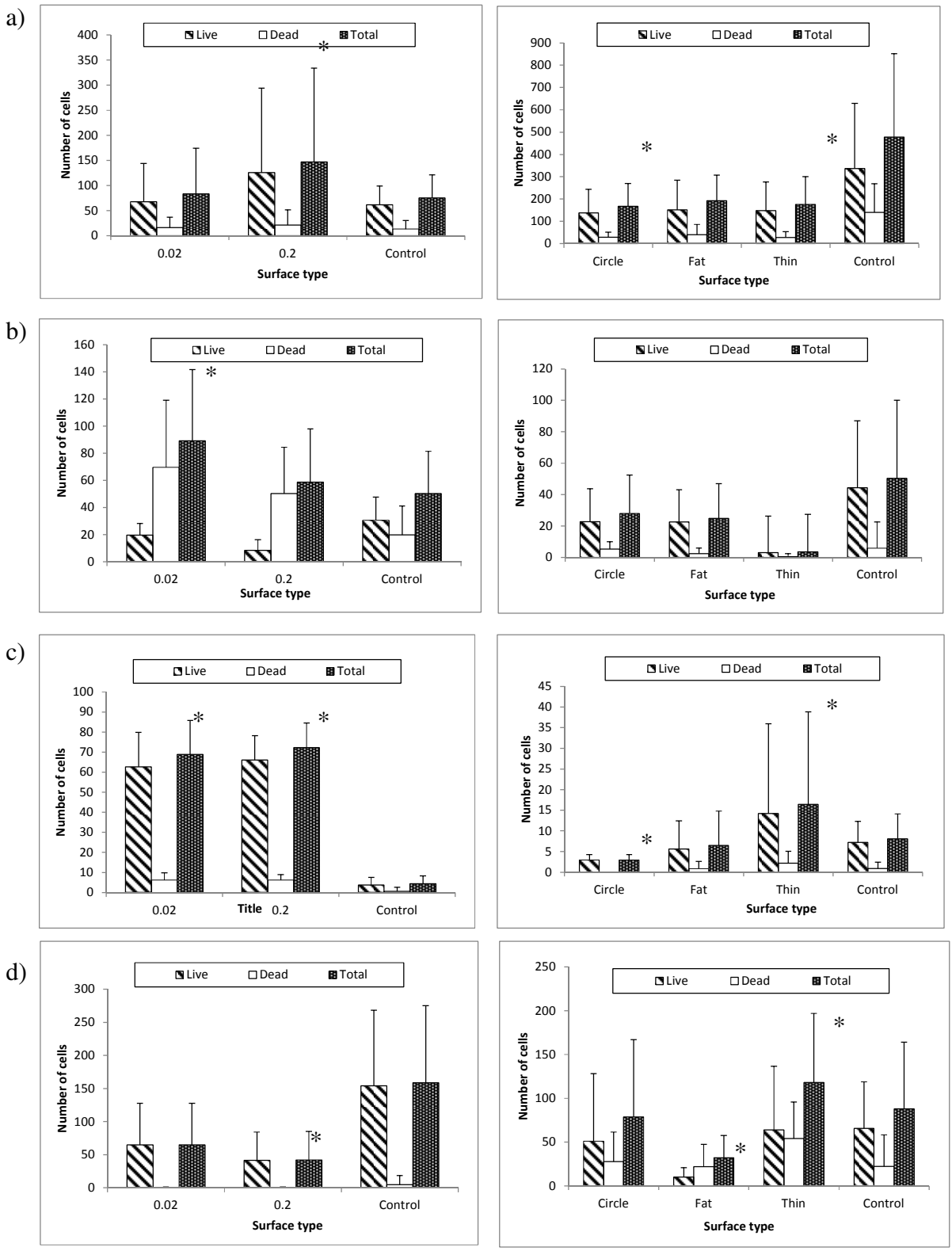

Figure 3.4. **Average number of attached cells after 30 minutes on alumina (left) and silica (right): (a) *E. coli* ATCC 25922; (b) *P. fluorescens* 1150; (c) *E. coli* O157:H7 4477; (d) *L. innocua* FSL C2-008**

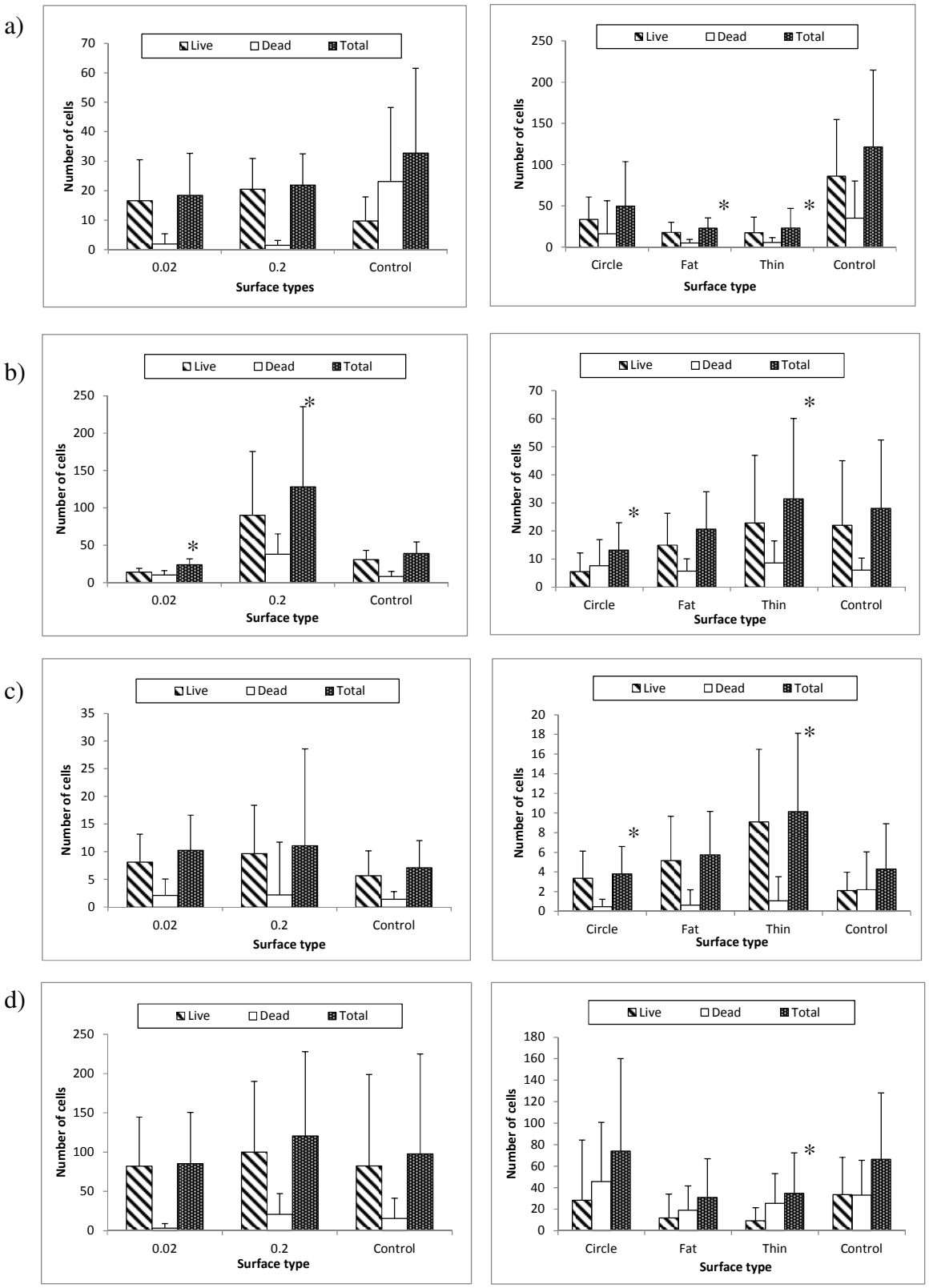

Figure 3.5. **Average number of attached cells after 24 hours on alumina (left) and silica (right): (a) *E. coli* ATCC 25922; (b) *P. fluorescens* 1150; (c) *E. coli* O157:H7 4477; (d) *L. innocua* FSL C2-008**

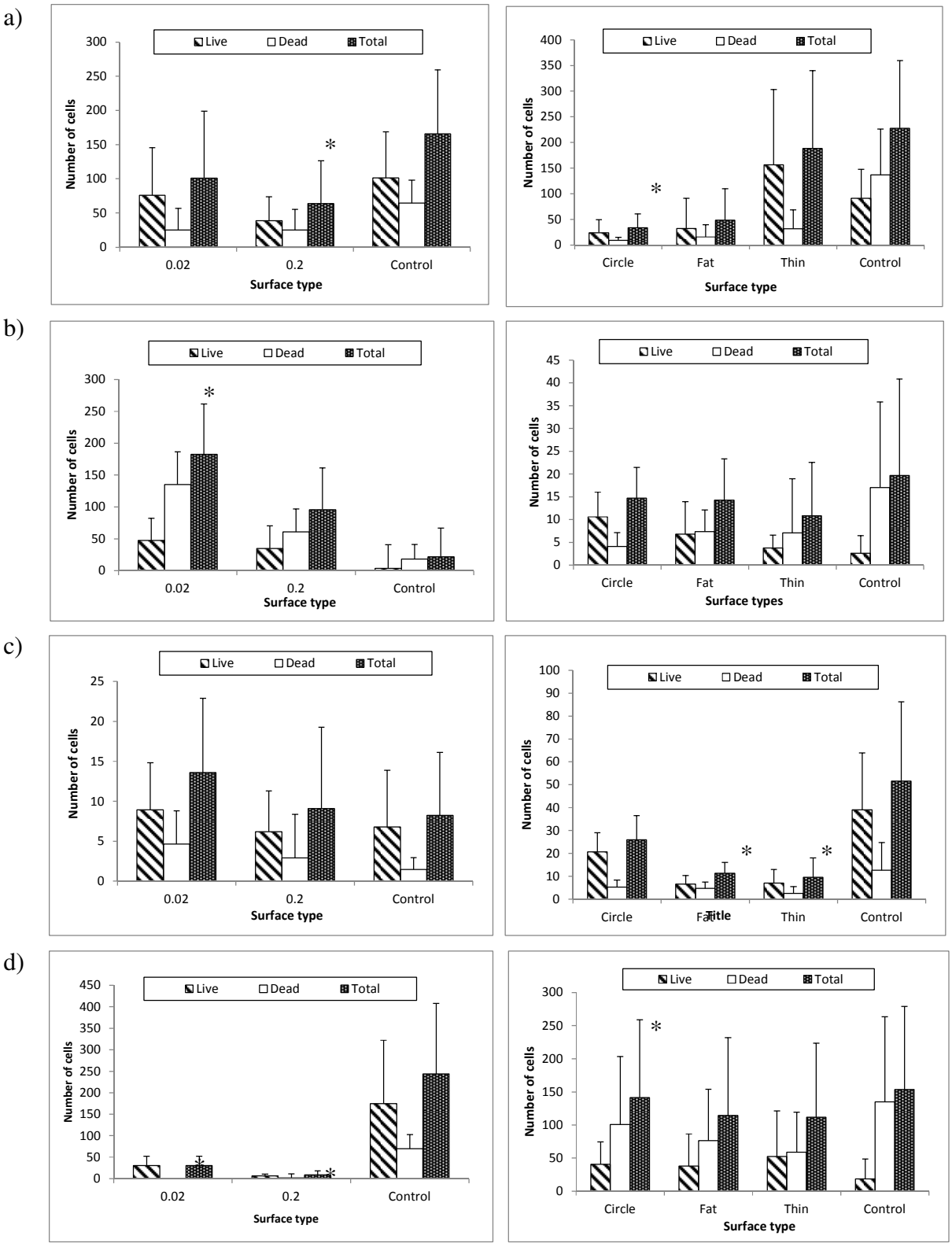

Figure 3.6. Average number of attached cells after 96 hours on alumina (left) and silica (right): (a) *E. coli* ATCC 25922; (b) *P. fluorescens* 1150; (c) *E. coli* O157:H7 4477; (d) *L. innocua* FSL C2-008

Cell morphology of attached bacteria

Scanning electron microscopy visualization of attached bacteria revealed striking physical differences between cells attached to different surface types, especially for *E. coli* ATCC 25922 and *P. fluorescens* 1150, after 24 hours incubation with the substrates (Figures 3.7 & 3.8). The 24 hour time point was chosen in order to have a sufficient number of attached cells remaining after sample preparation, but not so many cells as to obscure the initial layer of attached cells. Morphology of *E. coli* O157:H7 was not examined, due to having insufficent numbers of attached cells. Both *E. coli* ATCC 25922 and *P. fluorescens* 1150 expressed appendages that seemed to assist in their attachment to the surfaces. No appendages were observed with *L. innocua* (Figure 3.7c, 3.8c). For the strains that expressed appendages, the types of appendages that were present appeared to depend on the specific surface topography of the substrate. For example, *E. coli* ATCC 25922 exhibited long and relatively thick appendages that were few in number on both the smooth alumina (Figure 3.7a, top) and silica (Figure 3.8a, top) surfaces. On the 20 nm porous alumina membranes, a much more complex web of appendages was seen linking cells to each other, as well as to the surface (Figure 3.7a, middle). On the 200 nm porous membranes (Figure 3.7a, bottom), the cells expressed more numerous but thinner appendages that formed thick bundle structures. On all of the nanoengineered silica surfaces, *E. coli* cells expressed shorter and thinner appendages that often extended into the wells, even if the cell bodies themselves were not inside the wells (Figure 3.8a).

P. fluorescens also exhibited appendages of differing thicknesses and lengths, which varied with surface type. Unlike *E. coli*, which expressed long and thick appendages when attached to the smooth control surfaces, *P. fluorescens* expressed comparatively few appendages when attached to both the smooth silica and alumina surface, and those that were present were shorter than those present on *E. coli*, especially on the smooth silica (Table 3.2). Conversely, on

both the 20 nm and 200 nm porous alumina membranes, thick webs of appendages surrounded the cells and formed dense webs that connected cells to each other and the surface (Figure 3.7b). On the nanoengineered wide-welled or narrow-welled silica substrates, *P. fluorescens* expressed long appendages similar to that seen on the smooth silica surfaces (3.8c). However, the dense web-like network observed on the alumina membranes was not seen on any of the silica surfaces. Cells attached to the silica surfaces containing circular wells appeared to express little to no appendages, and the appendages were shorter than those seen with the other silica substrates.

a) b) c)

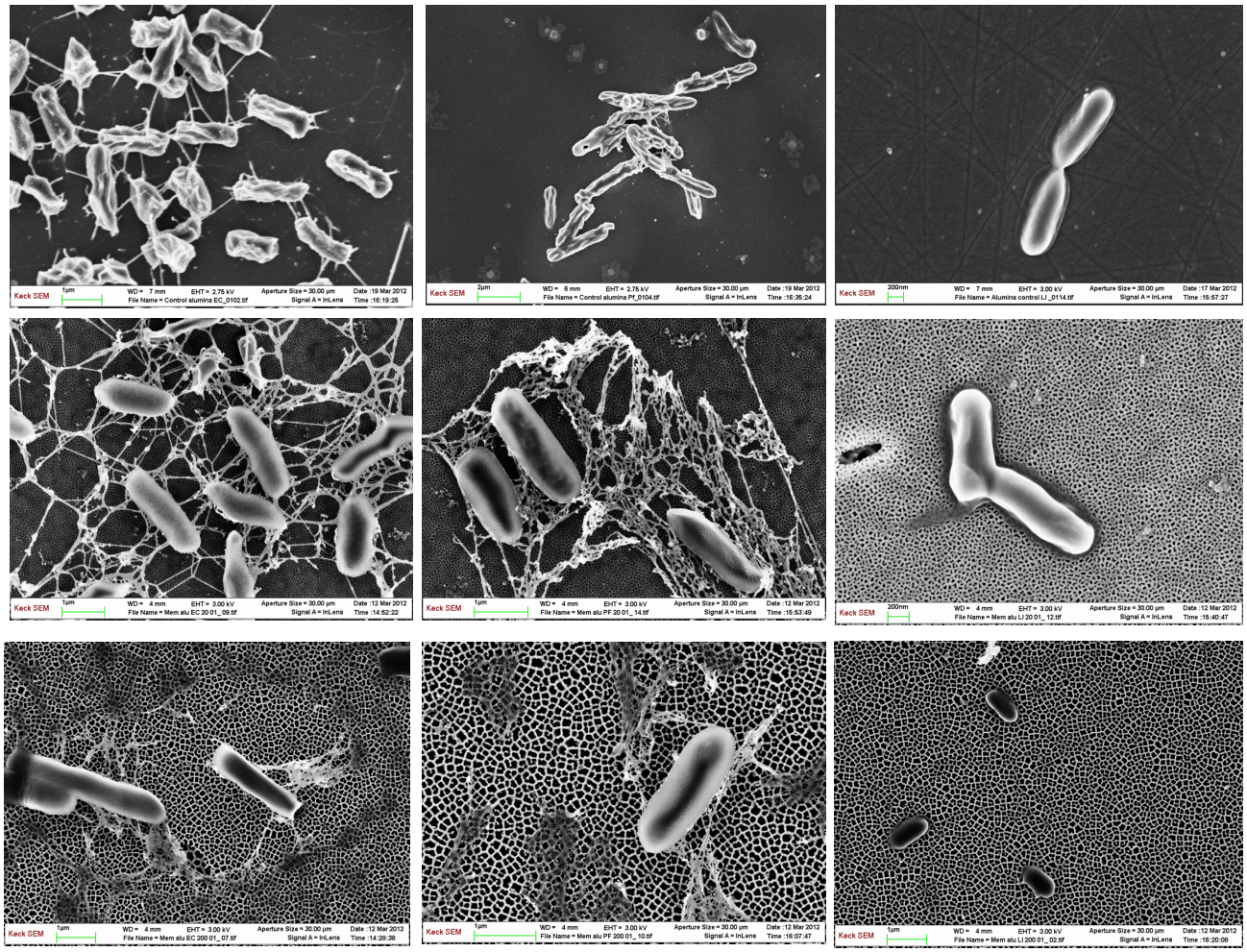

Figure 3.7. Scanning electron micrographs of bacterial cells attached to alumina substrates after 24 hours: a) [from top to bottom] *E. coli* ATCC 25922 on smooth alumina, 20 nm membrane, and 200 nm membrane; b) [from top to bottom] *P. fluorescens* 1150 on smooth alumina, 20 nm membrane, and 200 nm membrane; c) [from top to bottom] *L. innocua* FSL C2 – 008 on smooth alumina, 20 nm membrane, and 200 nm membrane

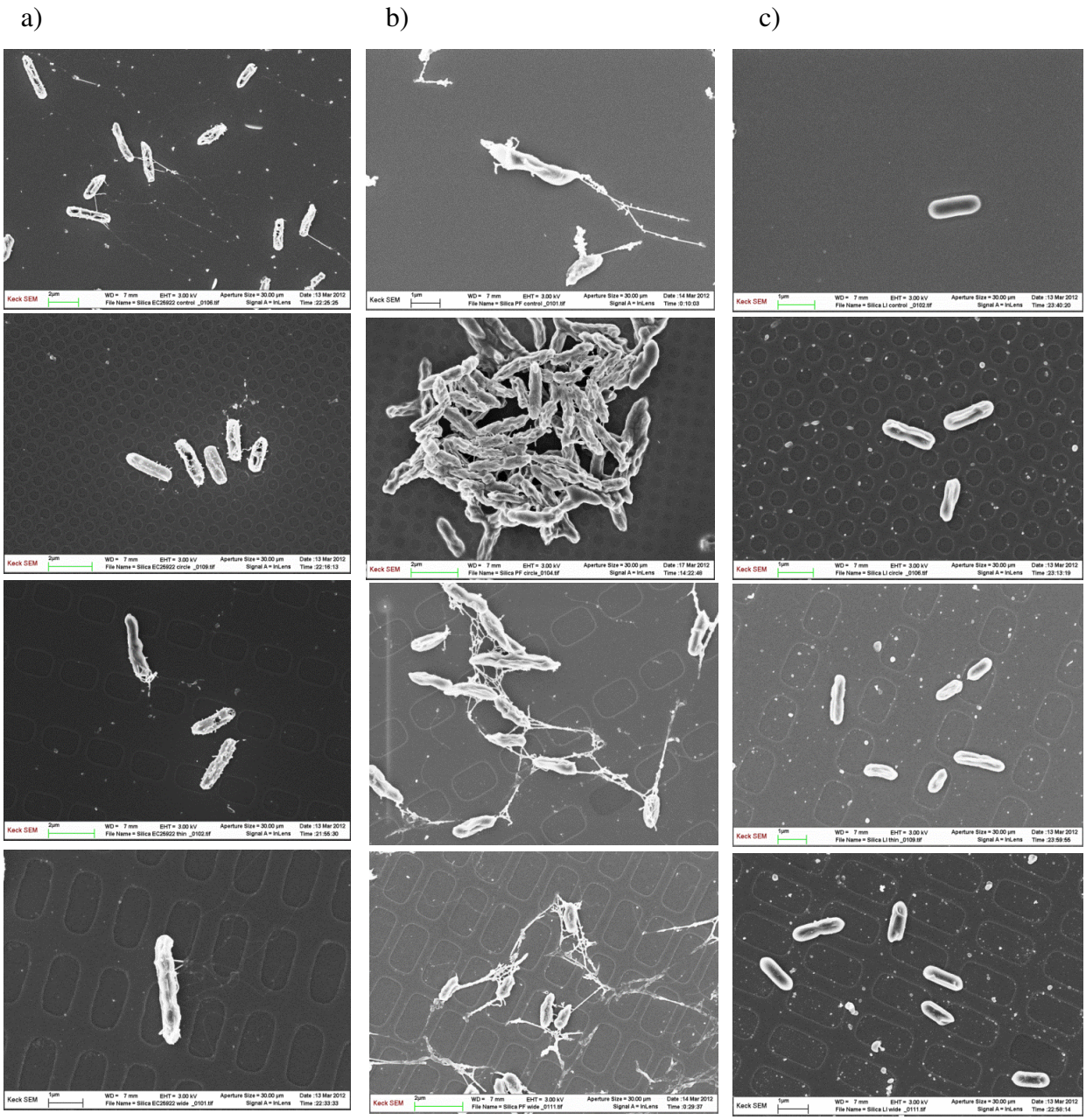

Figure 3.8. Scanning electron micrographs of bacterial cells attached to silica substrates after 24 hours: a) [from top to bottom] *E. coli* ATCC 25922 on smooth silica, circular wells, thin wells, and wide wells; b) [from top to bottom] *P. fluorescens* 1150 on smooth silica, circular wells, thin wells, and wide wells; c) [from top to bottom] *L. innocua* FSL C2 – 008 on smooth silica, circular wells, thin wells, and wide wells

Table 3.2 Cell and appendage dimensions for alumina substrates

E. coli	**Control**	**20 nm**	**200 nm**
Cell diameter, µm	0.576 ± 0.164	0.778 ± 0.074*	0.632 ± 0.208
Cell length, µm	2.104 ± 0.441	1.992 ± 0.241	2.599 ± 0.722*
Appendage diameter, µm	0.069 ± 0.01	0.050 ± 0.029	0.042 ± 0.009
Appendage length, µm	0.991 ± 0.523	1.085 ± 0.788	1.659 ± 1.178
L. innocua			
Cell diameter, µm	0.422 ± 0.041	0.529 ± 0.048*	0.494 ± 0.048
Cell length, µm	1.112 ± 0.065	1.364 ± 0.247*	1.161 ± 0.199
Appendage diameter, µm	---	---	---
Appendage length, µm	---	---	---
P. fluorescens			
Cell diameter, µm	0.525 ± 0.114	0.7621 ± 0.135	0.87 ± 0.089*
Cell length, µm	1.859 ± 0.451	2.289 ± 0.453	2.41 ± 0.601
Appendage diameter, µm	0.096 ± 0.024	0.0552 ± 0.019	0.06 ± 0.03
Appendage length, µm	0.894 ± 0.952	1.309 ± 0.552	1.19 ± 0.436

Table 3.3 Cell and appendage dimensions for silica substrates

E. coli	**Control**	**Circle**	**Thin**	**Wide**
Cell diameter, µm	0.631 ± 0.038	0.537 ± 0.071*	0.623 ± 0.086	0.587 ± 0.041
Cell length, µm	2.219 ± 0.294	2.12 ± 0.616	2.311 ± 0.543	2.479 ± 0.253
App. diameter, µm	0.071 ± 0.010	0.067 ± 0.016	0.072 ± 0.010	0.064 ± 0.015
App. length, µm	1.483 ± 0.556	0.562 ± 0.374	0.576 ± 0.463	1.623 ± 1.224
L. innocua				
Cell diameter, µm	0.524 ± 0.026	0.438 ± 0.065	0.451 ± 0.033	0.500 ± 0.026
Cell length, µm	1.263 ± 0.149	1.247 ± 0.118	1.142 ± 0.154	1.299 ± 0.192
App. diameter, µm	---	---	---	---
App. length, µm	---	---	---	---
P. fluorescens				
Cell diameter, µm	0.599 ± 0.094	0.566 ± 0.074	0.518 ± 0.060	0.488 ± 0.070
Cell length, µm	1.837 ± 0.511	2.484 ± 0.456	1.668 ± 0.293	1.536 ± 0.429
App. diameter, µm	0.096 ± 0.116	0.03 ± 0.008*	0.098 ± 0.023	0.095 ± 0.008
App. length, µm	0.815 ± 0.324	0.326 ± 0.124*	1.787 ± 0.894	1.486 ± 0.815

* represent statistically significantly different from controls

Quantification of the number of appendages (Figures 3.9-3.12) that appeared to emanate from the attached cells revealed an interesting trend. For both *E. coli* and *P. fluorescens*, it was observed that the cells attached to the nanoporous membranes expressed many more appendages than did cells attached to smooth alumina. However, there were no obvious trends with the cells attached to silica surfaces.

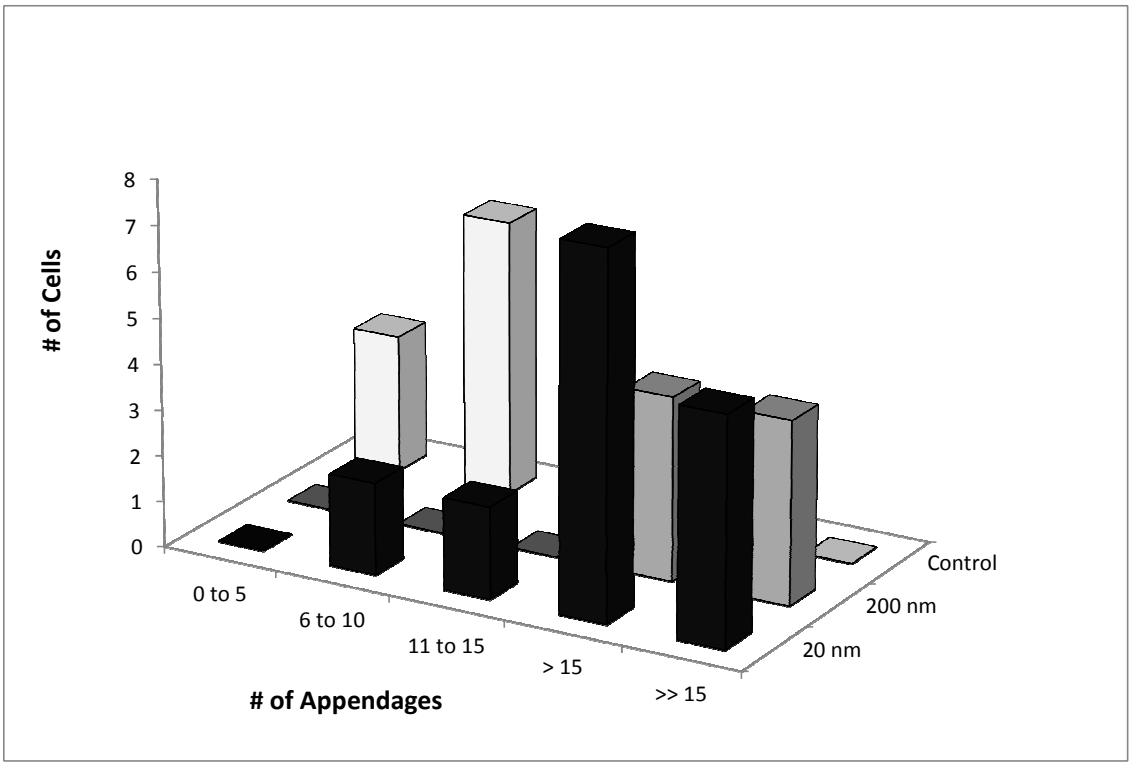

Figure 3.9 Number of appendages on *E. coli* cells attached to alumina substrates

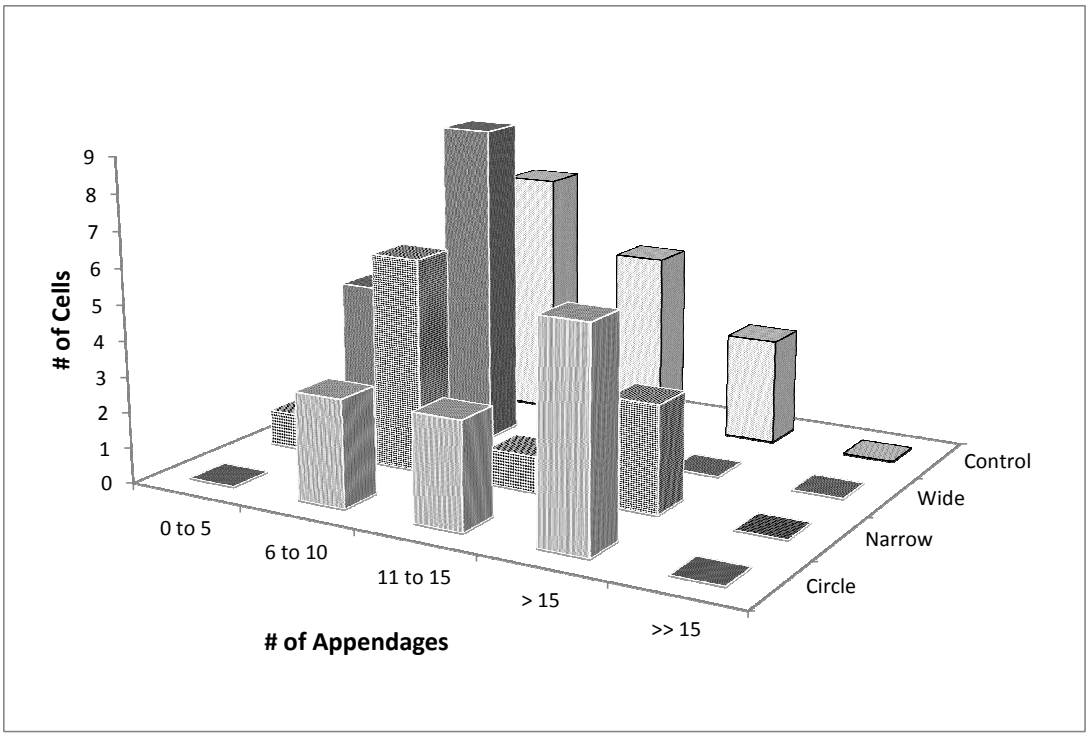

Figure 3.10 Number of appendages on *E. coli* cells attached to silica substrates

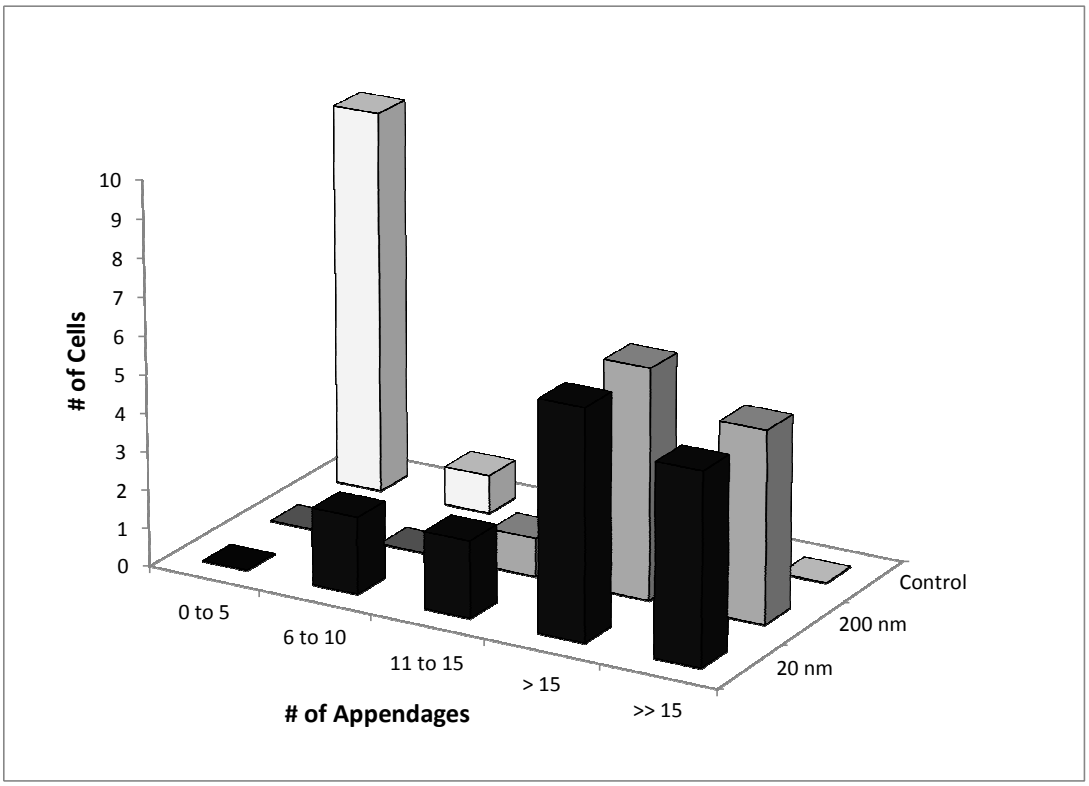

Figure 3.11 Number of appendages on *P. fluorescens* cells attached to alumina substrates

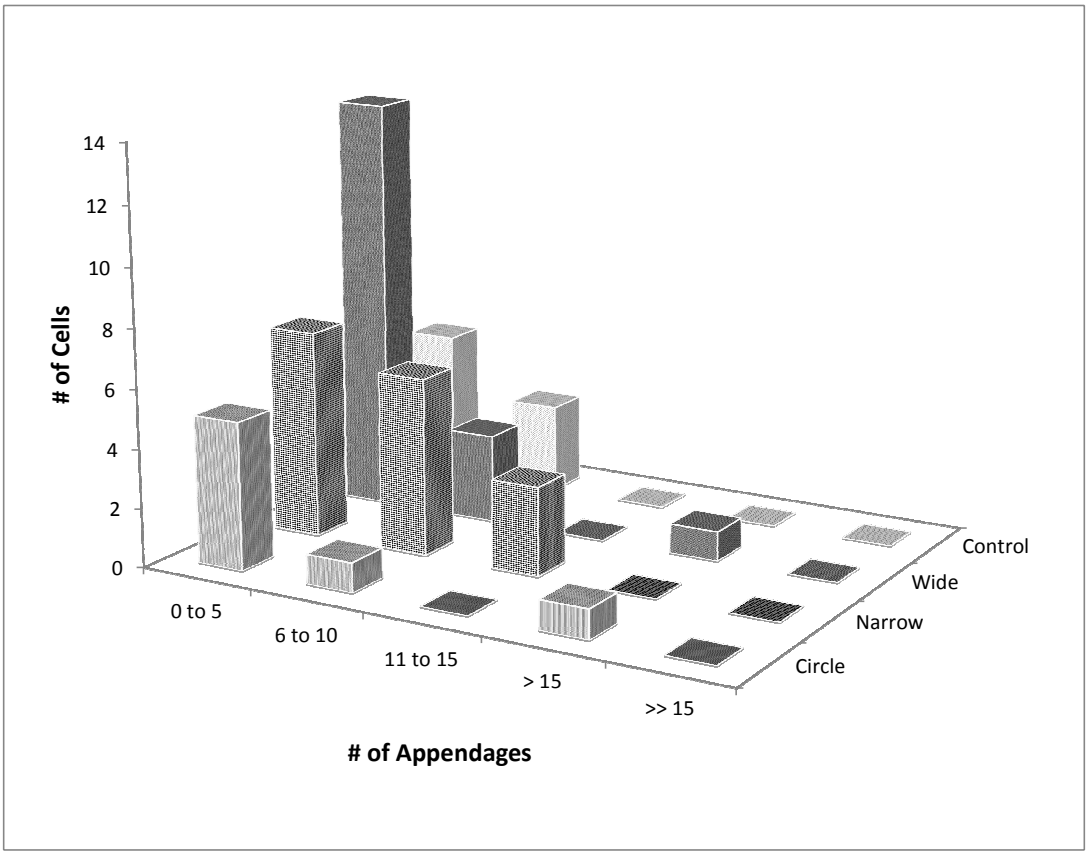

Figure 3.12 Number of appendages on *P. fluorescens* cells attached to silica substrates

DISCUSSION

The results of this study clearly demonstrate that substrate nanoscale topography does influence bacterial attachment behavior, both in terms of the orientation of the cells relative to the surface details, as well as the number of cells attached to a particular surface. It is clear that bacterial attachment is influenced by the shape and size of the nanoscale topographical features, as evidenced by the preferential orientation that cells exhibited on the silica surfaces. Cells aligned themselves in ways that would maximize contact area between the cell and the surface. This preferential alignment to nanoscale and sub-microscale surface details has been observed by others as well. Diaz et al. found that *P. fluorescens* attached in the channels of nanostructured gold (Diaz et al., 2007). Hochbaum and Aizenberg found that *P. aeruginosa* cells aligned

themselves horizontally in trenches when the vertical nanoposts were spaced far enough apart to accommodate the cells. However, when the inter-post spacing was smaller than the diameter of the cells, bacteria aligned themselves parallel to the vertical posts and perpendicular to the plane of the substrate surface (Hochbaum and Aizenberg, 2010).

From a quantitative perspective, the magnitude of the surface topography effect is not consistent, and no clear relationship between the surface topography and the number of attached cells at each time point was observed. Rather, the number of attached cells varied with each strain in addition to the surface type and the exposure time of the cell culture to the surface. This is not an unexpected result, as the outer membrane of bacteria can be vastly different between species. Conflicting results have been reported in the literature as well, with some researchers finding a greater level of attachment to nanophase surfaces compared to conventional surfaces (Park et al., 2008; Mitik-Dineva et al., 2007, Mitik-Dineva et al., 2008), while others found a bacterial-repelling effect of nanophase materials (Puckett *et al*., 2010; Diaz *et al*., 2009). Recent work performed by Singh et al. (2011) on titania thin films suggests a relationship between surface roughness and bacterial attachment: as roughness increased to approximately 20 nm, bacterial attachment increased as well; after 20 nm, significant inhibition of bacterial attachment and biofilm formation were observed. The authors hypothesized that surfaces with roughness greater than 20 nm exhibited a dramatic increase in adsorbed protein from the aqueous medium, and therefore hindered bacterial attachment (Singh et al., 2011). The nanoengineered silica surfaces had average roughness values between 5.2 and 6.7 nm, and thus might not have been rough enough to induce a repelling effect mediated by surface conditioning.

Perhaps the most compelling evidence of a substrate topography effect on bacterial attachment is the fact that the attached cells showed differences in their morphology that varied according to the surface details on the substrate. Overall, bacteria attached to the non-porous

surfaces, such as the nanoengineered silica substrates and the smooth alumina and silica control substrates, exhibited fewer individual appendages compared to cells attached to the nanoporous membranes. Additionally, the appendages were thicker for cells attached to the non-porous substrates compared to those present on the porous substrates. In a study by Rizzello *et al*., *E. coli* cells exposed to gold substrates with nanoscale topography did not express certain type-1 fimbriae, in contrast to cells exposed to smooth gold and glass surfaces. A comprehensive analysis of the *E. coli* proteome showed that in addition to fimbriae expression, genes involved in stress response and defense mechanisms were expressed differently in cells exposed to nanorough versus nanosmooth surfaces (Rizzello et al., 2011).

While it is not yet possible to definitively identify the types of appendages expressed by *E. coli* and *P. fluorescens* on the different surfaces in this investigation, visual analysis strongly suggests that the appendages are not the same. Quantitative analysis of the numbers of appendages emanating from attached cells further supports the conclusion that substrate surface topography is affecting attachment. Cells attached to nanoporous membranes had many more appendages than cells attached to smooth alumina. The fact that this was not the case for cells attached to silica substrates also implicates the nanoscale of the alumina topographical details compared to the micrometric scale of the silica surface details. All of this indicates that bacteria activate different mechanisms of attachment in response to different surface topography. Further investigations are needed to identify the particular appendages present on cells attached to different surfaces and elucidate the mechanisms that the cells employ using those appendages to adhere to surfaces.

CONCLUSIONS

Bacterial attachment is a complex phenomenon influenced by many factors, with

substrate topography playing a significant role. The results of this work show that substrate surface topography at the nanoscale affects bacterial attachment behavior in several ways. Cells seem to try to maximize contact area with the surfaces presumably to achieve a stronger and more stable attachment, and their alignment is thusly governed by substrate topographical details. Moreover, substrate topography either directly or indirectly induces expression of different appendages which appear to help mediate attachment. Food safety applications could benefit from surfaces which can repel bacteria, and therefore future work will focus on finding the appropriate size and shape of substrate topographical details to reduce bacterial attachment. Better understanding of the relationship between cell size and shape relative to substrate surface details, as well as the way in which the substrate details affect expression of appendages may allow the design and fabrication of surfaces with nanoscale topology that can effectively promote or prevent bacterial adhesion. This would greatly improve the overall sanitary quality of food processing facilities and reduce the risk for cross-contamination of pathogenic and spoilage microorganisms from food contact surfaces to foods, ultimately reducing the incidence of foodborne illness and improving the general safety and quality of the food supply.

ACKNOWLEDGEMENTS

Funding for this project was provided by USDA-NIFA Project 65210 – 20024 – 11 and USDA National Needs Grant no. 2006-04257. The fabrication of silica surfaces was performed by Joshua Phelps. His assistance with this project is acknowledged and tremendously appreciated. The author acknowledges the staff at the Cornell Nanobiotechnology Center and the Cornell Center for Materials Research, specifically Dr. Teresa Porri, Penny Burke, John Grazul, Mick Thomas, and John Hunt, for their assistance in using the tools and instruments in the Center, as well as for general upkeep of the facilities.

REFERENCES

Balasundaram, G., & Webster, Thomas J. (2006). A perspective on nanophase materials for orthopedic implant applications. Journal of Materials Chemistry, 16(38), 3737.

Beloin, C., Valle, J., Latour-Lambert, P., Faure, P., Kzreminski, M., Balestrino, D., Haagensen, J. A. J., Molin, S., Prensier, G., Arbeille, B. (2004). Global impact of mature biofilm lifestyle on *Escherichia coli* K-12 gene expression. Molecular Microbiology, 51(3), 659-674

Boyd, R. D., Verran, J., Jones, M. V., & Bhakoo, M. (2002). Use of the atomic force microscope to determine the effect of substratum surface topography on bacterial adhesion. Langmuir, 18(6), 2343-2346.

Bryers, J. D. (2000). Biofilm formation and persistence. In J.D Bryers (Ed.), Biofilms II: Process Analysis and Applications (pp. 45-88). Wiley-Liss.

Busscher, H. J., & Weerkamp, A. H. (1987). Specific and non-specific interactions in bacterial adhesion to solid substrata. *FEMS Microbiology Reviews*, 46, 165-173.

Carpentier, B., & Cerf, O. (1993). Biofilms and their consequences, with particular reference to hygiene in the food industry. *Journal of applied bacteriology*, 75(6), 499-511.

Chmielewski, R. A. N., & Frank, J F. (2003). Biofilm Formation and Control in Food Processing Facilities. *Comprehensive reviews in food science and food safety*, 2.

Collignon, S., & Korsten, L. (2010). Attachment and Colonization by *Escherichia coli* O157 : H7 *, Listeria monocytogenes , Salmonella enterica subsp . enterica serovar Typhimurium ,* and *Staphylococcus aureus* on Stone Fruit Surfaces and Survival through a Simulated Commercial Export Chain. *Journal of Food Protection*, 73(7), 1247-1256

Cookson, A. L., Cooley, W. A, Woodward, M. J. (2002). The role of type 1 and curli fimbriae of Shiga toxin-producing *Escherichia coli* in adherence to abiotic surfaces. *International journal of medical microbiology*, 292(3-4), 195-205.

Dalby, M. J., Riehle, M. O., Yarwood, S. J., Wilkinson, C. D. W., & Curtis, A. S. G. (2003). Nucleus alignment and cell signaling in fibroblasts: response to a micro-grooved topography. *Experimental Cell Research*, 284(2), 272-280.

Díaz, C., Cecilia, M., Laura, P., Gabriela, S., & Saravia, G. D. (2007). Influence of the nano-micro structure of the surface on bacterial adhesion. *Materials Research*, 10(1), 11-14.

Donlan, R. M. (2002). Biofilms: microbial life on surfaces. *Emerging infectious diseases*, 8(9), 881-90.

Flint, S. H., Brooks, J. D., & Bremer, P. J. (2000). Properties of the stainless steel substrate, influencing the adhesion of thermo-resistant streptococci. *Journal of Food Engineering*, 43(4), 235-242.

Frank, J. F., & Koffi, R. (1990). Surface-adherent growth of *Listeria monocytogenes* is associated with increased resistance to surfactant sanitizers and heat. *Journal of Food Protection*, 53(7), 550-554.

Hochbaum, A.I., and Aizenberg, J. (2010). Bacteria Pattern Spontaneously on Periodic Nanostructure Arrays. *Nano Lett*., 10 (9), 3717 – 3721.

Li, B., & Logan, B. E. (2004). Bacterial adhesion to glass and metal-oxide surfaces. *Colloids and surfaces B: Biointerfaces*, 36(2), 81-90.

Mitik-Dineva, N., Wang, J., Mocanasu, R. C., Stoddart, P. R., Crawford, R. J., & Ivanova, E. P. (2008). Impact of nano-topography on bacterial attachment. *Biotechnology journal*, 3(4), 536-44.

Mitik-Dineva, N., Wang, J., Truong, V. K., Stoddart, P., Malherbe, F., Crawford, R. J., Ivanova, E.P. (2009). *Escherichia coli, Pseudomonas aeruginosa*, and *Staphylococcus aureus* attachment patterns on glass surfaces with nanoscale roughness. *Current microbiology*, 58(3), 268-73.

Nguyen, V. T., Turner, M. S., & Dykes, G. a. (2010). Effect of temperature and contact time on *Campylobacter jejuni* attachment to, and probability of detachment from, stainless steel. *Journal of food protection*, 73(5), 832-8.

Park, M. R., Banks, M. K., Applegate, B., & Webster, Thomas J. (2008). Influence of nanophase titania topography on bacterial attachment and metabolism. *International journal of nanomedicine*, 3(4), 497-504.

Pawar, D. M., Rossman, M. L., & Chen, J. (2005). Role of curli fimbriae in mediating the cells of enterohaemorrhagic *Escherichia coli* to attach to abiotic surfaces. Journal of Applied Microbiology, 99, 418-425

Popat, K. C., Chatvanichkul, K.-isara, Barnes, G. L., Joseph, T., Jr, L., Grimes, C. A., Desai, T.A. (2006). Osteogenic differentiation of marrow stromal cells cultured on nanoporous alumina surfaces. *Journal of Biomedical Materials Research Part A*, 80(4), 955-964.

Pratt, L. A, & Kolter, R. (1998). Genetic analysis of *Escherichia coli* biofilm formation: roles of flagella, motility, chemotaxis and type I pili. *Molecular microbiology*, 30(2), 285-93.

Puckett, S. D., E. Taylor, et al. (2010). The relationship between the nanostructure of titanium surfaces and bacterial attachment. *Biomaterials* 31(4): 706-713

Ren, D., Bedzyk, L. A., Thomas, S. M., Ye, R. W., & Wood, T. K. (2004). Gene expression in *Escherichia coli* biofilms. *Applied microbiology and biotechnology*, 64(4), 515-24.

Rizzello, L., Sorce, B., Sabella, S., Vecchio, G., Galeone, A., Brunetti, V., Cingolani, R., & Pompa, P. (2011). Impact of nanoscale topography on genomics and proteomics of adherent bacteria. *ACS Nano*, 5 (3), 1865-76

Robbins, J. B., Fisher, C. W., Moltz, A. G., & Martin, S. E. (2005). Elimination of *Listeria monocytogenes* biofilms by ozone, chlorine, and hydrogen peroxide. *Journal of food protection*, 68(3), 494-8.

Ryu, J.-H., Kim, H., Frank, J. F., & Beuchat, L. R. (2004). Attachment and biofilm formation on stainless steel by *Escherichia coli* O157:H7 as affected by *curli* production. *Letters in applied microbiology*, 39(4), 359-62.

Scallan E., Griffin P. M., Angulo, F. J., Tauxe, R.V., and Hoekstra, R.M. (2011). Emerging Infectious Diseases, 17 (1): 16 – 22.

Scheuerman, T., Camper, A., & Hamilton, M. (1998). Effects of substratum topography on bacterial adhesion. Journal of colloid and interface science, 208(1), 23-33.

Singh., A.V., Vyas, V., Patil, R., Sharma, V., Scopelliti, P., Bongiorno, G., Podesta, A., Lenardi, C., Gade, W.N., & Milani, P. (2011). Quantitative characterization of the influence of the nanoscale morphology of nanostructured surfaces on bacterial adhesion and biofilm formation. PLoS ONE, 6 (9): e25029.

Van Houdt, R., & Michiels, C. W. (2005). Role of bacterial cell surface structures in *Escherichia coli* biofilm formation. Research in microbiology, 156(5-6), 626-33.

Verran, J, Rowe, D. L., & Boyd, R D. (2001). The effect of nanometer dimension topographical features on the hygienic status of stainless steel. Journal of food protection, 64(8), 1183-7.

Whitehead, K. A., Colligon, J., & Verran, J. (2005). Retention of microbial cells in substratum surface features of micrometer and sub-micrometer dimensions. Colloids and surfaces. B, Biointerfaces, 41(2-3), 129-38.

Woodling, S. E., & Moraru, C. I. (2005). Influence of surface topography on the effectiveness of pulsed light treatment for the inactivation of *Listeria innocua* on stainless-steel surfaces. Journal of food science, 70 (7).

CHAPTER 4

CONCLUSIONS AND FUTURE DIRECTIONS

As consumers become more conscientious of the quality and nutritive value of foods that they purchase, the food industry must employ multiple strategies for ensuring the microbiological safety of fresh, minimally-processed, and ready-to-eat foods. This dissertation presented two engineering-based approaches for eliminating the presence of harmful bacteria in foods or food processing environments that may be used synergistically to improve the quality and safety of the food supply. The first approach involved using a non-thermal technology, Pulsed Light, to inactivate microorganisms. A numerical model was developed that combined information about the spatial distribution of fluence and microbial inactivation kinetics to predict the spatial distribution of microbial inactivation. The major conclusions of this work are:

- Treatment intensity in PL treatment can vary dramatically depending on the location and orientation of the substrate relative to the lamp, and the geometrical and optical properties of the liquid substrate. As such, PL treatment would be the most effective for UV-transparent substrates in thin layers.
- Understanding the spatial distribution of fluence and microbial inactivation allows processors to judge whether or not PL would be a viable microbicidal treatment, as well as identify the weak spots in a substrate that must be considered when designing the PL treatment configuration, without extensive experimentation.

The knowledge gained from this work helps to increase the understanding of both the potential and pitfalls of using Pulsed Light to decontaminate liquid substrates. Future work could investigate the effects of PL on the nutritional and sensory properties of treated substrates, since significant negative changes to these properties would immediately discourage the use of PL treatment of foods.

In conjunction with using technology to inactivate microorganisms already present, food processors and manufacturers would greatly benefit from adopting measures to prevent bacterial

attachment to food processing surfaces. This would reduce the risk for cross-contamination from the processing environment to the consumables and therefore help ease the burden of responsibility that microbicidal treatments bear. This study explored the possibility of manipulating substratum surface topography at the nanoscale to control bacterial attachment. While this study did not find any universally observed trends in attachment behavior, it was clear that nanoscale topography did influence bacterial attachment. The major conclusions are:

- When possible, bacteria appear to orient themselves in ways that maximize contact area with the surface.
- Bacteria exhibit different cellular appendages when attached to chemically identical but topographically distinct surfaces, suggesting that the mechanisms of attachment utilized by the cells are influenced by surface topography.

Future work needs to focus on elucidating mechanisms of attachment in effectively control bacterial attachment behavior. Identifying the types of appendages that are expressed by cells attached to different surface types would give insight into the cellular pathways that are activated in response to different surface topographies. Additionally, it is likely that surface conditioning plays a role in bacterial attachment, and this effect needs to be understood before universally repellant surfaces can be engineered.